



**FINAL REPORT: Carbon Life Cycle Analysis of CO₂-EOR
for Net Carbon Negative Oil (NCNO) Classification**
WORK PERFORMED UNDER AGREEMENT DE-FE0024433

Vanessa Nuñez-López¹
Ramon Gil-Egui¹
Pooneh Hosseinioosheri²
Susan D. Hovorka¹
Larry W. Lake²

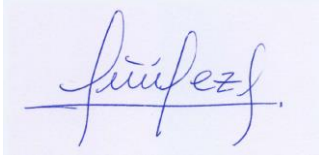
¹Gulf Coast Carbon Center, Bureau of Economic Geology, Jackson School of
Geosciences, The University of Texas at Austin.

²Hildebrand Department of Petroleum and Geosystems Engineering,
The University of Texas at Austin.

SUBMITTED TO
U.S. Department of Energy
National Energy Technology Laboratory
Mary Sullivan – Federal Project Manager
(412) 386-7484
mary.sullivan@netl.doe.gov

April 1, 2019

FINAL REPORT

Report Submitted to:	DOE-NETL
DOE Identification Number:	DE-FE0024433
Project Title:	“Carbon Life Cycle Analysis of CO ₂ -EOR for Net Carbon Negative Oil (NCNO) Classification”
Project PI:	Vanessa Nuñez-López Research Scientist Associate vanessa.nunez@beg.utexas.edu , Office number: (512) 471-5825
Submission date:	04/01/2019
DUNS Number:	170230239
Recipient Organization:	Bureau of Economic Geology, The University of Texas at Austin
Submitting Official: Vanessa Nunez-Lopez, PI:	

Disclaimer

This report was prepared as an account of work sponsored by an agency of the United States Government. Neither the United States Government nor any agency thereof, nor any of their employees, makes any warranty, express or implied, or assumes any legal liability or responsibility for the accuracy, completeness, or usefulness of any information, apparatus, product, or process disclosed, or represents that its use would not infringe privately owned rights. Reference herein to any specific commercial product, process, or service by trade name, trademark, manufacturer, or otherwise does not necessarily constitute or imply its endorsement, recommendation, or favoring by the United States Government or any agency thereof. The views and opinions of authors expressed herein do not necessarily state or reflect those of the United States Government or any agency thereof.

Report Summary

This final report summarizes the work that was conducted to achieve the project's general objective of developing a clear and repeatable methodology to determine whether the oil produced in a conventional CO₂ enhanced oil recovery (CO₂-EOR) operation can be classified as Net Carbon Negative Oil (NCNO). The report also summarizes the reservoir mass accounting methodology and the monitoring, verification, and accounting (MVA) methodology, which are critical elements that support the general objective and were conceived as project goals.

Because the purpose is to classify the EOR product (crude oil) and not the EOR project itself, and as the rate of crude oil production varies significantly with time, the methodology uses a novel dynamic carbon lifecycle analysis (d-LCA) that links instant energy demand and associated greenhouse gas (GHG) emissions to instant operational performance. The EOR operational performance is assessed through CO₂ utilization rates, which relate usage of CO₂ to oil production. This dynamic method provides a better understanding of the evolution of the environmental impact (CO₂ emissions) and mitigation (geologic CO₂ storage) associated with an expanded carbon capture, utilization and storage (CCUS) system, from start to closure of operations. The dynamic interplay between operational and environmental performance forms the basis of our CCUS technology analysis.

The LCA part of the work is meant to complement previous NETL LCA work, and so it focused on EOR/storage efficiency, its variability through time, and the impact of this variability on LCA results. The environmental impact of the CCUS system was assessed for 3 system boundaries: (1) gate-to-gate, (2) gate-to-grave, and (3) cradle-to-grave. The environmental impact was also assessed considering the electricity displacement from other generation facilities.

Another goal of our study was to use results to make recommendations on EOR field development strategies that are conducive to producing NCNO. Because field operational strategies have a significant impact on reservoir engineering parameters that affect both CO₂ storage and oil production (e.g., sweep efficiency, flood conformance, fluid saturation distribution), we conducted a scenario analysis that assesses the operational and environmental performance of four common and novel CO₂-EOR field development strategies. Results show that all CO₂-EOR evaluated scenarios start operating with a negative carbon footprint and, years into the project, transition into operating with a positive carbon footprint. Having achieved a result that proves that all CO₂-EOR operations produce NCNO during the first years of production is critical in the context of the urgency of climate change mitigation. Transition points are significantly different in each scenario.

In a cradle-to-grave CCUS system, if the capture facility displaces a conventional power source and credits are added for displacement, the adverse impact caused by the system expansion not only is reversed but transformed into a significant environmental benefit. The effect of the displacement more than compensates the emissions associated with the electricity generation requirements for the production of CO₂, as much more electricity will be displaced.

Results provide an understanding of the evolution of the system's net carbon balance of all four field development strategies studied. This information can be useful to CO₂-EOR operators seeking value in storing more CO₂ through a carbon credit program (e.g., the 45Q federal carbon credit program). Most importantly, this study serves as confirmation that CO₂-EOR can be operationally designed to both enhance oil production and reduce greenhouse gas emissions to the atmosphere.

Contents

Report Summary	i
Contents.....	iii
List of Figures	v
1. Introduction	1
2. Reservoir Mass Accounting Methodology	4
2.1 Preferred Mass Accounting Method	4
2.2 Mass Accounting Method with Recycle Mass Accounting	8
3. Integrated MVA Methodology.....	12
3.1 MVA Workflow.....	14
3.1.1 Definition of Project and Quantitative Success Criteria	16
3.1.2 Characterization as a Critical MVA Element.....	20
3.1.3 ALPMI Creation and Response Modeling	25
3.1.4 ALPMI Monitoring Execution	25
3.1.5 Verification and Accounting of Success Criteria.....	26
4. NCNO Methodology	27
4.1 Subsurface Modeling for EOR Operational Performance	27
4.2 Surface Modeling for CCUS Environmental Performance.....	30
4.2.1 Gate-to-Gate Carbon Emission Estimates	31
4.2.2 Gate-to-Grave Carbon Emission Estimates.....	34
4.2.3 Cradle-to-Grave Carbon Emission Estimates	35
4.2.4 Cradle-to-Grave Electricity Displacement	36
5. NCNO Results and Discussion	38
3.1 CO ₂ -EOR Reservoir Response	38
3.2 Gate-to-Gate Boundary	40
3.3 Gate-to-Grave Boundary.....	43
3.4 Cradle-to-Grave Boundary	47
3.4.1 Pulverized Carbon Power Plant	47
3.4.2 Natural Gas Combined Cycle Power Plant.....	50
6. Conclusions.....	54
Nomenclature	55
Acknowledgements	55

References	56
Appendix A: Review and Analysis of Existing Monitoring Methods and Tools.....	59
Appendix B: Gate-to-Gate & Gate-to-Grave Results	79
Appendix C: Cradle-to-Grave (Pulverized Coal Power Plant)	88
Appendix D: Cradle-to-Grave (Natural Gas Combined Cycle Power Plant)	94
Appendix E: Results with Public Relative Permeability Data	100

List of Figures

Figure 2.1. Elements of reservoir mass accounting.	7
Figure 2.2. Surface mass accounting monitoring locations	8
Figure 3.1. Steps of an integrated MVA methodology	15
Figure 3.2 (a) Stratal slice of the 3-D seismic survey, with interpreted channel morphologies in the Lower Tuscaloosa Formation “D-E” interval showing high-amplitude (red) sinuous fluvial channel loops. Dashed line shows location of cross section in Figure. (b) Interpreted channel morphologies in seismic profile, showing general reservoir architecture of a fluvial point-bar plain. Sandstones (red) appear to be discontinuous laterally, suggesting sinuous deposition in 3-D.	19
Figure 3.3. Reservoir heterogeneity of sand bodies (left). Grain size and sedimentary structure cross-section of Cranfield wells 31F-2 and 31F-3, 30 meters apart (right).....	21
Figure 3.4. Cranfield stratigraphic section showing injection zone and near-surface. From [33].....	22
Figure 3.5. Transect of Detailed Area of Study (DAS).	23
Figure 3.6. Flowchart used to improve Cranfield reservoir modeling by the integration of field data.....	24
Figure 4.1. (a) Structural contour map, (b) sector model showing structure and location of injection and production wells, (c) active and inactive grids used for reservoir simulation. Sealing fault is a closed boundary.	28
Figure 4.2. CCUS system components and carbon LCA boundaries	31
Figure 4.3. Methodology for direct and indirect CO ₂ emissions inventory at the EOR site.	32
Figure 5.1. (a) Cumulative oil production as a function of CO ₂ volumes injected. (b) CO ₂ storage as a function of CO ₂ volumes injected. HCPV = hydrocarbon pore volume.	39
Figure 5.2. (a) Net utilization ratio (purchased CO ₂ needed to produce one barrel of oil). (b) Gross CO ₂ utilization ratio (purchased plus recycled CO ₂ needed to produce one barrel of oil).	39
Figure 5.3. Instantaneous gate-to-gate GHG emissions rates per carbon intensive component: (a) CO ₂ injection compression, (b) water injection, (c) water disposal, and (d) total emissions without gas separation.....	41
Figure 5.4. Gate-to-gate GHG emission rate per gas separation process for (a) continuous gas injection, (b) water curtain injection, (c) water-alternating-gas, and (d) the hybrid scenario.	42
Figure 5.5. CO ₂ storage mass (grey curves) versus CO ₂ e emissions (color curves) of the gate-to-gate CCUS system for (a) continuous gas injection, (b) water curtain injection, (c) water-alternating-gas, and (d) the hybrid scenario.....	43
Figure 5.6. C Carbon intensity of gate-to-grave components in: (a) continuous gas injection, (b) water curtain injection, (c) water-alternating-gas, and (d) the hybrid scenario..	44

Figure 5.7. CO ₂ storage mass (grey curves) versus CO _{2e} emissions (color curves) of the gate-to-grave CCUS system for (a) continuous gas injection, (b) water curtain injection, (c) water-alternating-gas, and (d) the hybrid scenario.	45
Figure 5.8. Carbon balance (CO _{2e} emissions minus CO ₂ storage) of the gate-to-grave CCUS system for (a) continuous gas injection, (b) water curtain injection, (c) water-alternating-gas, and (d) the hybrid scenario.	46
Figure 5.9. Evolution of efficiency rates: (a) mass of CO ₂ injected per mass of CO ₂ stored, (b) oil production per Kg of CO ₂ injected, (c) gate-to-grave cumulative GHG emissions per mass of CO ₂ stored, and (d) gate-to-grave cumulative GHG emissions per barrel of oil produced.	47
Figure 5.10. CO ₂ storage mass (grey curves) versus CO _{2e} emissions (color curves) of the cradle-to-grave CCUS system with pulverized coal power plant for: (a) continuous gas injection, (b) water curtain injection, (c) water-alternating-gas, and (d) the hybrid scenario.	48
Figure 5.11. Carbon balance (CO _{2e} emissions minus CO ₂ storage) of the cradle-to-grave CCUS system with pulverized coal power plant for (a) continuous gas injection, (b) water curtain injection, (c) water-alternating-gas, and (d) the hybrid scenario.	48
Figure 5.12. Evolution of efficiency rates: (a) components upstream of the CO ₂ -EOR site, (b) the cradle-to-grave PC – CCUS system.	49
Figure 5.13. Effect of electricity displacement on the carbon balance (CO _{2e} emissions minus CO ₂ storage) of the cradle-to-grave CCUS system with pulverized coal power plant for (a) continuous gas injection, (b) water curtain injection, (c) water-alternating-gas, and (d) the hybrid scenario.	50
Figure 5.14. CO ₂ storage mass (grey curves) versus CO _{2e} emissions (color curves) of the cradle-to-grave CCUS system with Natural Gas Combined Cycle power plant for: (a) continuous gas injection, (b) water curtain injection, (c) water-alternating-gas, and (d) the hybrid scenario.	51
Figure 5.15. Carbon balance (CO _{2e} emissions minus CO ₂ storage) of the cradle-to-grave CCUS system with Natural Gas Combined Cycle power plant for (a) continuous gas injection, (b) water curtain injection, (c) water-alternating-gas, and (d) the hybrid scenario.	51
Figure 5.16. Evolution of efficiency rates: (a) components upstream of the CO ₂ -EOR site, (b) the cradle-to-grave NGCC – CCUS system.	52
Figure 5.17. Effect of electricity displacement on the carbon balance (CO _{2e} emissions minus CO ₂ storage) of the cradle-to-grave CCUS system with Natural Gas Combined Cycle power plant for (a) continuous gas injection, (b) water curtain injection, (c) water-alternating-gas, and (d) the hybrid scenario.	53

1. Introduction

Carbon dioxide enhanced oil recovery (CO₂-EOR) is a technology most commonly applied in the third and final stage of development of mature oil fields to enhance oil production. For this reason it is also referred to as a type of tertiary recovery. It has been applied successfully in the U.S. since the early 1970's, most extensively in the Permian Basin located in West Texas and eastern New Mexico where more than 50 CO₂-EOR projects operate [1]. The technology targets the residual oil in depleted oil reservoirs by injection of CO₂ [2].

The oil recovery process can be immiscible or miscible, with the highest oil recovery expected in miscible displacements [3]. In a miscible process CO₂ enhances oil production by mixing with the residual oil as a solvent agent at pressures above the minimum miscibility pressure (MMP), which is the minimum pressure at which miscibility is achieved [3]. The reduced viscosity and expansion of the new CO₂-oil phase decreases flow resistance toward oil producing wells. The produced CO₂ is separated from the produced fluids, re-injected back into the reservoir and the process is repeated in a loop. However, not all the injected CO₂ is produced back to the surface, as several mechanisms such as capillarity, dissolution, and the geologic structure, trap a significant percentage (as much as 50%) of the CO₂ injection stream within the reservoir [4,5]. For oil field operators the mass of CO₂ trapped in the reservoir represents a loss which needs to be replaced with purchased CO₂ in order to maintain the required CO₂ injection rates. In cases where anthropogenic CO₂ captured from industrial facilities is used for EOR, the anthropogenic CO₂ lost into the formation could be considered as a geologically stored CO₂ mass, a mass that would have entered the atmosphere as a greenhouse gas had it not been captured and utilized for EOR. Because of the latter, CO₂-EOR technologies that use anthropogenic CO₂ are also considered carbon capture, utilization, and storage (CCUS) technologies.

However, some have questioned the validity of CO₂-EOR as an alternative for greenhouse gas emission reduction, as CO₂ emissions result from the energy consumption throughout the EOR operation and, more significantly, from the combustion of the incremental oil produced. To answer the question of how much carbon is emitted in CO₂-EOR projects, several carbon lifecycle analysis (LCA) have been conducted and are available in the literature.

LCA is a process that assesses the environmental impact that occurs throughout a product's lifecycle, from raw materials acquisition through production, use, final treatment, recycle, and disposal. The process is standardized in ISO 14044:2006 [6] and encompasses four distinctive phases: (1) goal and scope definition, (2) inventory analysis, (3) impact assessment, and (4) interpretation. Table 1.1 provides a list of the most relevant CO₂-EOR LCA studies to date.

Table 1.1. GHG emissions from previous LCA studies on CO₂-EOR, from oil field site to end product combustion.

Reference	Study Remarks	GHG Emissions		
		CO ₂ -EOR Field Site	Refinery Operations	Product Combustion
Aycaguer [7]	Storage: 2.6 kg CO ₂ /kg of oil produced (4.5 kg CO ₂ /kg gasoline produced) and 0.1 kg CH ₄ per kg oil. General conclusion: GHG generated by gasoline combustion is offset by CO ₂ storage in the reservoir.	0.4 kg CO ₂ /kg oil		4.8 kg CO ₂ /kg gasoline
Suebsiri [8]	Storage: 18.60 Mton CO ₂ . General conclusion: EOR has the capacity to store 30% of the total CO ₂ emissions from the EOR process through the refinery and end usage.	1.4 Mtonne CO ₂ (0.06 ton CO ₂ /ton CO ₂ recycled)	3.3 Mtonne CO ₂ /130 MMbbl	61 Mtonne CO ₂ /130 MMbbl
Hertwich [9]	General conclusion: a combined cycle power plant with carbon capture has substantially lower GHG emissions than a gas power plant without CCS.	19.1 kg CO ₂ e per standard cubic meter of oil		
Jaramillo [10]	Storage (SACROC case): 85 Mtonne CO ₂ e Storage: 0.2 tonnes CO ₂ /bbl oil produced Emissions: 3.7–4.7 ton CO ₂ emitted/ton CO ₂ injected General conclusion: 0.62 tonnes of CO ₂ will need to be injected (and stored) per bbl of oil produced in order to offset system emissions.	SACROC case: 22.7 Mtonne CO ₂ e	SACROC: 20.1 Mtonne CO ₂ e	SACROC: 159 Mtonne CO ₂ e
DOE-NETL [11]	This study quantifies electricity requirements of CO ₂ -EOR expressed in kWh per barrel of incremental oil.	27–98 kWh/bbl		
Fox [12]	Net Storage at EOR site: 241.5 Mton CO ₂ . (93% of CO ₂ purchased) Net storage including product combustion: 126.5 Mton CO ₂ sequestered (49%)	18.5 Mtonne CO ₂ (0.1 ton CO ₂ /bbl)		97 Mtonne CO ₂
Cooney [13]	LCA analysis on 3 system boundaries: Gate-to-gate, cradle-to-gate, and cradle-to-grave.	60–165 kg CO ₂ e/bbl (including land use + construction)		

*Mtonne = million metric ton, MMbbl = million barrel.

Other studies address the issue of the potential disparity between the goals of EOR and the goals of carbon storage. In fact, the subject of co-optimization has been a focus of carbon capture, utilization, and storage (CCUS) research studies during the last decade [14–16]. In most

studies, co-optimization is the process of finding a balance between the goals of EOR (produce more oil/money with less purchased CO₂) and the goals of carbon storage (store more purchased CO₂), which seem in conflict. In our study, we expand the goals of carbon capture and storage (CCS) from just storing CO₂ to reducing greenhouse gas emissions, which requires a carbon balance analysis of CO₂-EOR that accounts for CO₂ emissions throughout the CCUS system.

The efficient displacement of reservoir fluids with CO₂ is a critical process which, when optimized, provides an opportunity for simultaneously enhancing oil production and associated carbon storage. Oil field operators develop their fields so that maximum oil production is obtained within the constraints of their field specific settings. Many challenges (economic, geologic, resource access, etc.) are site specific and thus vary at each EOR field development. These differences influence the selection of CO₂ injection strategies.

Throughout the history of CO₂-EOR technology applications [17], several CO₂ injection strategies have been developed to overcome operational shortfalls, such as early CO₂ breakthrough due to viscous fingering or gravity override, and injectivity loss, among others. Water-alternating-gas (WAG) strategies, which alternate injection of brine and CO₂, were designed and implemented to improve flood conformance by reducing the mobility contrast between the displacing and displaced fluids. The goal of such strategies is to avoid high residual oil saturations in un-swept or poorly swept rock volumes. However, loss of injectivity occurs to some degree during WAG in most floods [18, 19], particularly in those with reservoir permeabilities below 10 millidarcies. To reduce injectivity loss, operators started adjusting WAG ratios and drilling new wells, all of which led to a significant variety of CO₂ injection configurations that are EOR site specific.

EOR operational considerations, such as the ones described, greatly affect associated geologic carbon storage volumes, which in turn affect the net carbon balance of the EOR operation. In fact, carbon storage is the only parameter in the net carbon balance equation that counters the environmental impact (CO₂ emissions) of CCUS systems. Given the importance of this volume in the context of CCUS carbon lifecycle, we focus on the understanding of reservoir responses to different field development schemes for EOR and how those schemes affect the energy demanding components of CCUS systems. To this end we conducted a scenario analysis that captures the range of reservoir responses to different CO₂ injection strategies and analyzed the interplay between the subsurface performance and the energy needed to run the operation in the different scenarios. This dynamic approach provides a better understanding of the evolution of the environmental impact (CO₂ emissions) and mitigation (geologic CO₂ storage) associated with an expanded carbon capture, utilization and storage (CCUS) system, from start to closure of operations.

2. Reservoir Mass Accounting Methodology

In the context of greenhouse gas (GHG) emission reduction, the mass of CO₂ that can qualify as permanently stored in the oil reservoir through the process of EOR, constitutes the only parameter in the carbon balance equation that can contribute to this reduction. Quantifying CO₂ storage mass with a robust mass accounting methodology and assuring geologic permanence through a fit-to-purpose monitoring, verification, and accounting (MVA) program are critical tools that we provide in this study.

The target of our reservoir mass accounting methodology is the mass of purchased CO₂. It is expected that the overall amount of CO₂ stored in the reservoir during the flood be approximately the amount of CO₂ delivered to the EOR site for injection.

In this sense, our preferred methodology differs from most current methodologies in that we recommend not to account for recycle gas, as it introduces significant complexities which lead to significant mass accounting errors. Another difference is that we do propose accounting for CO₂ subsurface losses, both laterally and vertically outside of a pre-established subsurface volume. The latter is in agreement, however, with the International Organization for Standardization (ISO 27916:2019), which includes quantification of losses from the “EOR complex.”

We also developed an alternative methodology to our preferred one, because existing local regulations, contractual structures, financial expectations, etc., might require that the EOR operator report recycle mass accounting. Both methodologies include losses of CO₂ at the surface, which correspond to CO₂ releases from surface equipment during a number of identified expected and unexpected events. We received valuable input and review from Hilcorp and the Petra Nova team on practical aspects of EOR operations that were necessary in the development of the methodologies.

2.1. Preferred Mass Accounting Method

All carbon capture, utilization and storage (CCUS) projects sponsored by the DOE regional sequestration partnership are required to report the volumes/mass of carbon geologically stored through the process of CO₂ EOR. These projects report their mass accounting similarly: total injected CO₂ minus total produced/recycle CO₂. SECARB’s Early Project at Cranfield, for example, used equation (1) below, which corrects for methane concentration both in the purchased CO₂ and in the produced gases. Most of these projects, including Cranfield, did/do not include CO₂ losses due to subsurface or surface leakage.

$$\text{Net CO}_2 \text{ Stored} = (\text{Total CO}_2 \text{ Injection} - \text{Average CH}_4 \text{ in Injection Stream}) - (\text{Total CO}_2 \text{ Produced} - \text{Average CH}_4 \text{ in Production/Recycle Stream}) \quad (\text{eq. 1})$$

EPA's greenhouse gas reporting program Subpart RR §98.442, however, does require the accounting of CO₂ leakages at the surface (see eq. 2, corresponding to eq. RR-11 in subpart RR), and makes the distinction between surface CO₂ leakage (through the surface interface) and CO₂ equipment leakage (as described in table 2.2). Similarly, ISO 27916:2019 states that the mass of CO₂ stored should be quantified as in eq. 3. Note: the methodologies presented here were developed prior to the release of ISO 27916:2019.

$$CO_{2\text{sequestered}} = CO_{2\text{injected}} - CO_{2\text{produced}} - CO_{2\text{surf leakage}} - CO_{2\text{equip leakage}} \quad (\text{eq. 2})$$

$$m_{\text{stored}} = m_{\text{input}} - m_{\text{loss operations}} - m_{\text{loss EOR complex}} \quad (\text{eq. 3})$$

Our preferred methodology differs from the mentioned methodologies in that it follows purchased CO₂ as the key mass accounting parameter -instead of total injected CO₂- in order to avoid the accounting of recycle gas, as it introduces significant complexities which lead to significant mass accounting errors.

One of the issues associated with CO₂ recycle accounting include cumulative errors that arise from the use of a larger number of measuring equipment. Based on EOR operator experience (verbal communication), the sum of CO₂ injection volumes from wellhead flow meters does not conform exactly to the total volume of purchased CO₂. This inconsistency not only comes from equipment errors in CO₂ volume calculations that are intrinsic to the flow meters used in oil and gas operations but also from equipment calibration issues.

Errors are also introduced when converting volume to mass or vice versa. At most locations at the field, Coriolis flowmeters are used which measure mass per unit of time. Recycle gas however is commonly measured with volumetric flowmeters, so knowledge of the fluid density is required for the calculation of an accurate mass flow rate. Because the CO₂ recycling stream has varying density, this relationship is not simple and results in errors in the order of a couple percentage points (verbal communication). In addition to calculation errors, equipment calibration is frequently needed as it is affected by changes in the vibration of the flow lines through which the fluids flow.

Another complexity of recycle mass accounting is introduced in CO₂ EOR operations, such as Cranfield, where the CO₂ is not separated from the produced gases before re-injection. The concentration of produced hydrocarbon gases, most commonly methane, in the recycling stream increases with time as more gases are stripped out of the oil. In this case, gas analysis is required at the time of measuring.

We propose the use of eq. 4 as the basis and preferred method of our reservoir mass accounting methodology, as it results in a more direct and accurate mass accounting protocol.

$$M_{stored} = M_{purchased} - M_{lost\ subsurface} - M_{lost\ surface} \quad (\text{eq. 4})$$

where,

M_{stored} = mass of CO₂, in metric tons, geologically stored in the reservoir through CO₂ EOR during x reporting period. It equals the mass of CO₂ purchased minus subsurface and surface CO₂ losses. If there aren't losses, the mass of CO₂ stored/retained in the subsurface should simply equal the mass of CO₂ purchased.

$M_{purchased}$ = mass of CO₂, in metric tons, delivered to the EOR site from the CO₂ capture facility, measured at the transfer meter during x reporting period, see "M₁" location in figure 2.2. Any CO₂ impurities in the purchased stream need to be subtracted using the CO₂ purity provided by the CO₂ capture facility. A measurement error needs to be included. The meter used could be a mass flow meter or a volumetric flow meter.

$M_{lost\ subsurface}$ = mass of CO₂, in metric tons, that migrated outside of a subsurface volume (see fig. 2.1), which has been previously defined by a monitoring, verification, and accounting (MVA) program. The subsurface volume is the volume within the oil field lease boundary, above the base of deepest EOR producing Formation, and below the base of an *above zone monitoring interval* (AZMI)*. This subsurface volume may include some zones in conventional oil/gas production. If CO₂ should migrate out of the CO₂ injection zone and reach other producing zones, the EOR operator should quantify CO₂ losses via production testing of all actively producing zones. These losses should be reported quarterly.

Similarly, if CO₂ should migrate laterally outside of the EOR lease boundary, this loss should be quantified. An MVA program should provide this information during the operation. Reservoir modeling can be used pre CO₂ injection for the estimation of these potential losses. Lateral migration of CO₂ is considered a loss because CO₂ that flows into a neighboring lease might get produced in adjacent operations. These losses should be reported quarterly.

*AZMI is a laterally continuous, thin, subsurface layer that lies above the CO₂ injection zone. This interval needs to be carefully selected to monitor vertical CO₂ migration as part of an MVA program (see next chapter and Appendix A). AZMIs should satisfy specific petrophysical conditions needed for CO₂ leakage detection assurance.

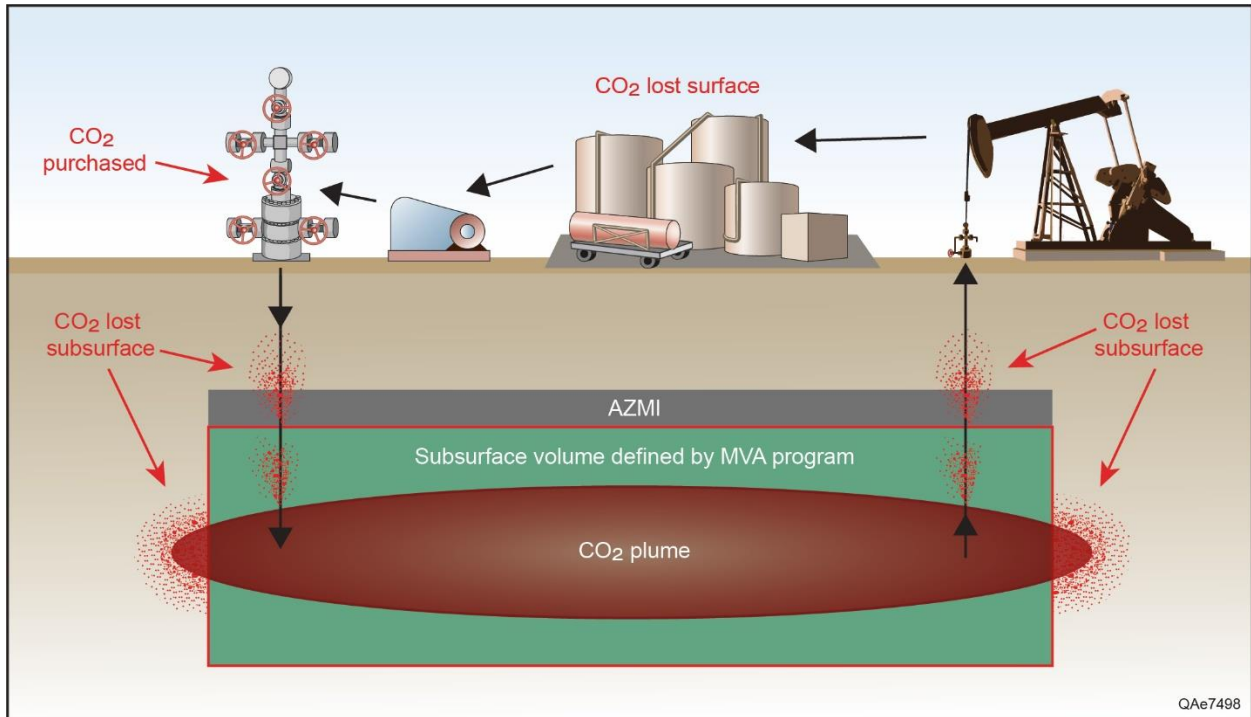


Fig. 2.1. Elements of reservoir mass accounting. *Not to scale.

$M_{lost\ surface}$ = mass of CO₂, in metric tons, lost at the surface. These losses include any potential leakage from surface equipment, which for the purpose of this methodology include (see "M_s" locations in fig. 2.2):

- (1) Blowdown valve releases: a safety release of gas accumulated in equipment, such as the recycle gas compressors. These are low frequency events. We recommend that the number of these events be assessed during the first year of operation in order to determine the significance of the CO₂ volumes released.
- (2) Maintenance releases: any CO₂ release during maintenance operations, including releases to depressurize equipment for safety reasons.
- (3) Troubleshooting releases: any CO₂ release during troubleshooting operations, including repair of faulty electrical systems, equipment leaks, etc.

- (4) Venting: A potentially continuous release at the EOR site. Fugitive emissions should be allocated under this category. A vapor recovery unit (VR) could be used to estimate vented/fugitive emissions.
- (5) Unusual events: any CO₂ release from pipelines and wells, including blowouts, workovers, leaks.
- (6) Flare releases: Another potentially continuous release of CO₂ at the flare. It is a type of venting located after the extra low-pressure equipment. A vapor recovery unit (VR) could be used to estimate vented/fugitive emissions.

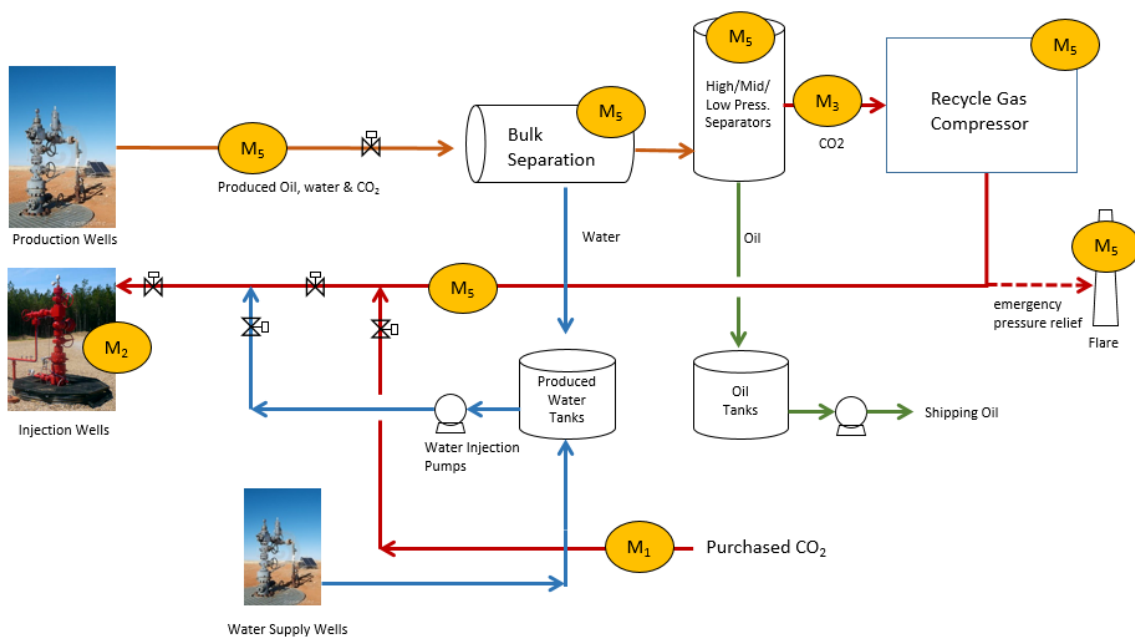


Fig. 2.2. Surface mass accounting monitoring locations. The subscript number in M_# represents the mass accounting element # in Table 2.1.

2.2. Mass Accounting Method with Recycle Gas Accounting

The role of recycling has been widely misunderstood in CCUS. Many reputable accounting methods use a traditional petroleum engineering method that is based on pore volumes swept based on a total mass injected, which is the sum of all the CO₂ injected. As the project matures the total CO₂ injected will include new CO₂ from the capture plant plus recycled CO₂.

As it was explained in the previous section, accounting for recycle CO₂ is a complex task, which results in inaccuracies. However, existing local regulations, contractual structures, financial expectations, etc., might require that the EOR operator report recycle mass accounting. If this is the case, we recommend the use of equation 5.

$$M_{stored} = M_{total\ injected} - M_{recycle} - M_{lost\ subsurface} - M_{lost\ surface} \quad (\text{Eq. 5})$$

Where,

$M_{total\ injected}$ = total mass of CO₂, in metric tons, injected into the reservoir during x reporting period. If the EOR operation is inclusive of a CO₂ separation facility, where the CO₂ is separated from produced reservoir gases, then the cumulative mass of CO₂ injected will be the sum of all the CO₂ injected, which as the project matures will include new CO₂ from the capture plant (purchased CO₂) plus recycled CO₂.

$M_{recycle}$ = Mass of CO₂, in metric tons, produced from the reservoir, separated, processed, compressed, and reinjected into the reservoir during x reporting period. If the CO₂ produced from the reservoir is not separated from other produced hydrocarbon gases, as it is commonly the case in Gulf Coast CO₂ floods, the mass of CO₂ recycled needs to be corrected for the continuous increase in the concentration of impurities in the CO₂ injection stream. This concentration increases with every new injection cycle, as more hydrocarbon gases get produced along with the oil and the CO₂. In this case, the operator needs to establish and implement gas analysis procedures that measure the concentration of these impurities (mostly CH₄) in the recycle stream at the time of reporting.

For increased accuracy, the total injected CO₂ mass should be the sum of the purchased CO₂ mass (measured by a flow meter at the transfer location) plus the CO₂ recycle mass measured by a flow meter located upstream of the recycle gas (RC) compressor/s, see “M₃” location in fig. 2.2. The purchased CO₂ mass also needs to be corrected by the CO₂ concentration at the measuring locations. Therefore, a gas analysis is required at the time of reporting.

We do not recommend the estimation of the total CO₂ injection mass as the sum of the CO₂ injection mass of individual injection wells. However, wellhead flow meters at CO₂ injection wells are still needed for allocation purposes.

There are two reasons for this recommendation, (1) having less measuring points decreases flow meter errors and prevents inconsistencies, and (2) the highest quality meters are the ones located upstream of the recycle gas compressor/s. Note that even these higher quality meters (i.e. V-cone flow meter), which are differential pressure meters, produce errors of +/- 0.5%

according to manufacturers, and errors as large as +/- 1 % according to operators (personal communication).

Table 2.1 lists the all the parameters needed in the use of equations 3 and 4 and their proposed reporting frequency. Table 2.2 compares the parameters required in our proposed mass accounting methodology with the parameters required in Subparts RR and UU of EPA's greenhouse gas reporting program §98.442.

Table 2.1. Mass accounting parameter and frequency of reporting.

#	Proposed Mass Accounting Parameter	Frequency	
1	Mass of CO ₂ purchased	Quarterly	
2	Mass of CO ₂ injected*	Quarterly	
3	Mass of CO ₂ recycled*	Quarterly	
4	Mass of CO ₂ lost in the subsurface	Quarterly	
5	Mass of CO ₂ lost in the surface	Blowdown releases	Assess during 1st year to establish significance
		Maintenance releases	Record date of event
		Troubleshooting releases	Record date of event
		Venting	Quarterly
		Unusual events (pipeline releases, well releases: blowouts, workovers, leaks)	Record date of event
		Flare releases	Quarterly
6	Mass of CO ₂ geologically stored	Quarterly	

* Required if equation 5 is used.

Table 2.2. Comparison of required mass accounting parameters.

GHGs to be reported	Subpart RR	Subpart UU	Our proposed reporting
Mass of CO ₂ received	✓	✓	✓
Mass of CO ₂ injected into the subsurface	✓		✓*
Mass of CO ₂ produced	✓		
Mass of CO ₂ emitted by surface leakage	✓		
Mass of CO ₂ equipment leakage and vented CO ₂ emissions from surface equipment located between the injection flow meter and the injection wellhead	✓		✓
Mass of CO ₂ equipment leakage and vented CO ₂ emissions from surface equipment located between the production flow meter and the production wellhead	✓		✓
Mass of CO ₂ sequestered in subsurface geologic formations	✓		✓
Cumulative mass of CO ₂ reported as sequestered in subsurface geologic formations in all years since the facility became subject to reporting requirements under subpart RR	✓		
Mass of CO ₂ recycle			✓*

* In the case equation 4 is used.

3. Integrated MVA Methodology

Monitoring, Verification and Accounting (MVA) programs at CO₂-EOR sites overlap with EOR operation surveillance practices but expand to include the elements of carbon storage by documenting that injected CO₂ is retained within the reservoir. CO₂-EOR surveillance is described first, followed by additions to document storage.

CO₂-EOR surveillance is primarily designed with the goal of optimizing the performance of CO₂ floods in order to maximize oil production. Flood performance is improved by maximizing the effectiveness of the areal sweep, vertical conformance, and displacement efficiency of the miscible (or near-miscible) process, and includes effective manage of CO₂. Numerical models of CO₂ floods are heavily reliant on the analysis of primary, secondary, and when available tertiary production data, provide a rich source of information on reservoir geometry, rock properties, and fluid characteristics and distribution.

These data are used in pre-injection modeling to provide guidance to investment decision makers, and to inform the design and operation of the CO₂ flood. During the CO₂ flood, EOR monitoring during operations is usually driven by material balance techniques [27], which aim to balance the volumes injected with those produced. Material balance is an effective optimization methodology because fluid flow during EOR is highly managed by the injector-producer patterns. Surveillance of pressure at wellhead as well as intermittent collection of down-hole pressure is also a common technique to assure that the flood is being conducted as planned. The operator may decide to conduct additional surveillance in order to manage the flood and deliver timely intervention to control unpredicted flow behavior. Unpredicted flow behavior results from the inherent complexity of the oil reservoir and typical adjustments, known as “balancing the flood” are required to maximize production.

Examples of additional surveillance are production or injection profiles, cased hole wireline logging for fluid saturation using pulsed neutron or sonic logging, and borehole or surface geophysics. Material balance and other types of surveillance are typically held proprietary. Only in select cases are data shown at professional conferences or published.

EOR operations are required to provide assurance that groundwater quality is being protected, under Class II of the Underground Injection Control Program (UIC). Typically the focus of the regulations is in correct construction and maintenance of wells in terms of mechanical integrity. Monitoring of above reservoir units or near surface is not a typical part of EOR projects.

The objectives of monitoring programs associated with carbon storage projects additionally include evidence that long term CO₂ containment within the target formation will

be accomplished. Areal sweep, vertical conformance, and displacement efficiency continue to be important in carbon storage projects as these performance metrics relate to the effective use of the pore space, which translates into larger ultimate CO₂ storage volumes and smaller project footprints. Assuring long term CO₂ permanence, however, not only requires changing the approaches within the target formation, but also broadens the area of study to include monitoring activities outside of the target formation and adds the requirement of post operational monitoring and modeling activities to document retention.

Storage monitoring starts with the delineation of the planned containment area. Boundaries are defined by the maximum acceptable lateral extent of the CO₂ plume and the size of the associated pressure plume, but can be adapted to focus on the area currently underlain by CO₂, with increases in the area as the area underlain by the CO₂ plume and elevated pressure increase.

Monitoring is closely linked to modeling. Initial work on rock and fluid characterization and dynamic modeling of the CO₂ flood is needed to document that retention of the planned volume is expected. Uncertainties in the characterization phase are used to create multiple probabilistic representations of the impact of these uncertainties on the performance of the flood, and uncertainties with potential to damage the performance of the flood in a material way are highlighted in the risk assessment. Risk assessment schemes are used to structure material uncertainties and stakeholder concerns in an orderly format, and can be loosely to closely integrated with modeling. Risk assessment then drives the definition of the monitoring strategy. Monitoring should be designed to reduce risk and uncertainties leading to material impact/damage and to poor flood performance.

Ideally, monitoring can be used to systematically reduce uncertainties, increase confidence in the injection operation, and lead to closure with high confidence in long term retention. Monitoring can also be designed to provide early warning of a trajectory that would lead to damages, allowing operation to be modified prior to any undesirable occurrence. Other types of risk however may be underlain by uncertainties that cannot be reduced by observations, and monitoring must continue over the lifespan of the project and into the closure period in sentinel mode, observing that no damage has occurred and that no mitigation is needed. Still other monitoring types are needed should an unexpected or damaging condition develop, in order to design mitigation and remediation plans, and assess any penalty incurred, such as loss of credit for storage.

The mechanism by which the implications of monitoring are assessed is via comparison of the observed response with the modeled response. In some situations that comparison can be a simple threshold, however other comparisons will be against output from an analytical model, a geochemical model, a geomechanical model, a multiphysics model, or a geocellular

fluid flow model. The robustness of the history matching capability depends heavily on the quality of the data collected. The targeted data needs can only be met with a carefully designed, carefully deployed, fit-for-purpose monitoring strategy. It is important to answer not only the normal question “is the flood performing as expected?” but also the more difficult inverse question “is it possible that the flood is performing unacceptably?”

3.1 MVA Workflow

Our proposed MVA methodology is based on a formal and reproducible process that links critical elements of risk assessment, modeling, and monitoring of CO₂-EOR systems. The process described here is referred to as “Assessment of Low Probability Material Impacts (ALPMI).”

The ALPMI process quantitatively and reproducibly evaluates how much monitoring is needed to achieve project goals and subsequently provides rigorous criteria on which to base the verification of achievement of those goals. Most geologic storage projects conduct a similar process informally and intuitively, so the proposed ALPMI concept is not new; it is rather a straightforward application of hypothesis-driven scientific inquiry. However, the method provides guidance on how scientific assessment can be used in a regulatory context. The ALPMI process is a more completely developed version of the common recommendation to monitor likely leakage points. It improves on this recommendation by 1) recognizing that in a well-selected, characterized and operated project, all the leakage risks have been reduced to “unlikely”. In addition, ALPMI provides a framework within which monitoring deployment is targeted to detect the material impact.

Material impact in this method is defined by important stakeholders as an event or trend that they would consider unacceptable, such that it would constitute project failure. Project developers generally avoid terms such as “unacceptable” and “failure”; this more neutral terminology is proposed to facilitate needed discussion. Many deviations from the planned and expected evolution of a project may occur, however only a subset would constitute material impacts.

The most commonly discussed material impacts in projects that our group has reviewed are unacceptable leakage and unacceptable induced seismicity. However, the method is also open to other stakeholder concerns. In this formulation it is essential that the stakeholders quantitatively define the material impact in terms of magnitude, location, temporal parameter, and certainty of measurement or prediction. For example, leakage of greater than a specified mass of CO₂ or brine across a specified physical space (e.g. out of a storage complex or from the subsurface into atmosphere and/or aqueous environments) is defined as a material impact.

Conversely, smaller amounts or slower leakage is defined as having negligible impact. For leakage, the temporal parameter set by stakeholders could be for a measurement period, or for a future period to be determined by a model-based prediction. The leakage metric for the mass of CO₂ or brine could be set by (1) a health or environmental concern, (2) a concern for groundwater protection, or (3) an atmospheric impact. For a seismic impact, probabilistic specification of seismic hazards and risks using the correct terminology for this discipline is needed. In all cases, a certainty required for the assessment should be specified.

Most geologic storage projects have been so far conducted in a developing regulatory regime. Meeting regulations that specify exactly what is to be done would not use the ALMPI method. For this discussion, we assume regulations are to some extent non-prescriptive; that is, 1) they require that the project developer justify selection of some monitoring tools and sidelining of others, 2) the details of tool type and instrument design are to be justified, and 3) the frequency and spacing of data collection will be specified.

The following sections provide a review of the general parts of the ALMPI process (fig. 3.1).

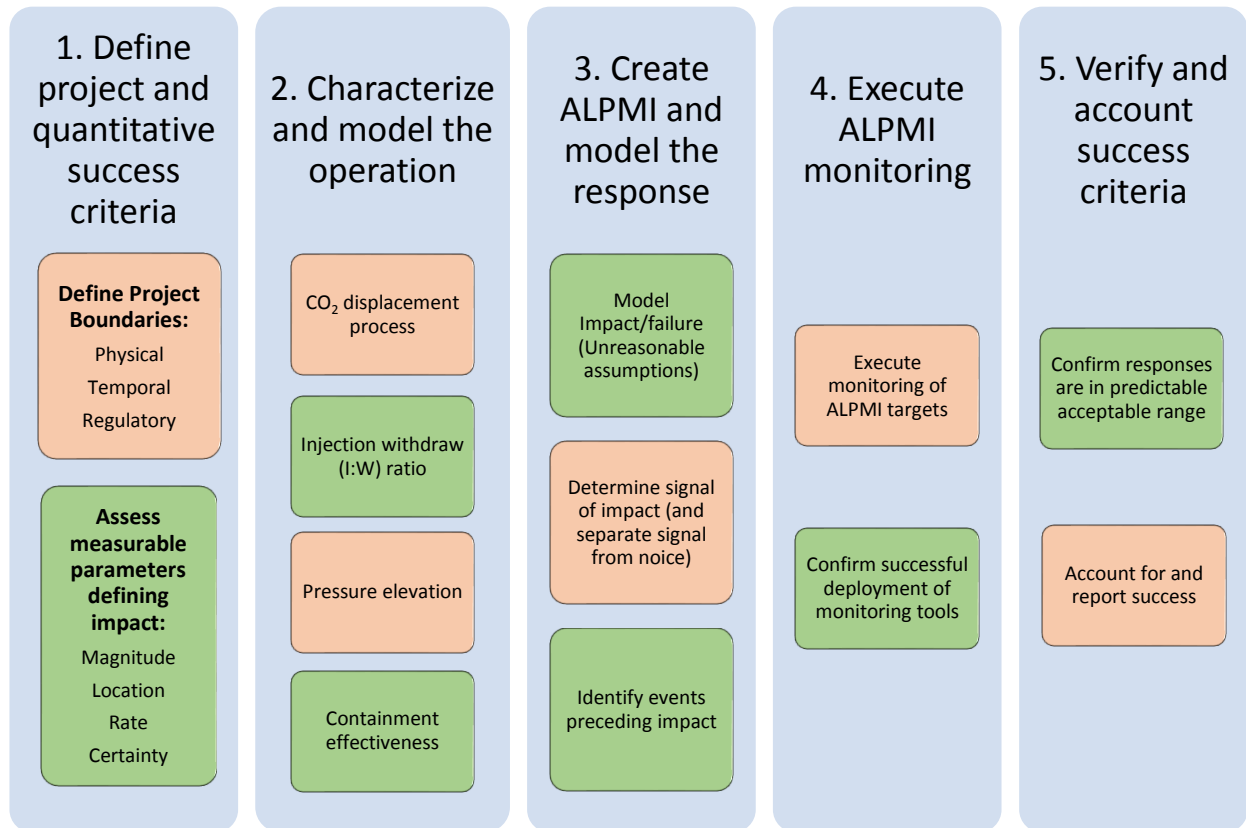


Fig. 3.1 Steps of an integrated MVA methodology

3.1.1 Definition of Project and Quantitative Success Criteria

An integrated monitoring program starts with the project definition, including the identification of the physical (surface and subsurface maps and cross-sections), temporal (history, start and end of mass accounting), and regulatory boundaries. As emphasized in the previous chapter, the mass accounting methodology requires that the boundaries of a project volume be defined in order to properly account for subsurface CO₂ vertical and lateral losses (fig. 2.1).

Physical Boundaries

For most projects, the physical boundaries would be defined by a combination of site specific geologic features and existing regulatory requirements. For example, in the case of CO₂ storage in saline formations, the risks of lateral migration are defined under the Underground Injection Control Program (UIC), in the Class VI program. Two elements are recognized; the area underlain by CO₂ and the area of elevated pressure. Class VI requires that the operator identify any features that might allow migration of fluids to the freshwater, known in UIC program as underground sources of drinking water (USDW).

Conduits for leakage to USDW can be natural (faults) or human made (wells). In the case of water injection under the UIC class I program, injection pressure is the driving force behind leakage. In the case of injection of a buoyant fluid, such as CO₂, gravity forces continue acting even after dissipation of pressure produced by injection. This phenomenon adds a third avenue for leakage, in which CO₂ migrates updip beneath the gently-dipping seal, potentially moving long distances laterally. Long migration paths may allow CO₂ to encounter upward connectivity of transmissive zones.

Understanding the potential for lateral migration requires then a good understanding of the reservoir geology. Geologic storage modeling and field studies demonstrate how reservoir heterogeneity and gravitational segregation interact to control the vertical distribution of CO₂ within the reservoir and limit the lateral expansion of flow paths. Improved understanding of geological controls on lateral flow assists in selecting an adequate monitoring approach as well as in implementing a more effective injection strategy for a projected maximum and ultimate extent of the CO₂ plume.

The following paragraphs summarize field observations that can inform the selection of physical monitoring boundaries:

Juanes and others [28] studied the evolution of an immiscible CO₂ plume footprint in a homogenous aquifer. In this geological setting, the plume is governed by gravitational

buoyance arising from the density difference between CO₂ and brine as well as the capillarity between reservoir fluids and rock that limits the lateral dimensions of the plume. As CO₂ is injected into the reservoir, the less wetting CO₂ displaces the more wetting brine via a drainage-like process. The plume continues to displace gas in an imbibition process as gravity effects produce an upwelling of CO₂, while the backflow of brine at the trailing edge of the plume contributes to the distinctive shape of the plume-shaped gravity tongue [29]. As the plume encounters an impermeable confining system at the top of the reservoir, the CO₂ accumulates beneath the layer and hereafter rapidly spreads laterally.

Spatially heterogeneous rock properties (e.g. permeability and capillary pressure) can create preferential flow paths acting to dictate lateral plume propagation (Bryant and others 2008), and can favor large lateral extents of plumes. Reservoir heterogeneity features can be a product of geological depositional history, post-depositional diagenetic processes, structural deformation or the precipitation of asphaltene and heavy oil “flocs” during CO₂-EOR operations at a site.

All these factors have an influence on fluid flow, which can significantly affect channelization or fingering behavior of CO₂ and the overall character of the plume. A comprehensive assessment of reservoir heterogeneity characteristics will be important to establish an accurate projection of reservoir fluid flow evolution and to ultimately promote a more effective CO₂ flood conformance strategy. Two types of heterogeneity interact: (1) heterogeneity in map view, in which the CO₂ plume grows preferentially in some rock volumes, such as along the channel-axis where high permeabilities are found, leading to an elongated or spider-form plume, and (2) vertical heterogeneity, in which some zones of a rock sequence are more permeable and accept most of the CO₂, leading to a thick reservoir in which only a small part of the sequence accepts CO₂, which then leads to large lateral spread. These factors have long been recognized in EOR floods as reasons for by-pass.

A reservoir depositional history comprised of sedimentation along the lobes and branches of fluvial channels can also comprise a heterogeneity feature that can affect the plume shape evolution and migration characteristics. In such a system, the difference in permeability between channels and the surrounding sediment will dictate the preferred fluid flowpaths as the CO₂ will tend to migrate along higher permeability channel structures (Thatcher and others, 2011).

The preferred migration of CO₂ along fluvial channels has been observed in field studies during subsurface monitoring of CO₂ injection at SECARB’s phase-III Cranfield site, where monitoring large volume injection into a heterogeneous amalgamated fluvial reservoir with wide lateral continuity but containing many internal high permeability zones, as well as likely zones that baffle flow (fig. 3.2), demonstrated some of the impacts of reservoir heterogeneity on

fluid flow. Although this field was developed as an EOR flood, the development of the flood was excellent for making observations. Rather than being developed as a phase of water flood, Cranfield was abandoned and shut in in 1966, so that pressure and fluids could re-equilibrate prior to initiation of the flood in 2008. Additionally, the operator Denbury Onshore LLC, operates the field by direct CO₂ injection (no WAG), and waits for CO₂ arrival and reservoir pressure to build to drive production. Therefore, the early stages of field development are simple injection, like a storage-only site.

Pressure response through the reservoir showed that pressure communication through the water phase was very good, with only a crestal graben fault segmenting the reservoir. However, CO₂ breakthrough showed strong evidence that two-phase flow was dominated by preferential flowpaths over short distances. At one monitoring well location (EGL7), CO₂ arrival was delayed compared to model predictions by almost a year and a half. This corresponds to faster than modeled arrival at others wells. Another transect in which wells were placed close together and monitored repeatedly showed clear interaction of the two-phase fluid flow with reservoir heterogeneity.

At high injection rates, CO₂ flow rates measured by tracers arrived faster at the more distant well at 100 meters downdip of the injector, by-passing the nearer observation well at 60 m. This behavior shows preferred flow through sinuous channel geometry. In addition, cross-well surveys show that the CO₂ accessed two layers of the possible 60 m-thick interval, by-passing much of the permeable reservoir formation [32, 33]. Modeling could not identify a single realization of the channel geometry that matched required all observations; however an array of realizations could bound the observed conditions [20].

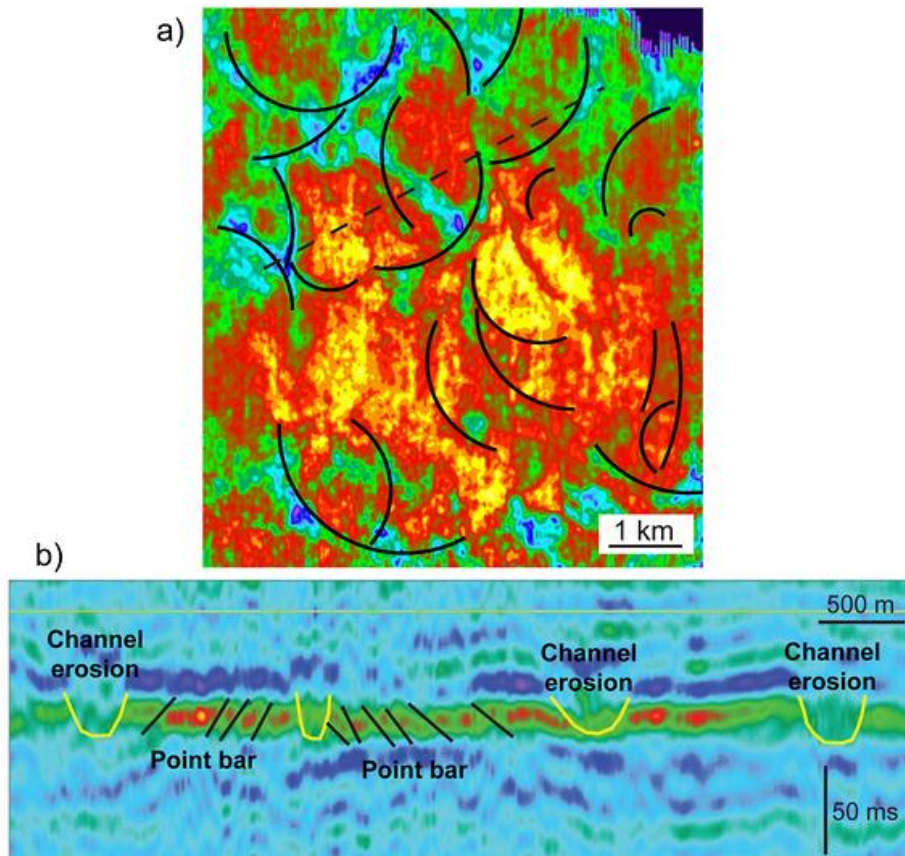


Fig. 3.2. (a) Stratal slice of the 3-D seismic survey, with interpreted channel morphologies in the Lower Tuscaloosa Formation “D-E” interval showing high-amplitude (red) sinuous fluvial channel loops. Dashed line shows location of cross section in Figure. (b) Interpreted channel morphologies in seismic profile, showing general reservoir architecture of a fluvial point-bar plain. Sandstones (red) appear to be discontinuous laterally, suggesting sinuous deposition in 3-D. Location of cross section marked by dashed line in Figure a. [35]

Another important type of heterogeneity is structural heterogeneity. At the In Salah CO₂ storage site, Algeria, the influence of structural deformation on CO₂ migration in the subsurface has been demonstrated in relation to a network of intra-reservoir faults and fractures. The reservoir is extensively fractured along a predominant joint set (NW-SE) in close alignment with the present-day stress field and is also faulted by a series of strike-slip faults (E-W) stemming from basin inversion [34].

The Krechba reservoir at In Salah is comprised of a 20 m thick homogeneous sandstone with fluid flow from three injection sites (Kb501, Kb502 and Kb-503) directed by and entrained at topographic traps along the reservoir-confining system interface (J.P. Deflandre and others, 2011). The network of faults at In Salah act as a barrier to fluid flow and simulations studies suggest they locally restrict the CO₂ around the injection wells and channelize flow toward topographic traps at the reservoir-confining system interface [34].

Quantitative definition of material impacts

An important part of the project definition is to quantitatively define material impacts. Success defined by qualitative terms such as “safe”, “secure”, “effective”, “permanent”, cannot be rigorously demonstrated. Without a quantitative definition of project success, monitoring may be either too extensive, measuring parameters that are not material to success, or under developed, missing developing trends that will lead to project failure.

It is likely that iterative interaction with stakeholders to develop material impact descriptions will benefit projects. For example, an ALMPI process can be used to assess the cost of attaining a measurement to several thresholds. Stakeholders can then make informed decisions about the cost vs. value of different levels of assurance. Quantification will depend on the impact being assessed, however it should be multifaceted. A starting list of parameters defining material impact is:

- Magnitude of the impact (mass, volume, concentration, or vector)
- Location at which material impact is assessed (e.g., a volume outside of a storage compartment, a groundwater resource, or a surface such as base of freshwater, or ground surface. The geographic location of the 3-D volume over which it is to be assessed should also be specified).
- Temporal definition of when and over what duration the impact defined is specified. Leakage mass = leakage rate × time, so the time term is critical to monitoring design. Many monitoring parameters such as pressure, temperature and concentration are sensitive to leakage rate.
- Certainty of measurement or prediction defines the amount of data needed to establish an acceptable result.

3.1.2 Characterization as a Critical MVA Element

Site characterization is an essential element in the success of fit-to-purpose monitoring programs. The nature of site characterization in carbon storage settings is different from characterization for resource production only. In a hydrocarbon field, the fluids are in place and characterization is the tool used to locate them and optimize extraction. Combined with carbon storage, characterization is needed to provide information on how CO₂ can be injected under conditions where it will be retained.

Site characterization protocols for geologic carbon storage at EOR sites predominantly revolve around assessing the injection withdraw ratio (I:W ratio), area of pressure elevation and containment effectiveness of the storage complex, while establishing a framework of field proven and repeatable monitoring methods capable of assessing the suitability of the oil field as a sequestration site. A suitable storage site, including EOR fields, must provide effective

trapping mechanisms, competent bounding seals, hydraulic isolation from overlying aquifers, an appropriate hydrogeological regime, and minimal potential pathways for both vertical and lateral CO₂ migration through faults or fractures [36]. In a carbon storage context, these data are collected and quantified for input to models. In a typical oil reservoir development the collection of some of these data is not common practice, hence procedures and techniques differ.

In contrast to business as usual CO₂-EOR, carbon storage requires the assessment of the entire storage system, which lies within the boundaries previously delineated for the MVA program. Whole-system thinking can add value to the design and optimization of EOR floods. For example, correct assumptions about pressure increase are needed to optimize purchase and recycle volumes, and water curtains.

Whole-system characterization includes the reservoir (production history, boundary conditions, modeling injection), the trap (quality, uncertainty, spill points), and the overburden. Vertical and areal reservoir heterogeneities are major features of interest because they significantly affect both migration direction of the plume and its extent [30], in turn affecting reservoir-capacity estimates through sweep efficiency and injectivity.

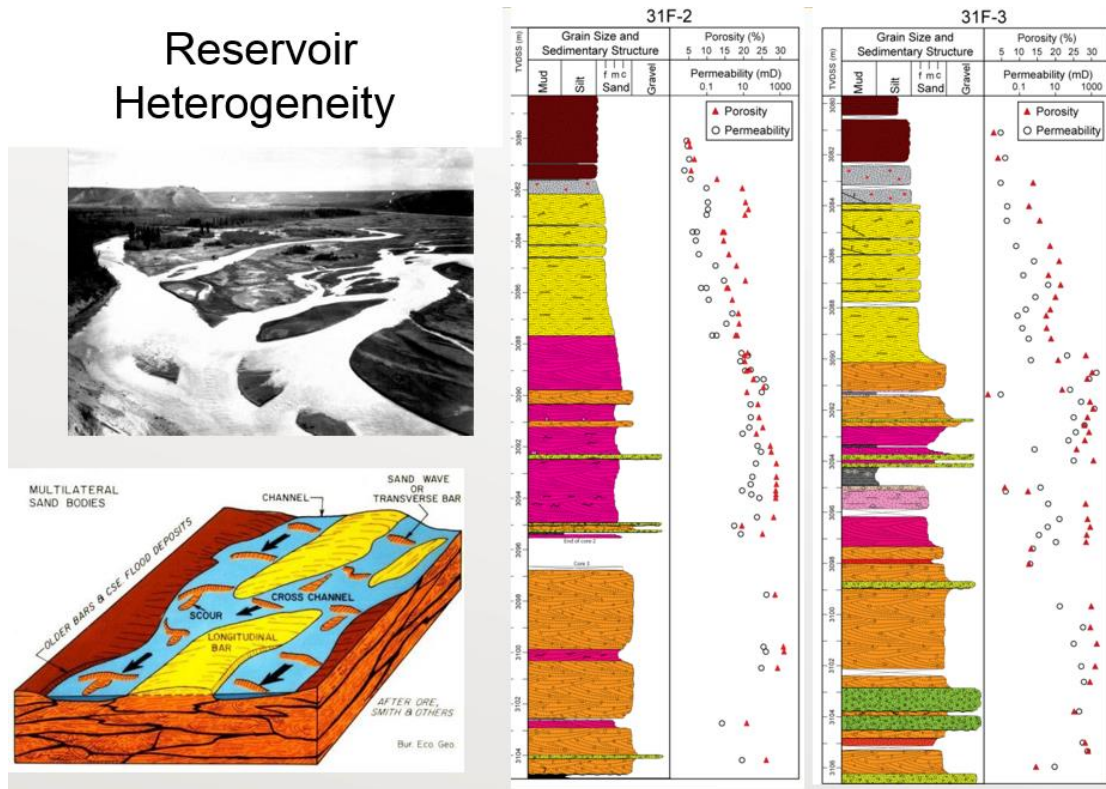


Fig. 3.3. Reservoir heterogeneity of sand bodies (left). Grain size and sedimentary structure cross-section of Crandfield wells 31F-2 and 31F-3, 30 meters apart (right).

One example of the effect of reservoir heterogeneity and the importance of its characterization is in Cranfield, our case study site. At Cranfield, the reservoir architecture is superficially quite simple, with the reservoir composed of a 15-to 20 m thick conglomeritic sandstone interval that can be mapped over most of the field. As shown in Fig. 3.4, only thin discontinuous dark mudstones compartmentalize the basal sandstone. However, observation at both the field scale and interwell scale studied at the detailed area of study (DAS) shows that CO₂ exhibits strong preferential flow. At the DAS (fig. 3.5), CO₂ arrival at the 31-F3 observation well, 112 meters from the injection zone, was shortly after arrival at the 31-F2 observation well, only 68 m away, showing preferential flow.

In addition, as injection rate increased, tracers arrived faster at well 31-F3 well than at 31-F2 [31]. However, this faster arrival was not linear with injection rate, but was retarded relative to what would have been extrapolated based on lower rates. Therefore at higher rates, more of the formation was accessed. This may demonstrate a mechanism by which pattern floods can augment production, in that developing plumes access additional pore volume in response to fluctuations in injection rate and fluid – pore interaction.

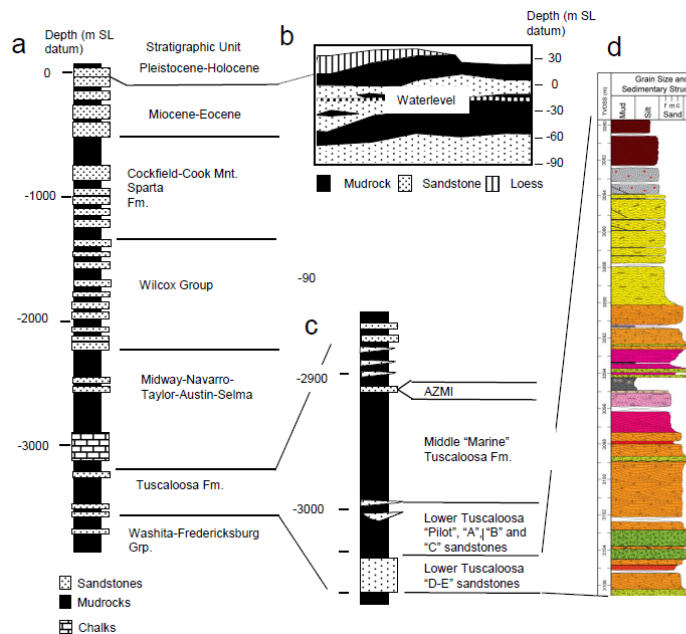


Fig. 3.4. Cranfield stratigraphic section showing injection zone and near-surface. From [33].

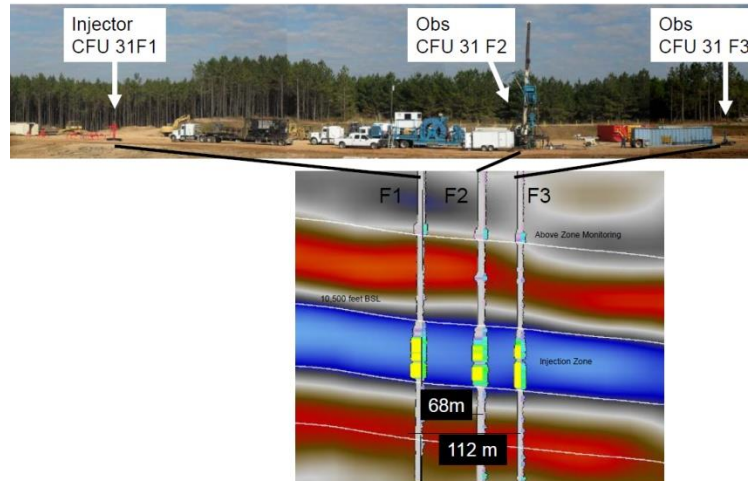


Fig. 3.5. Transect of Detailed Area of Study (DAS). From [33].

Monitoring is closely linked to modeling. Initial work on rock and fluid characterization and dynamic modeling of the CO₂ flood is needed to design the injection plan. Uncertainties in the characterization phase are used to create multiple probabilistic representations of the impact of these uncertainties on the performance of the flood, and uncertainties with potential to damage the performance of the flood in a material way are highlighted in the risk assessment.

In almost all reservoir settings, the complex fluid history introduces significant uncertainty in the distribution of reservoir properties, leading to mismatches between fluid-flow model predictions and observed reservoir response. In EOR, this uncertainty has important commercial consequences, for example in early- and late-responding wells. Early responding wells can lead to faster-than-optimal recycling of CO₂ and are indicators that large parts of the reservoir were not contacted by CO₂. Slow response leads to slow return on investment and may also indicate that CO₂ is not sweeping the reservoir as designed, but migrating to zones not targeted for flooding. Documentation of reservoir and fluid complexities under storage conditions therefore have good potential for improving flood design and response to non-optimum flood response in EOR context.

In an effort to reduce uncertainty, a step-by-step static and dynamic modeling approach was developed for Cranfield [20], where model parameter uncertainties are reduced by field data integration and multiple, sequential stochastic reservoir modeling (fig. 3.6). In this approach, the first step defines absolute permeability and porosity by modeling single phase flow with small-scale data obtained from a well test experiment. A second step addresses boundary conditions and global reservoir connectivity, focusing on the injection induced pressure rise. A third step studies injection and observation wells' bottom hole pressure (BHP). Only models that match field data move on through the steps.

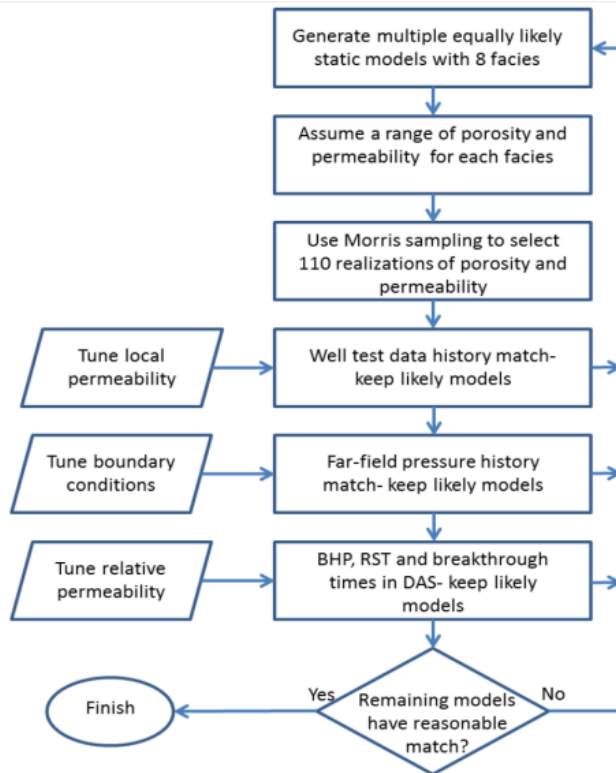


Fig. 3.6. Flowchart used to improve Cranfield reservoir modeling by the integration of field data

The field observations, some not typically taken in EOR projects, used for relative permeability end points and local heterogeneity validation include injection zone pressure from pressure gauges installed in injection and observation wells, CO₂ saturation evolution from time-lapse reservoir saturation tool, or RST (a cased-hole pulsed neutron well logging tool later explained), and breakthrough time from U-tube gaseous-phase compositional samples. Time-lapse RST, proved useful in reducing the range of relative permeability model parameters, such as end-point saturations, which directly affect plume size and long-term estimates of residual trapped gas saturations. Assigning different relative permeabilities and capillary-entry pressures to sand and shale facies helped in correctly addressing sweep efficiencies in the Lower Tuscaloosa formation.

At Cranfield, detailed cross-well surveillance at less than pattern scale showed how geologic heterogeneity led to preferential flow. At the inter-well scale, the CO₂ could only access a fraction of the 20-m-thick sandstone. Results from imaging tools and tracer tests show that the flowpaths evolved over time, with flow rate being influential. Boundary condition assumptions are crucial for pressure response matching. Caution is advised, however, as under multi-phase flow conditions several realizations can be matched to the reservoir pressure

response [33]. Results from these tools could be used to improve understanding of the subsurface, benefiting the management of a CO₂ flood in the EOR context.

3.1.3 ALPMI Creation and Response Modeling

The rare occurrences of material impacts from geologic storage and the limited quantitative descriptions of analog geologic failure events limit our knowledge on the conditions that lead to them and the type and magnitude of the signals resulting from them. In instances like this, a negative outcome needs to be modeled, or physically created in an analog site, in order to obtain a response and determine its resulting signals (pressure, temperature, geochemistry, seismic signals, etc.). Negative outcomes are commonly identified as events that lead to the contamination of underground sources of drinking water or the atmosphere, such as CO₂ leakage through faults and/or wells, geomechanical failure of reservoir/caprock, induced seismicity, etc.

An example of a physically created negative outcome is a controlled CO₂ release, such as the ZERT site in Montana, USA, [38] and the Ginninderra site in Canberra, Australia [39]. In controlled releases, a response from a created CO₂ leakage is evaluated under controlled and safe conditions.

A clear advantage of negative outcome creation is the improved information relevant to material impact prevention and remediation. A modeling exercise that lays out the elements that lead to a material impact can improve the understanding of the conditions or events that precede an undesirable outcome. This advanced knowledge can be crucial in decision making regarding the design of an operation or the need for changes in an operating project.

3.1.4 ALPMI Monitoring Execution

The execution of the ALPMI monitoring plan includes the selection of monitoring tools that will detect the material impact or trend toward material impact. Please refer to Appendix A for a review and analysis of existing monitoring methods and tools. ALPMI should, in general, avoid the need for rerunning complex models with updated data. However, a trend or exceedance of a threshold may not uniquely indicate project failure. It could be a result of an error in characterization or model design, so that additional modeling during project execution should be budgeted as a contingency. Attribution of signal (to the material impact or to an unrelated event), quantification, mitigation and remediation are dealt with outside of the ALPMI method.

Because the material impacts are already determined to be low probability, the expected outcome is a non-detection. Design such that a none-detection leads to a conclusion is essential. For example, the reservoir heterogeneity is less than the threshold that leads to migration of CO₂ out of the storage volume. In situ test of the monitoring network capacity can be valuable and therefore recommended. For example, detection of shot points shows that a seismic network could detect a certain threshold of seismic event even if microseismicity is created during injection.

3.1.5 Verification and Accounting of Success Criteria

The ALMPI method is designed to facilitate straightforward reporting of the high-likelihood of success. In ALPMI, success means that the risk is eliminated by non-detection of material impact during monitoring. Detection of responses in the predicted and acceptable range are used to systematically eliminate risk of material impacts. Only via such a hypothesis-driven method can the expected finding be rigorously and simply presented. However, if project success required modification, mitigation, remediation, quantification of leakage, more complex reporting outside of the ALMPI method would be needed.

4. NCNO Methodology

Our developed methodology is based on the coupling of two models: (1) a subsurface model that predicts reservoir responses in the form of incremental oil recovery, CO₂ storage mass, and CO₂ utilization rates; and (2) a dynamic lifecycle analysis (*d-LCA*) based surface model that estimates instant greenhouse gas emissions associated with operating a defined CCUS system.

The subsurface model needs to be designed to capture the time evolution of CO₂ utilization ratios. A reliable subsurface model increases confidence in LCA results as CO₂ flood performance affects significantly the carbon balance of the CCUS system. Results from the model are then used to assess how CO₂ utilization rates affect energy intensive system components.

Because CO₂ flood efficiency varies depending on the chosen EOR field development plan, we conducted a scenario analysis that captures the range of reservoir responses to different CO₂ injection strategies. Reservoir responses are given in terms of CO₂ utilization rates (an operational performance indicator) and carbon storage (an environmental performance indicator). Utilization rates refer to the volume of CO₂ (in thousand standard cubic feet (Mscf)) that needs to be injected into the reservoir in order to produce one barrel of oil.

The surface model is designed to estimate both the indirect carbon emissions associated with the electricity required to operate a CCUS system with defined boundaries and the direct carbon emissions within the boundary. An important distinction between emission types is that direct emissions are those emitted directly into the atmosphere within the system boundary, whereas indirect emissions are those emitted into the atmosphere outside the boundary from the energy consumption within the boundary.

4.1 Subsurface Modeling for EOR Operational Performance

A significant time was devoted to the subsurface modeling part of the study. As Cooney and others state in [13], the efficiency of the EOR process –which they describe as barrels of produced crude per ton of CO₂ sequestered- is “key in determining the life cycle results for the EOR supply chain.”

Our scenario evaluation was performed on an ongoing CO₂-EOR operation in Cranfield field, a 3,000 m. deep clastic reservoir in southwestern Mississippi, USA. The CO₂ injection zone in the Lower Tuscaloosa Formation is a four-way anticline with a diameter of 6.4 km (4 mi). The domal structure was created by a deep-seated inactive salt dome. In the Tuscaloosa interval, the

formation dip angle ranges from 1° to 3° , with a structural closure of ~ 75 m and an average thickness of ~ 25 m. A NW-SE-trending crestal graben drops the apex of the dome, and one of the bounding normal faults offsets the Tuscaloosa reservoir in the area of study with a throw equal to the interval thickness. Differing water oil contacts (WOC) on either side of the fault at the time of field discovery, non-propagation of pressure during CO_2 injection, and well-breakout observations suggest that the normal fault is non-transmissive in the horizontal direction, and that that the current maximum horizontal stress tends to close the fault.

We performed compositional numerical reservoir simulation on a Cranfield pre-existing static model described in detail by Hosseini et al. [20]. Compositional numerical simulation was preferred over a black oil model to more accurately simulate the solvent CO_2 -EOR process, where CO_2 is expected to dissolve into the oil phase to enhance oil production. Because compositional numerical simulation requires a large computational load, we used the north-eastern section of the static model (Figure 4.1), which is separated from the rest of the reservoir by the non-transmissive fault. We assumed that the modeled section (sector model), composed of 82,559 grid blocks, has minimum interaction with the producing zones in the south and west sides of Cranfield.

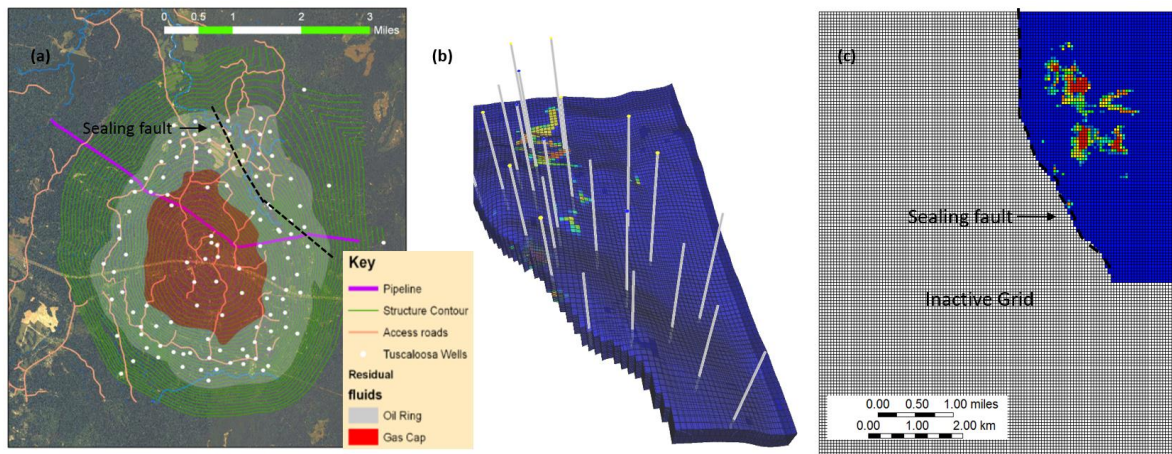


Figure 4.1. (a) Structural contour map, (b) sector model showing structure and location of injection and production wells, (c) active and inactive grids used for reservoir simulation. Sealing fault is a closed boundary.

We then used a commercial package (CMG-GEM) to run the numerical simulations. GEM is an advanced general equation-of-state compositional simulator, which includes equation of state, CO_2 miscible flood, CO_2 /brine interactions, and complex phase behavior. The simulator is set up to model three fluid phases including water, oil, and gas. Compositional models inherit a heavy computational load because of the high number of chemical components in the system.

The Peng Robinson equation of state was used in this study to model reservoir fluid properties. Our fluid model is composed of 7 different components including CO₂. The thermodynamic model and component properties were tuned based on Cranfield fluid data published by [37]. The fluid data used for this purpose included bubble point pressure, solution gas-oil-ratio, formation volume factor, oil and gas viscosities. One important factor during modeling of CO₂-EOR and storage processes in reservoirs with aquifers is to correctly generate the CO₂/brine solubility data. CO₂/water solubility in the current model is modeled using Henry's Law. Henry's Law assumes a linear relationship between CO₂ partial pressure/fugacity and solubility in water.

To calibrate our model, we history matched oil and gas production from 1944 to 1964, as well as a shut-in period from 1964 to 2008 and the first four years of the current EOR tertiary stage.

The sector model includes 11 injection wells and 10 production wells (Figure 4.1b). Injection rates were constrained based on known injection volumes available from the observed CO₂ injection period at each well location. A period of 25 years of injection was simulated for each CO₂ injection scenarios. A detailed description of the numerical reservoir simulation can be found in Hosseini et al. [21]. There is a difference, however, in the simulation results presented in this report as the CO₂-brine relative permeability curves used were not from public data as in Hosseini's article, but obtained from laboratory experiments on a Cranfield core, funded by this project. The simulation results, as well as the NCNO results, from the simulations run with public relative permeability data are included in Appendix E.

Water-alternating-gas (WAG) has been the EOR development strategy of choice in the Permian Basin, where the history of CO₂-EOR is richer, for several technical and economic reasons. However, continued CO₂ injection (CGI), as opposed to WAG, was initially selected as the injection strategy to develop the much more porous and permeable clastic depositional systems of the onshore Gulf Coast. The use of CGI in this younger EOR region, resulted in CO₂ injection volumes significantly larger (up to 6 times larger) than those of the Permian Basin. In the case of Cranfield, a Gulf Coast oil field, the operator selected CGI because it also operated a nearby natural CO₂ accumulation, which made CO₂ more readily available to the EOR site. Such decisions illustrate how the selection of field development strategies are site specific. Even though the CO₂ used in Cranfield is from a natural source, we assume the use of anthropogenic CO₂ in all our scenarios.

Based on the history of CO₂-EOR in the USA, we selected the four following CO₂ injection scenarios:

1. Continuous gas injection (CGI), where CO₂ is injected continuously into the oil bearing formation (this is the field development strategy at Cranfield);

2. WAG, where CO₂ and brine are injected in an alternating fashion to improve flood conformance and economics. We selected a WAG ratio of 1:1, 6 months of CO₂ injection alternated with 6 months of brine injection;
3. Water curtain injection (WCI), a continuous gas injection with the addition of peripheral water injection (commonly along the oil-water contact) in order to create a pressure barrier/curtain that contains the CO₂ within the desired rock volume; and,
4. Hybrid WAG + WCI.

4.2 Surface Modeling for CCUS Environmental Performance

Our environmental performance parameter is associated with net volumes of CO₂ emission reduction, which is the difference (or balance) between the CO₂ permanently stored in the oil reservoir and the greenhouse gas (GHG) penalty imposed by direct and indirect CO₂ emissions in relation to a pre-established CCUS system boundary. In our lifecycle approach, the environmental impact is strictly related to these direct and indirect CO₂ emissions. This impact is countered by the geologic CO₂ storage that occurs through the process of EOR, which represents the only means for CO₂ emission reduction.

Estimates of energy consumption are required for the carbon emissions accounting. This accounting is performed with a novel, dynamic LCA (d-LCA) approach with the goal of estimating the carbon balance evolution of the CCUS system as it operates. In our study, we refer to the term *carbon balance* as the difference between GHG emissions and CO₂ storage. A negative carbon balance indicates that more CO₂ is sequestered than it is emitted. We consider the CO₂-EOR operation to produce net carbon negative oil (NCNO) when, and for as long as, the CCUS system operates under a negative carbon balance.

Unlike the LCA studies in Table 1.1, which estimate a single value of carbon emissions (usually at the end of the studied projects) our d-LCA produces monthly estimates of carbon emissions that are coupled with the subsurface model. This is an important contribution to LCA studies on CO₂-EOR, as the production rate of the EOR product (oil) is highly variable throughout the operation, and so are the CO₂ utilization rates.

In LCA studies, the definition of boundaries is very important and is part of the goals and scope definition. We estimated the energy consumption and associated direct and indirect carbon emissions in relation to the three most common boundaries used in CCUS systems: (1) gate to gate, (2) gate to grave, and (3) cradle to grave. Figure 4.2 shows the general components of CCUS systems and the lifecycle boundaries most commonly used, which we also use in this study.

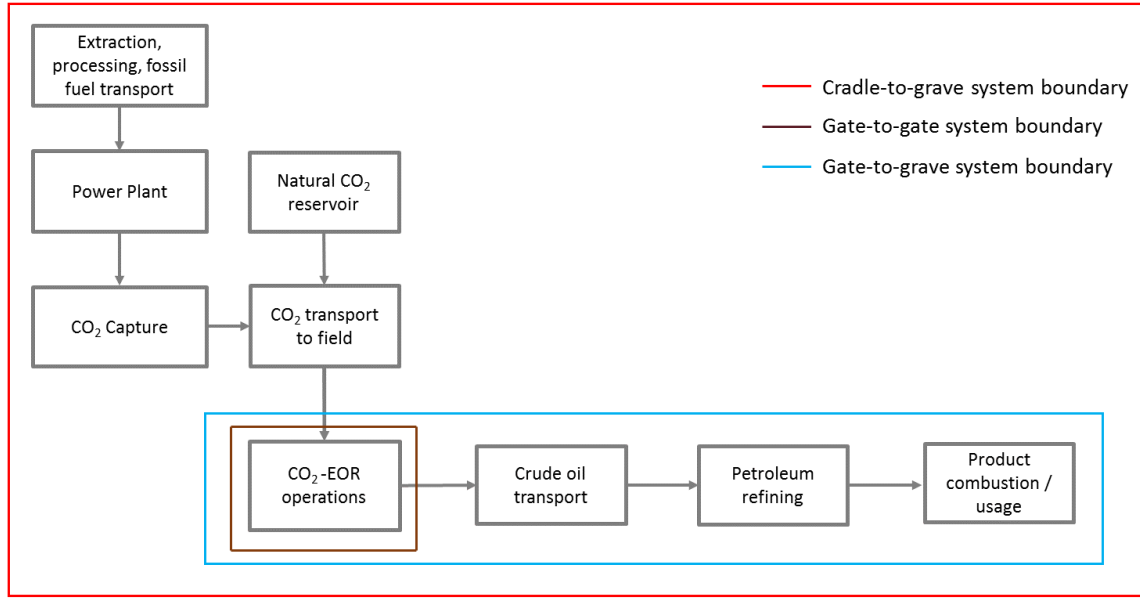


Figure 4.2. CCUS system components and carbon LCA boundaries.

4.2.1 Gate-to-Gate Carbon Emission Estimates

In a gate to gate system boundary, purchased CO₂ (regardless of the source) enters the gate and crude oil exits through the other gate. For this boundary the functional unit is mass of CO_{2e} emitted per barrel of produced oil. As CO₂-EOR operations vary from site to site, we developed a methodology for the LCA inventory of direct and indirect CO_{2e} emissions at the EOR site. The methodology follows a decision making diagram (Figure 4.3) that covers most CO₂-EOR configurations and indicates the type and location of emission estimations.

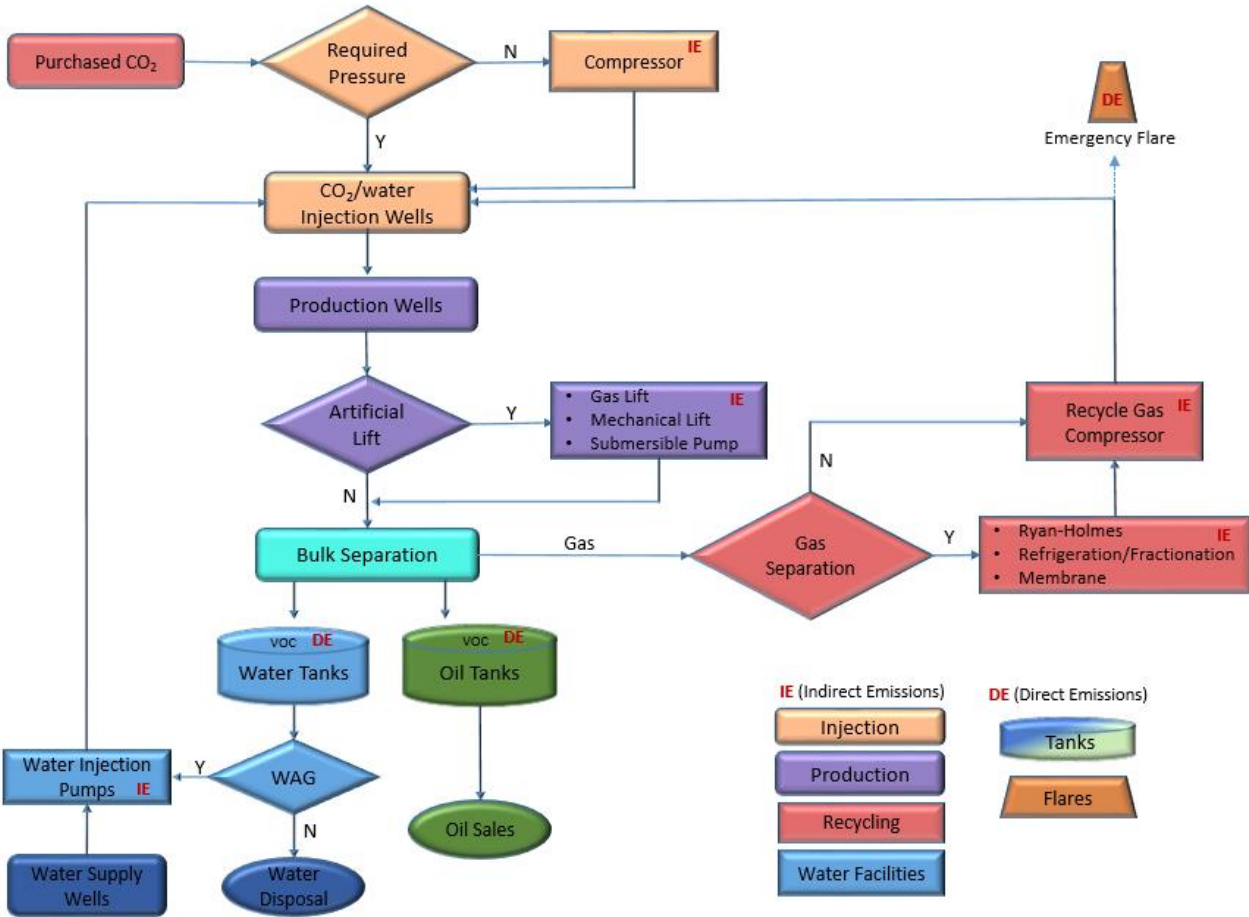


Figure 4.3. Methodology for direct and indirect CO₂ emissions inventory at the EOR site.

Gas compression for injection is a significant energy intensive component. At Cranfield, purchased CO₂ enters the field at a pressure of 12,411 kPa. Produced CO₂, which is recycled back into the oil reservoir, circulates through a Central Facility at an average pressure of 4,826 kPa. Purchased and recycle CO₂ are compressed to the required injection pressure of 20,684 kPa. We used Equation (1) to estimate the horsepower requirements to compress the recycled CO₂ to 20,684 kPa [12].

$$HP = 22 \times R_s \times S \times Q \times F \quad (1)$$

where,

R_s = compression ratio per stage

S = number of stages

Q = gas flow rate, MMscf/D

F = correction factor

The number of compression stages (S) depends on the compression ratio per stage, the theoretical discharge temperature and the operating regime (100% assumed). In order to avoid excessive material degradation or excessive thermal expansion, the compressor's discharge temperature needs to remain below 149 °C (759 °R). So we assumed $T < 149$ °C (137 °C for the recycling gas and 117 °C for purchased CO₂). The integer value S (2 for the recycling gas compressor and 1 for purchased CO₂ compressor) was estimated through an iterative process between Equations (2) and (3), satisfying the temperature condition.

$$R_s = (P_d/P_s)^{1/S} \quad (2)$$

where,

P_d = discharge pressure (psi)

P_s = suction pressure (psi)

$$T_d = T_s * R_s^{(k-1)/k} \quad (3)$$

where,

T_d = discharge temperature (°R)

T_s = suction temperature (°R)

k = specific heat ratio

We assumed a conservative estimate for $k = 1.33$ (the heat ratio of carbon dioxide), which is around 4% higher than the result of the produced gas samples from Cranfield. All these parameters have high impact on the total required compression horsepower. Hydraulic horsepower was converted to kilowatt (1 HP = 0.7457 kW). We assumed 24 hours of daily operations.

Analyses mimicked Cranfield operations to the extent possible. Production wells are gas lifted with CO₂ during the first 3 months of activity to kick off production. After 3 months, production is sustained by the energy of the reservoir, which is maintained by the CO₂ injection. Gas and liquids are separated at the surface and produced gases (CO₂ plus reservoir gases) are recycled back into the reservoir, without separation. Unlike in Cranfield, re-injecting produced, contaminated CO₂ into the reservoir is not common practice in the Permian Basin, where CO₂ is separated from the reservoir gases (methane, propane, others) to purify the CO₂ injection stream. Contaminants in the CO₂ can increase the minimum miscibility pressure, which reduces the effectiveness of the miscible displacement. However, gas separation facilities are expensive, and the gas separation process is energy intensive. Nuñez-López et al. [22] estimated the GHG

intensity of different energy-demanding, CO₂-EOR site components, including injection and production, bulk fluid separation, compression, and gas processing, and concluded that compression and gas separation were the most energy consuming processes within a gate-to-gate system.

Because the carbon balance of the operation changes depending on the decision to separate produced gases before re-injection, and on the type of gas separation technology selected, our energy consumption model includes the variability of these operational choices. Gas separation technologies include: (1) fractionation, (2) refrigeration, (3) Ryan-Holmes, and (4) membrane. Results where production gases are re-injected (no separation) are also included. The utility requirements (electricity and natural gas) for the four gas separation processes considered are in Table 4.2.

Table 4.2. Utility requirement for gas separation processes. Modified from [11].

Gas Processing Energy Requirements	Fractionation	Refrigeration	Ryan-Holmes	Membrane
Electricity (KWh/Tonnes gas)	13.8	13.8	62.8	26.1
Natural Gas (kg natural gas/kg EOR gas)	1.91×10^{-6}	1.45×10^{-6}	n/a	6.64×10^{-2}

The horsepower requirement for the energy intensive components of the gate-to-gate system (compression of injection gasses, gas lifting of production wells, surface fluid handling, and separation of produced gases) was estimated. As electricity networks have a different mix of electricity generation (coal, natural gas, solar, wind, etc.), the indirect emissions associated with the horsepower requirement estimates were calculated based on the local electricity grid (SRMV), which emits 468 kgCO_{2e}/MWh and experiences 4.97% grid losses [23], where CO_{2e} is carbon dioxide equivalent, a standard term used for measuring carbon footprint. It allows the inclusion of other GHG emissions in a common unit, based on their relative global warming potential (GWP) GWP factors (CH₄: 25 and N₂O: 298, 100-year GWP).

4.2.2 Gate-to-Grave Carbon Emission Estimates

In a CO₂-EOR gate-to-grave system, the gate is again the point where CO₂ enters the oil field, regardless of the source, and the grave represents the combustion of the refined product, which in our study is a national average mix of combustible products (gasoline, diesel, kerosene, etc.) plus non-combustible products such as paraffin. The components inside the gate-to-grave boundary are (1) the CO₂-EOR operation, (2) the transportation of crude oil from the

field to the refinery, (3) the crude oil refinery, and (4) the combustion of the mix of combustible products.

Because we assume the end product to be an average mix of combustible products contained in a barrel of crude oil, this boundary still allows for the use of a single functional unit which, as in the gate-to-gate boundary is mass of CO_{2e} emitted per barrel of produced oil. We assumed a maximum pipeline transportation distance of 300 miles from the Cranfield field to the closest concentration of refineries in the USA. This cluster refines about 75% of the total crude oil processed in the USA Gulf Coast area. Based on Cooney et al. [13], we assumed that USA crude oil is transported from the field to the refineries with an energy intensity of 260 BTU/tonne-mile or 189 J/kg-Km. We also assumed that this energy is 100% supplied by the local grid (SRMV). We estimated the refinery emission factor using a national average [24], determined from 2008 to 2014, of the fuel/energy consumption required to refine the produced crude oil, its energy content [11] and the emission factor per fuel used [23]. Emissions from electricity consumption include a 9% average penalty for national transmission losses. Finally, we estimated the end product combustion emission factor [10], assuming that 93% of the crude refined in the USA will produce CO₂ emissions at the combustion end process. According to Jaramillo [10], the average heat content of crude oil refined at USA refineries is 6120 MJ/STB, with an average carbon content of 19.17 Tg C/EJ.

4.2.3 Cradle-to-Grave Carbon Emission Estimates

In a cradle-to-grave system boundary the CCUS system expands to include GHG emissions upstream of the CO₂-EOR site. These emissions are added to gate-to-grave emissions and account for extracting, processing, and transporting the primary energy that is combusted at the power plant. In this study we assess the impact of two different anthropogenic sources of CO₂: (1) a pulverized coal-fired power plant (PC) and, (2) a natural gas combined cycle (NGCC) power plant; both with enough capacity to supply all the new CO₂ required at the CO₂-EOR site. Both plants use amine absorbers to capture the CO₂.

A remarkable complexity of CCUS cradle-to-grave systems is that upstream of the CO₂-EOR site the product is electricity, not oil, although some studies refer to electricity as a system's co-product. To solve the problem of the functional unit, we estimated the energy (kWh) generation required to supply the CO₂ needed at the EOR site. The GHG emissions associated with this energy generation (KgCO_{2e}/kWh) are then related to the barrels of crude oil produced.

The emission factors for each capture facility are in Table 4.3. As each capture facility has different emission factors, each facility is assumed to generate a different amount of electricity, each enough to supply the required mass of CO₂ for EOR. The NGCC plant, a much cleaner plant, will have to produce more than twice the energy to supply the same mass of CO₂ as a PC

plant.

An aspect worth noting is that emission factors for the elements upstream of the plants (0.131 and 0.191 KgCO₂/kWh for coal and natural gas, respectively) compensate the differences between the net emission factors of each plant (0.1107 and 0.0426 CO₂eKg /kWh for PC and NGCC respectively) resulting in a very similar total emission factor for the upstream around 0.2 CO₂eKg/kWh. So, the impact of the emissions upstream of the EOR site depends on the amount of electricity required to produce the CO₂ supply needed for EOR.

Table 4.3. Upstream emissions accounting

ELEMENTS UPSTREAM OF THE PLANT (*)		
	Coal Mining and Transport	NG production, Transport and Process
CO ₂ emission factor (Kg/kWh)	0.131	0.191

PLANT COMBUSTION (**) CO ₂ Capture: 90%		
	Supercritical Pulverized Coal Power Plant	Natural Gas Combined Cycle
Gross Power Output (MWh _e)	663	511
Net Power Output (MWh _e)	550	474
Net Plant HHV Heat Rate BTU/KWh	12,002	7,968
Gross CO ₂ e emissions (Kg/kWh)	0.8020	0.3647
Net CO ₂ e emissions (Kg/kWh)	0.1107	0.0426
Auxiliary power requirement (MW)	113	37.4
Net Plant efficiency (%)	28.4	42.8
CO ₂ e displacement factor (Kg/KWh)	0.611	0.611

* Modified from [25]. ** Modified from [26]

4.2.4 Cradle-to-Grave Electricity Displacement

In this scenario carbon-intensive electricity is being displaced with captured electricity, and the power produced from that system receives a credit for this displacement.

Emission displacement is determined by multiplying the emission factor of the electricity source to be displaced by the electricity required to produce the required CO₂ supply. The electricity displaced (and associated emissions) are assumed to be from the mix of the USA Electric Grid (2013) with an emission factor of 0.611 KgCO₂e/Kwh. The mass of GHG displaced

is added to the total emissions accounting as a credit.

In this study we will first show the impact of expanding the system to include upstream emissions (Cradle-to-Gate) without accounting for the GHG credits. Subsequently we will show the full impact of electricity displacement and how it affects the carbon balance curves of all studied scenarios. It is assumed that with an 85% capacity factor (full capacity operation) each option can fully satisfy all the CO₂ required by the EOR site.

5. NCNO Results and Discussion

5.1 CO₂-EOR Reservoir Response

One of the goals of our scenario analysis was to capture a range of reservoir responses to different CO₂ injection strategies. Results from our compositional numerical reservoir simulation for cumulative oil production and for geologic carbon storage in the northeastern quadrant of Cranfield are shown in Figure 5.1. Both parameters are plotted for our four CO₂ injection scenarios as a function of the volumes of CO₂ injected into the reservoir (hydrocarbon pore volumes). The end points of all curves represent the closure of the 25 year injection period.

Figure 5.1a shows how injection volumes are largest in the continuous gas injection scenarios (CGI and WCI). However, WAG produces more oil than WCI and produces 90% of the oil produced by CGI with only 58% of the injected CO₂. Figure 5.1b shows how CO₂ storage reaches a maximum and then decreases with time. In all carbon storage curves the maximum point is reached when CO₂ recycle exceeds the CO₂ injection rate. Excess recycled gas is then assumed to be sent to adjacent CO₂-EOR floods. As the excess CO₂ exits the boundaries of the system, it is subtracted from the storage volumes.

In CGI and WCI, CO₂ recycle volumes beyond the maximum storage point satisfy the CO₂ injection requirements, so CO₂ demand from the capture facility stops at that point for that specific flooding area (the northeastern quadrant of the field). In both WAG scenarios, the cyclic nature of the flood demands CO₂ from the capture facility throughout the operation, as gas production exits the boundaries of the flood during water injection and the lost CO₂ needs to be replaced for the next cycle of CO₂ injection.

As expected, CO₂ injection strategies that produce the most oil also store the most CO₂ (CGI and WAG), which confirms the argument that increased oil production also increases ultimate CO₂ storage volume.

A better indicator of the efficiency of the CO₂-EOR flood, commercially speaking, are the CO₂ utilization rates (Figure 5.2), which refer to the volume of CO₂ that needs to be injected to produce one barrel of oil. Net utilization rates (Figure 5.2a) only consider purchased CO₂, whereas gross utilization rates (Figure 5.2b) include total CO₂ injection (purchased plus recycled CO₂).

As expected, the lowest gross utilization rates are attributed to the two WAG scenarios, because CO₂ is not injected continuously. An important observation is the variability in both net and gross utilization rates as the EOR operation progresses, particularly during the first six - eight years of operation. Net utilization rates are lowest in our two water curtain scenarios.

Even though cumulative oil production is lowest in these two cases, the low net utilization shows the efficiency of the water curtain in assisting oil recovery with less purchased CO₂. Most carbon lifecycle analyses use an average for EOR/storage efficiency in their calculations, but as demonstrated here, CO₂ utilization rates vary significantly throughout the life of the project. Such simplifications affect carbon balance results. Previous NETL LCA studies such as Cooney et al. [10], acknowledge this as a potential improvement, which we have contributed to in this study.

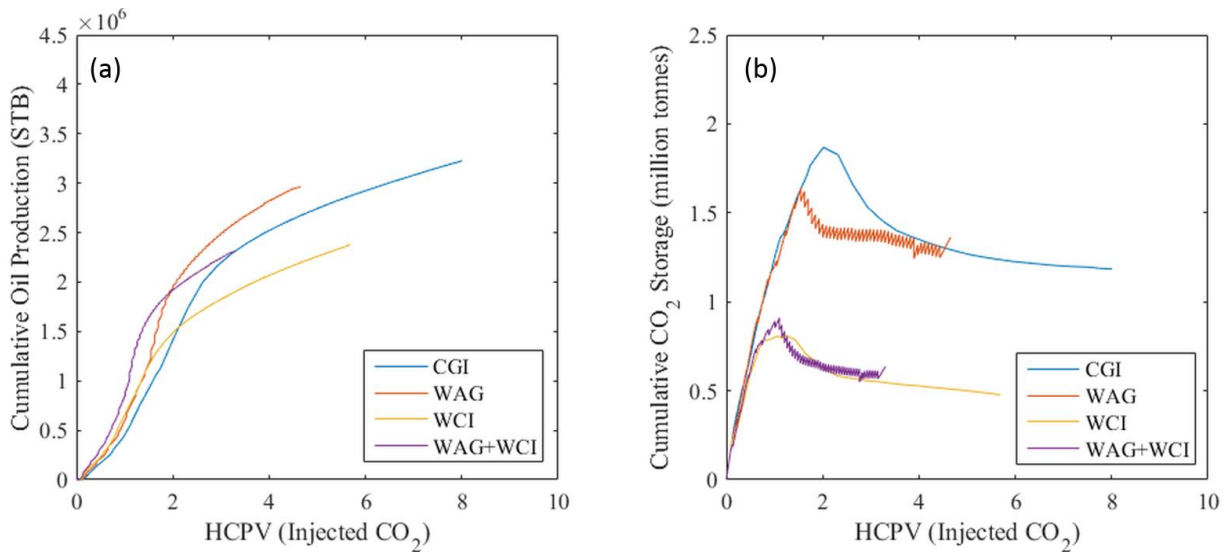


Figure 5.1. (a) Cumulative oil production as a function of CO₂ volumes injected. (b) CO₂ storage as a function of CO₂ volumes injected. HCPV = hydrocarbon pore volume.

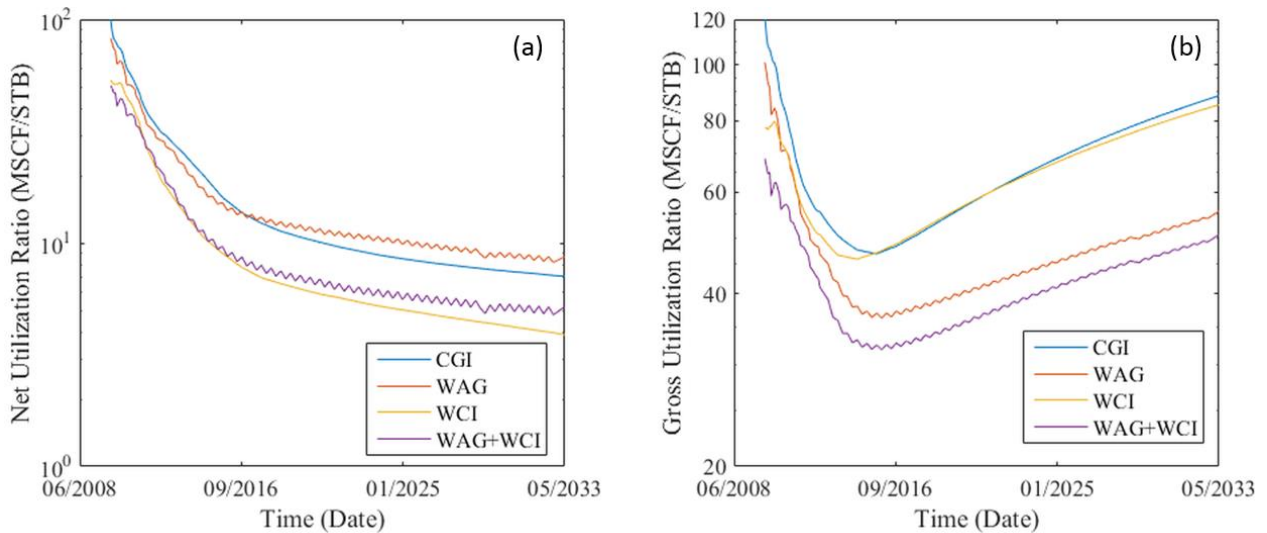


Figure 5.2. (a) Net utilization ratio (purchased CO₂ needed to produce one barrel of oil). (b) Gross CO₂ utilization ratio (purchased plus recycled CO₂ needed to produce one barrel of oil).

5.2 Gate-to-Gate Boundary

Within this boundary the most carbon intensive components are those that keep fluids flowing at the required pressures, rates, composition, and fluid phase; namely compression, pumping and gas processing. Gas compression for re-injection and the separation of produced gases are the two most significant carbon intensive processes. Compression of recycle gas is necessary in all our CO₂ injection scenarios in order to inject the CO₂ at injection pressures that assure a supercritical fluid phase.

The energy use for gas compression significantly overwhelms all components in a gate-to-gate system where gases are not separated. This relationship can be observed in Figure 5.3, where plots show the instant CO₂ emission rate, which refers to the mass of CO₂ emitted per barrel of oil produced at that point in time. Emission rates associated with gas compression and fluid handling are plotted. WAG cycles can be easily identified in the plots with each cycle marked by the fluctuation between zero and an instant emission rate value. End member scenario results show that in a WAG scenario, gas compression accounts in average for 95% of the carbon emissions, water injection for 4.7%, and water disposal for 0.3%. In a CGI scenario, gas compression accounts for 99.87%, with water production disposal contributing insignificantly. The time evolution of these contributions is also variable.

Gas separation and the type of gas separation process is a site specific operational choice. The impact of this decision on gate-to-gate GHG emissions is shown in Figure 5.4, which also shows significant emission variability over time for the three gas separation technologies studied, plus a case where production gases are re-injected without processing. In CGI, where the largest volumes of gas need to be processed, if Ryan Holmes separation (the most carbon intensive separation process) is used, the gate-to-gate emission rate varies from as low as 60 KgCO₂e/STB reached in the fourth year of injection to as much as to 650 KgCO₂e/STB at the end of the operation.

If fractionation/refrigeration is used the gate-to-gate emission rate varies from as low as 40 KgCO₂e/STB reached also in the fourth year to as much as to 330 KgCO₂e/STB at the end of the operation. All plots in Figures 5.3 and 5.4 show a large jump during the first months of injection. The jump coincides with the first barrel of oil produced, to which all GHG emissions from start of injection to that point are assigned. After first production, an accelerated decrease in emissions per produced barrel is observed. Maximum gate-to-gate environmental performance is attained at the minimum emission rate value. Emission rates steadily increase from the point of maximum environmental performance until the end of the CO₂-EOR operation.

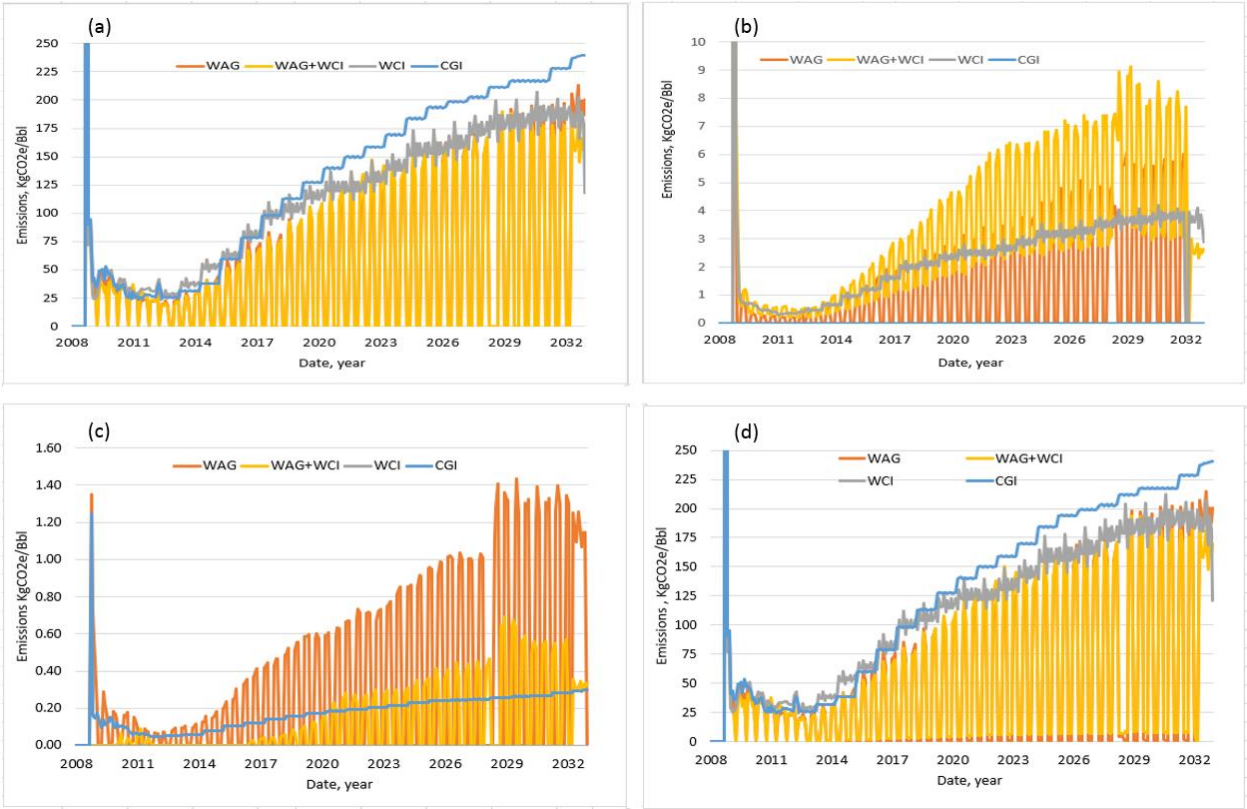


Figure 5.3. Instantaneous gate-to-gate GHG emissions rates per carbon intensive component: (a) CO₂ injection compression, (b) water injection, (c) water disposal, and (d) total emissions without gas separation.

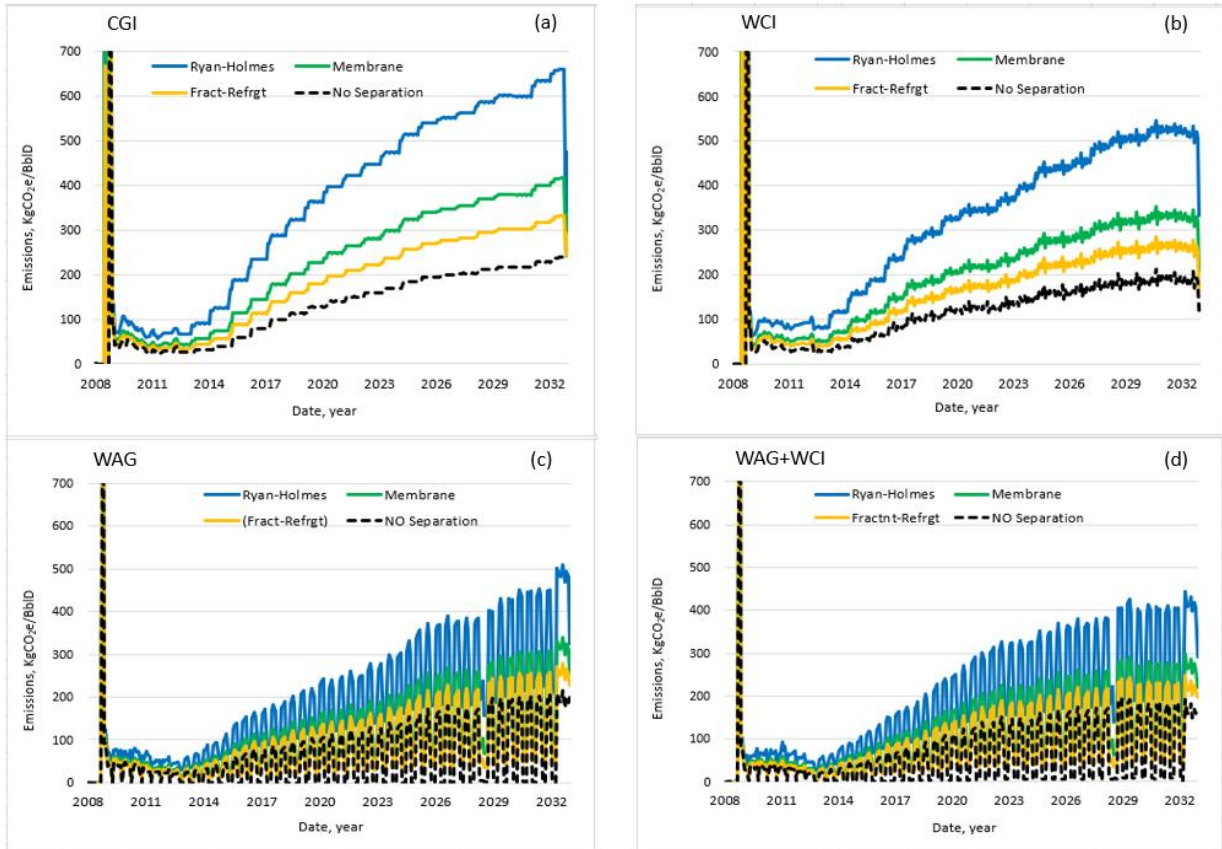


Figure 5.4. Gate-to-gate GHG emission rate per gas separation process for (a) continuous gas injection, (b) water curtain injection, (c) water-alternating-gas, and (d) the hybrid scenario.

The gate-to-gate CO₂e emission curves obtained with our surface model are superimposed on the CO₂ storage curves (Figure 5.5) to help visualize the dynamic relationship between GHG emissions and CO₂ storage. The storage curve does not intersect the emission curves in any of the scenarios, with the exception of WCI with Ryan Holmes gas processing, where the curves intersect one year before the end of the operation. As more CO₂ is stored than GHG's are emitted in association with the gate-to-gate boundary, most scenarios produce net carbon negative oil throughout the life of the EOR production and WCI with Ryan Holmes produces net carbon negative oil for 24 years. Please refer to Appendix B for complete set of gate-to-gate results.

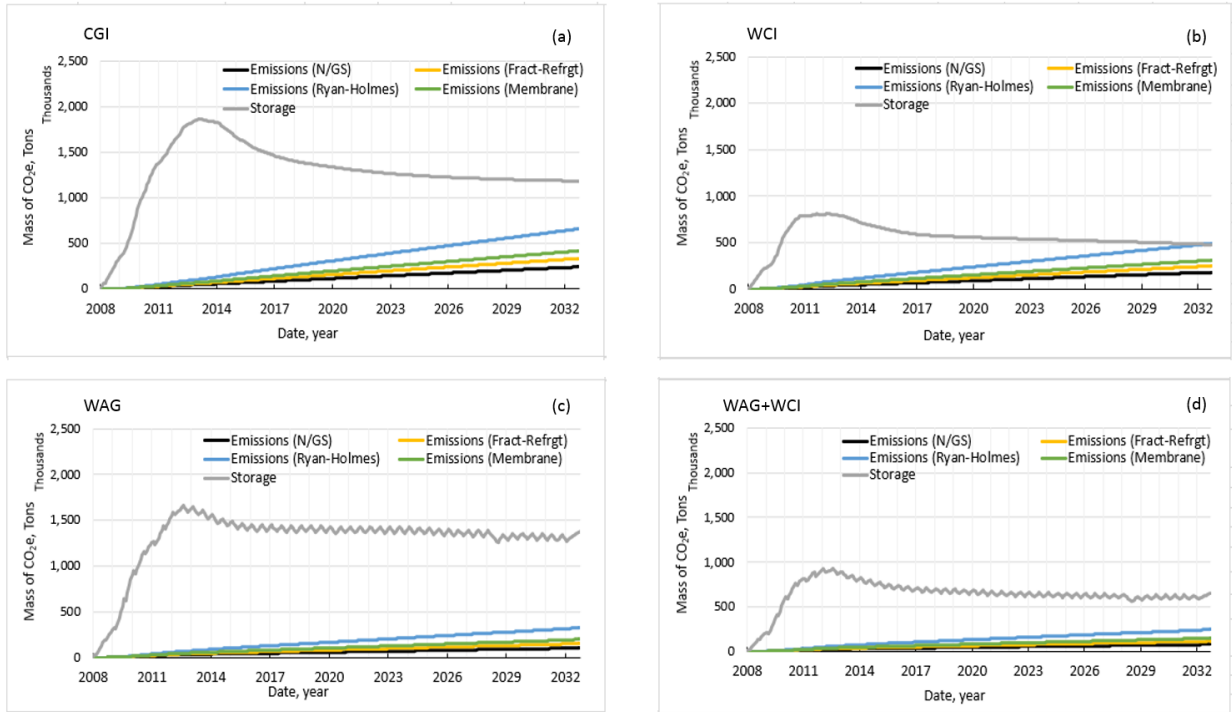


Figure 5.5. CO₂ storage mass (grey curves) versus CO₂e emissions (color curves) of the gate-to-gate CCUS system for (a) continuous gas injection, (b) water curtain injection, (c) water-alternating-gas, and (d) the hybrid scenario.

5.3 Gate-to-Grave Boundary

In this boundary the most carbon intensive component is the combustion of the refined product, particularly during the first years of operation when the CO₂ flood is most efficient. The contribution of product combustion to carbon intensity gradually decreases with time until it reaches an average of 65% of total system emissions. Figure 5.6 illustrates the carbon intensity of gate-to-grave system components (CO₂-EOR site, refinery, and product combustion) for our four CO₂ injection scenarios.

The gate-to-grave CO₂e emission curves obtained with our surface model are superimposed on the carbon storage curves (Figure 5.7) to observe their relationship and identify the point at which CO₂ storage and GHG emissions cross in all our scenarios. Results show that the net carbon balance range is widest for the CGI scenario, which has the best initial environmental performance (it stores the most CO₂). CGI remains carbon balance negative for twelve to fifteen years depending on the decision to purify the recycle gas and on the type of gas separation technology selected, whereas WAG remains negative for eighteen to twenty two years, a remarkably longer period. The two scenarios with water curtain injection have the lowest environmental performance because of the significantly smaller volumes of stored CO₂.

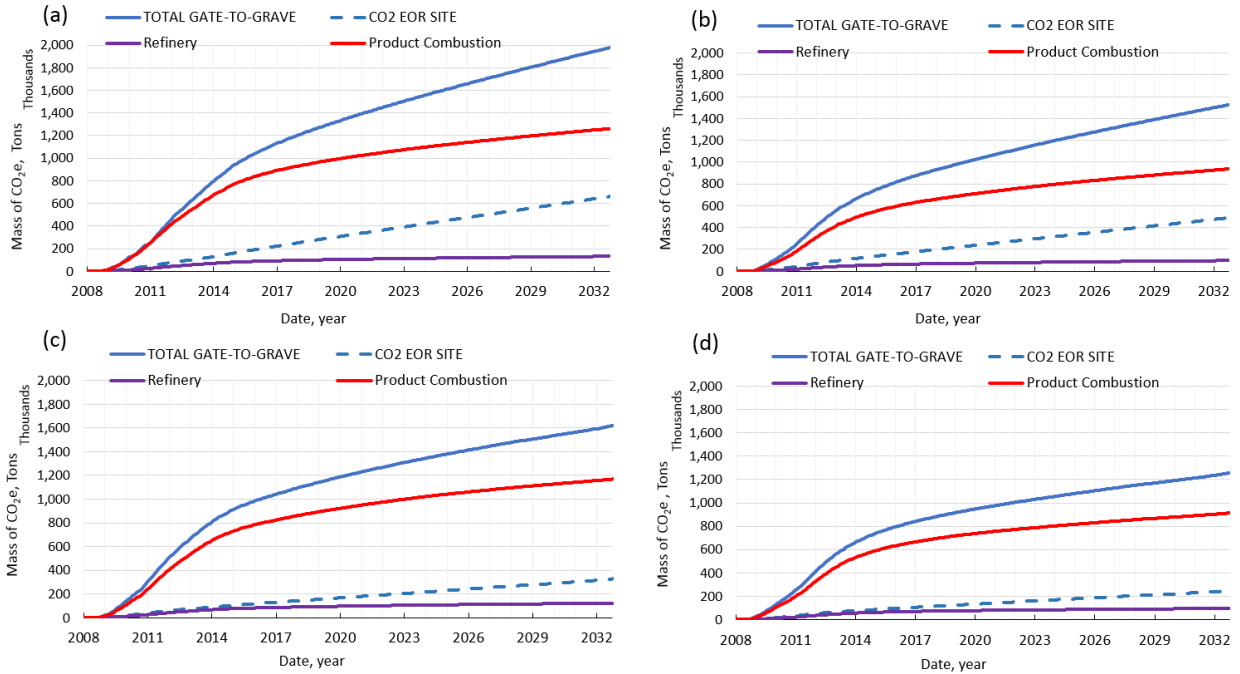


Figure 5.6. Carbon intensity of gate-to-grave components in: (a) continuous gas injection, (b) water curtain injection, (c) water-alternating-gas, and (d) the hybrid scenario.

The evolution of the carbon balance of the gate-to-grave CCUS system is plotted in Figure 5.8 to help visualize the emission/storage relationship. A negative carbon balance (associated with the CCUS boundary) means that more CO₂ has been stored than has been emitted into the atmosphere at that point in time. It also means that during a negative carbon balance period the oil produced is net carbon negative and the CCUS system has operated with a negative carbon footprint. The main takeaway from Figure 5.7 and Figure 5.8 is that all four scenarios start operating with a negative carbon footprint and, after years of operation transition into operating with a positive carbon footprint. Important decision making parameters at this transition point representing the end NCNO production, such as cumulative oil production, cumulative carbon storage, length of the negative carbon footprint period, and CO₂e emission rates are included in Table 5.1.

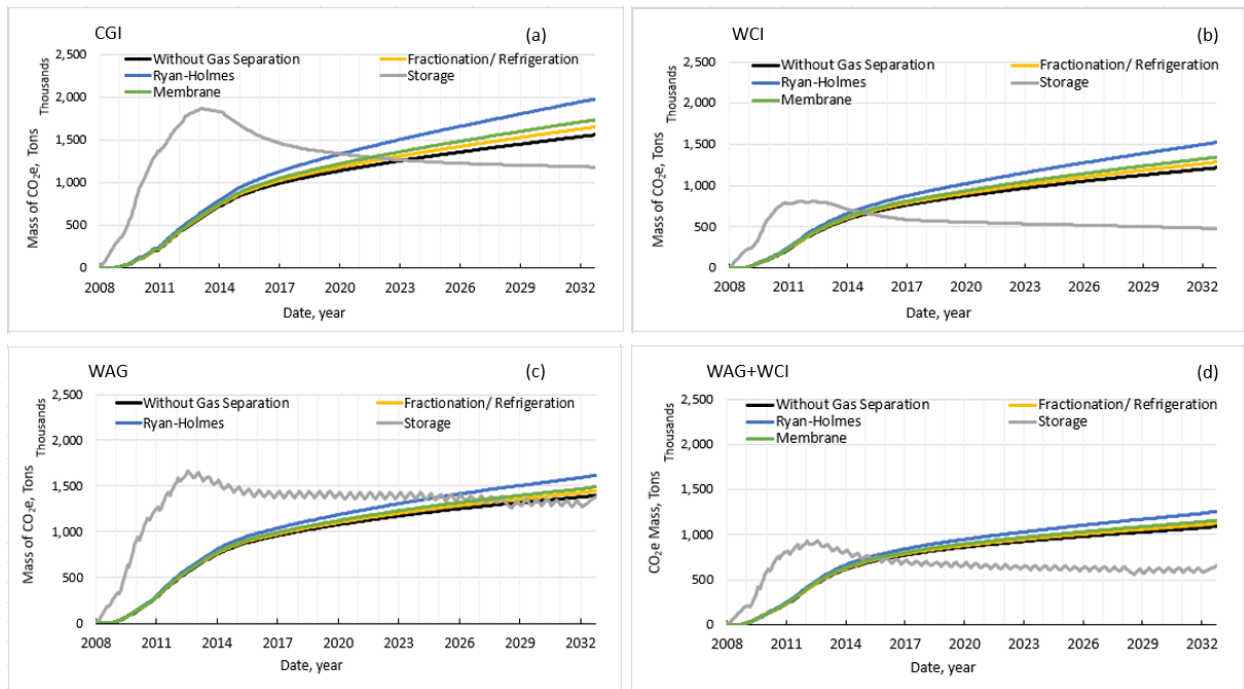


Figure 5.7. CO₂ storage mass (grey curves) versus CO₂e emissions (color curves) of the gate-to-grave CCUS system for (a) continuous gas injection, (b) water curtain injection, (c) water-alternating-gas, and (d) the hybrid scenario.

Understanding the carbon balance evolution of CCUS systems is one of the main contributions of this work. All pertinent LCA studies to date [7 to 13] have presented single-point results, commonly at the end of the EOR operation. Under that approach, we would have concluded that all scenarios had a positive carbon footprint, missing the important fact that all cases operate with a negative carbon footprint during the first years of CO₂ injection, with this period lasting over half the life of the operation in CGI and WAG scenarios.

Figure 12 illustrates the evolution of the gate-to-grave system's efficiency rates both operationally and environmentally. The figure reinforces the conclusion that WAG strategies are operationally efficient and have the lowest emission intensity in Kg CO₂ per barrel of oil produced. Please refer to Appendix B for complete set of gate-to-grave results.

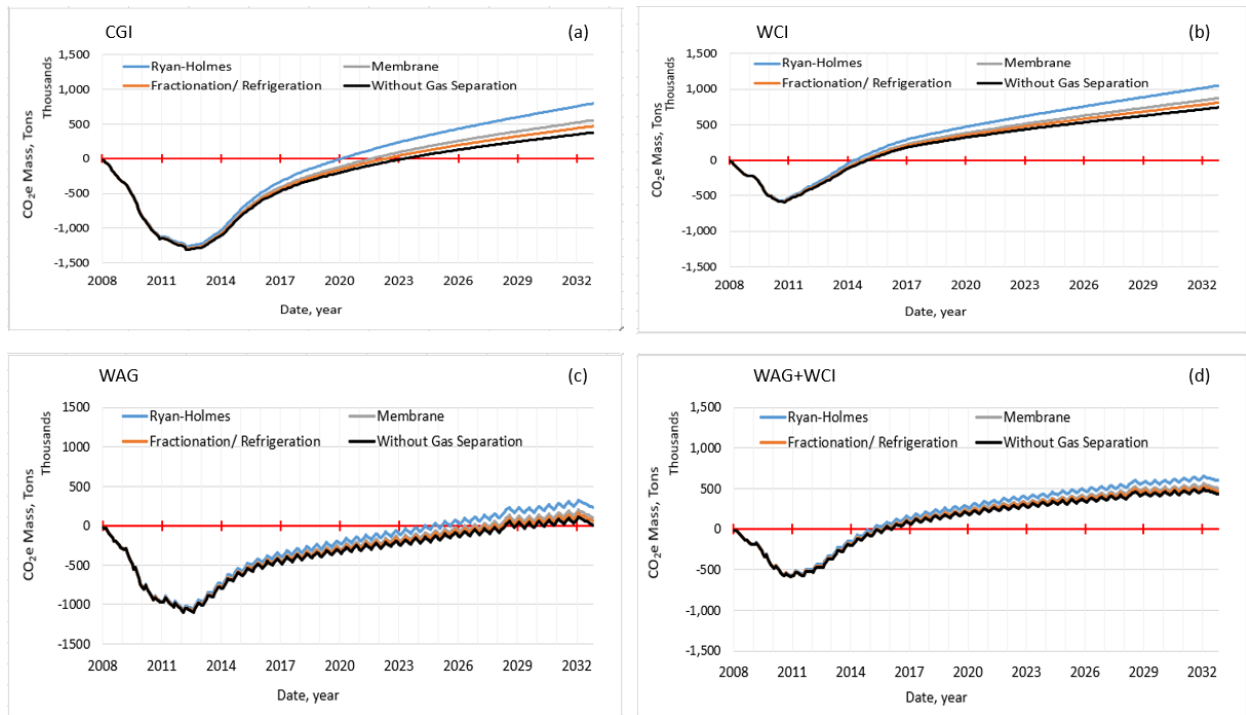


Figure 5.8. Carbon balance (CO₂e emissions minus CO₂ storage) of the gate-to-grave CCUS system for (a) continuous gas injection, (b) water curtain injection, (c) water-alternating-gas, and (d) the hybrid scenario.

Table 5.1. Important CCUS parameters at transition point (CO₂ storage = CO₂e emissions). Gate-to-grave boundary.

Parameter at transition point	CGI				WCI			
	N/S	R-H	Mem.	F/R	N/S	R-H	Mem.	F/R
Cumulative oil production (million barrels)	2.76	2.56	2.66	2.70	1.48	1.40	1.44	1.47
Percent of ultimate recovery (%)	86	79	82	84	48	55	56	57
Cumulative carbon storage (million tons)	1.26	1.34	1.30	1.28	0.69	0.72	0.70	0.70
Negative carbon footprint period (yrs.)	15.2	12.1	13.6	14.3	6.7	6.1	6.4	6.6
Negative carbon footprint period (% of project life)	61	49	55	57	27	24	26	26
Emission rate (tons CO ₂ e/barrel)	0.46	0.52	0.49	0.47	0.47	0.51	0.49	0.48

Table 5.1 (Cont.)

Parameter at transition point	WAG				WAG+WCI			
	N/S	R-H	Mem.	F/R	N/S	R-H	Mem.	F/R
Cumulative oil production (million barrels)	2.81	2.63	2.73	2.79	1.43	1.37	1.42	1.41
Percent of ultimate recovery (%)	95	89	92	94	46	60	62	61
Cumulative carbon storage (million tons)	1.32	1.37	1.35	1.34	0.66	0.69	0.67	0.65
Negative carbon footprint period (yrs.)	20.9	16.8	18.9	20.3	6.7	6.2	6.5	6.4
Negative carbon footprint period (% of project life)	84	67	76	82	27	25	26	26
Emission rate (tons CO ₂ e/barrel)	0.47	0.53	0.49	0.49	0.46	0.50	0.47	0.47

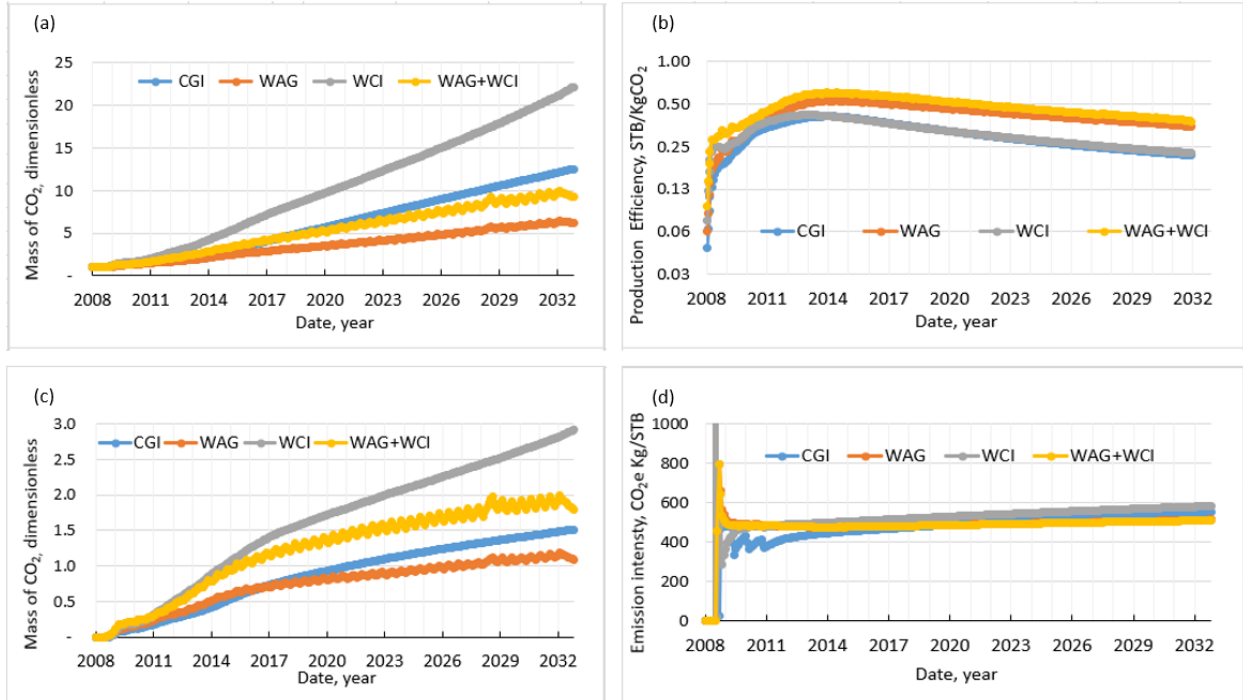


Figure 5.9. Evolution of efficiency rates: (a) mass of CO₂ injected per mass of CO₂ stored, (b) oil production per Kg of CO₂ injected, (c) gate-to-grave cumulative GHG emissions per mass of CO₂ stored, and (d) gate-to-grave cumulative GHG emissions per barrel of oil produced.

5.4 Cradle-to-Grave Boundary

5.4.1 Pulverized Carbon Power Plant

In general, expanding the gate-to-grave system to include GHG emissions upstream of the CO₂-EOR site has a significant adverse impact on the carbon lifecycle and balance of the CCUS system (Figures 13 and 14). In our study, the system expansion shortens the period of NCNO production by several years for all operational scenarios where CO₂ was supplied by a PC plant. Net carbon emissions at the end of the project increase significantly.

Both CO₂ injection strategies that use water alternating gas (WAG and Hybrid) are the most adversely impacted as CO₂ purchases continue throughout the life of the project, which in turn demands the associated electricity generation. We assumed that a continued CO₂ purchase from the capture plant is necessary because during the cycles of water injection produced CO₂ that cannot be stored at the site exits the system, so new CO₂ is purchased for the cycles of CO₂ injection. This has a tangible effect on the generation of energy and associated emissions. Figure 15 shows the evolution of emission intensities for both upstream components and the cradle-to-grave PC-CCUS system. In CGI, for example, the emission intensity increases from 550 Kg CO₂/STB in the gate-to-grave system to 800 Kg CO₂/STB in the cradle to grave system at the end of the project, whereas in WAG emission intensity increases from 500 Kg

CO₂/STB to 1,050 Kg CO₂/STB.

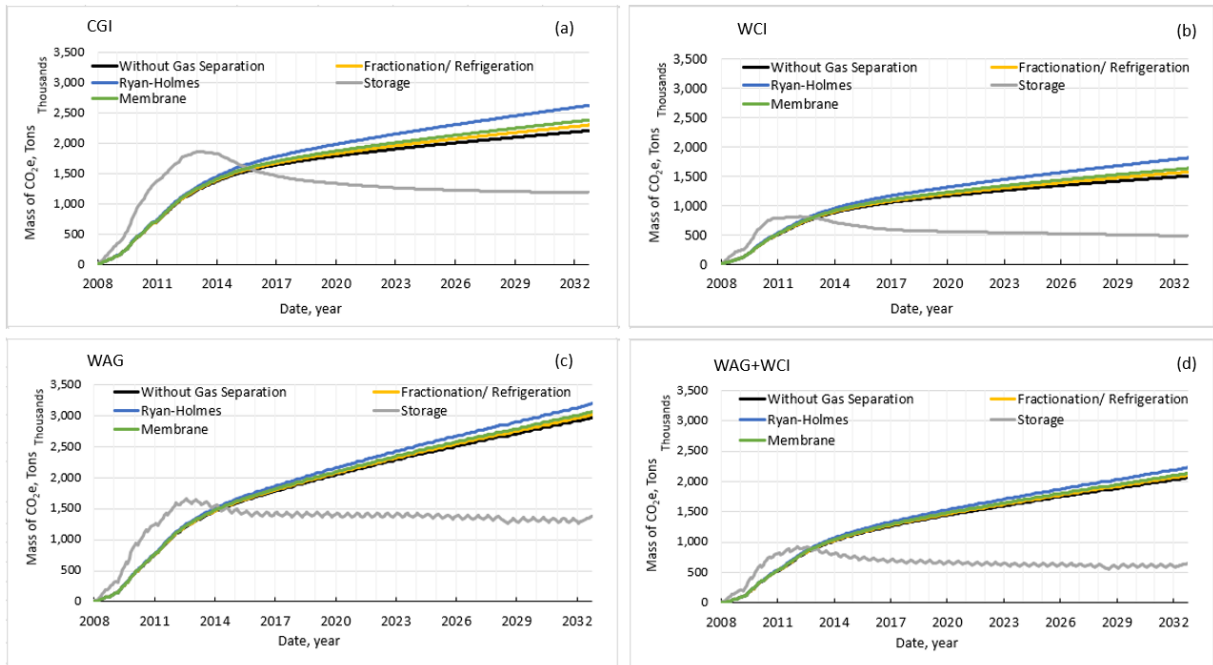


Figure 5.10. CO₂ storage mass (grey curves) versus CO₂e emissions (color curves) of the cradle-to-grave CCUS system with pulverized coal power plant for: (a) continuous gas injection, (b) water curtain injection, (c) water-alternating-gas, and (d) the hybrid scenario.

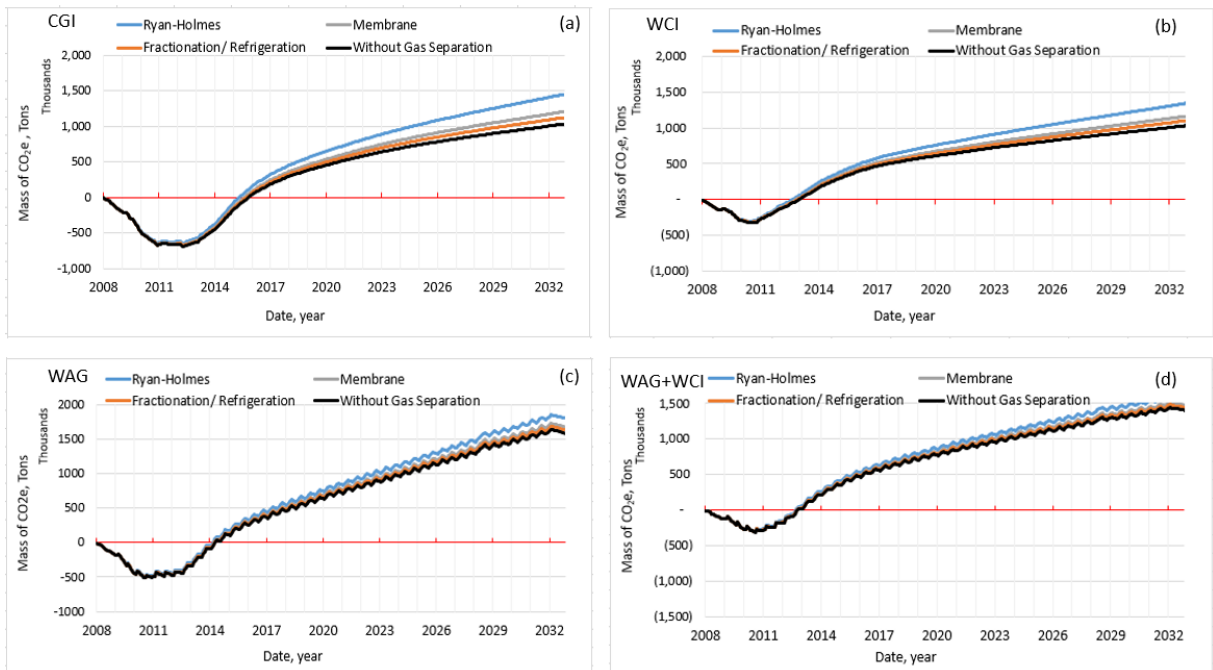


Figure 5.11. Carbon balance (CO₂e emissions minus CO₂ storage) of the cradle-to-grave CCUS system with pulverized coal power plant for (a) continuous gas injection, (b) water curtain injection, (c) water-alternating-gas, and (d) the hybrid scenario.

Important decision making parameters at this transition point, such as cumulative oil production, cumulative carbon storage, length of the negative carbon footprint period, and CO₂e emission rates are included in Table 5.2.

Table 5.2 Important CCUS parameters at transition point (CO₂ storage = CO₂e emissions). Cradle-to-grave boundary with Pulverized Coal power plant.

Parameter at transition point	CGI				WCI			
	N/S	F/R	R-H	Mem.	N/S	F/R	R-H	Mem.
Cumulative oil production (million barrels)	2.12	2.10	2.04	2.08	1.07	1.05	0.99	1.03
Percent of ultimate incremental recovery (%)	66	65	63	65	36	44	42	43
Cumulative carbon storage (million tons)	1.57	1.59	1.63	1.60	0.79	0.79	0.80	0.79
Negative carbon footprint period (yrs.)	7.8	7.7	7.3	7.6	5.0	4.9	4.7	4.8
Negative carbon footprint period (% of project life)	31	31	29	30	20	20	19	19
Emission rate (tons CO ₂ e/barrel)	0.74	0.76	0.80	0.77	0.73	0.75	0.80	0.77

Table 5.2 (Cont.)

Parameter at transition point	WAG				WAG+WCI			
	N/S	F/R	R-H	Mem.	N/S	F/R	R-H	Mem.
Cumulative oil production (million barrels)	1.70	1.70	1.69	1.70	1.08	1.08	1.06	1.06
Percent of ultimate incremental recovery (%)	57	57	57	57	36	47	46	46
Cumulative carbon storage (million tons)	1.70	1.70	1.69	1.70	0.86	0.86	0.89	0.89
Negative carbon footprint period (yrs.)	6.3	6.3	6.2	6.3	4.8	4.8	4.8	4.8
Negative carbon footprint period (% of project life)	25	25	25	25	19	19	19	19
Emission rate (tons CO ₂ e/barrel)	1.00	1.00	1.00	1.00	0.80	0.80	0.84	0.84

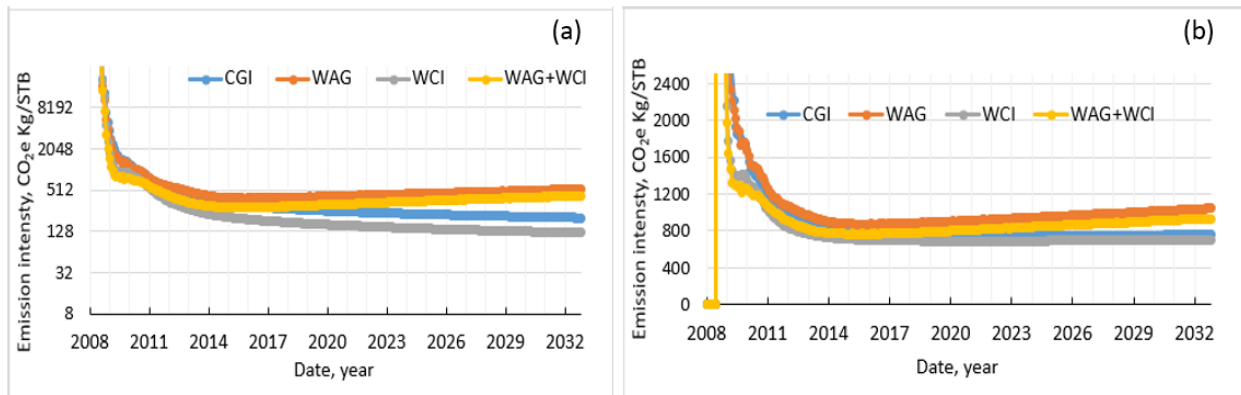


Figure 5.12. Evolution of efficiency rates: (a) components upstream of the CO₂-EOR site, (b) the cradle-to-grave PC – CCUS system.

If the capture facility displaces a conventional power source and credits are added for displacement, the adverse impact caused by the system expansion not only is reversed but transformed into a significant environmental benefit (Figure 5.13). The effect of the displacement more than compensates the emissions associated with the energy generation requirements for the production of CO₂, as much more electricity will be displaced.

As in all previous carbon balance curves, the balance reaches an optimum point (after 4.8 years of injection in the CGI case) when maximum storage is attained. In both WAG cases

after the optimum (minimum) point is reached the carbon balance increases but shortly after it starts to decrease again. This is the point at which carbon credits from electricity displacement exceed the carbon storage mass. WAG strategies are noticeably favored by electricity displacement as it occurs throughout the life of the operation. Please refer to Appendix C for complete set results.

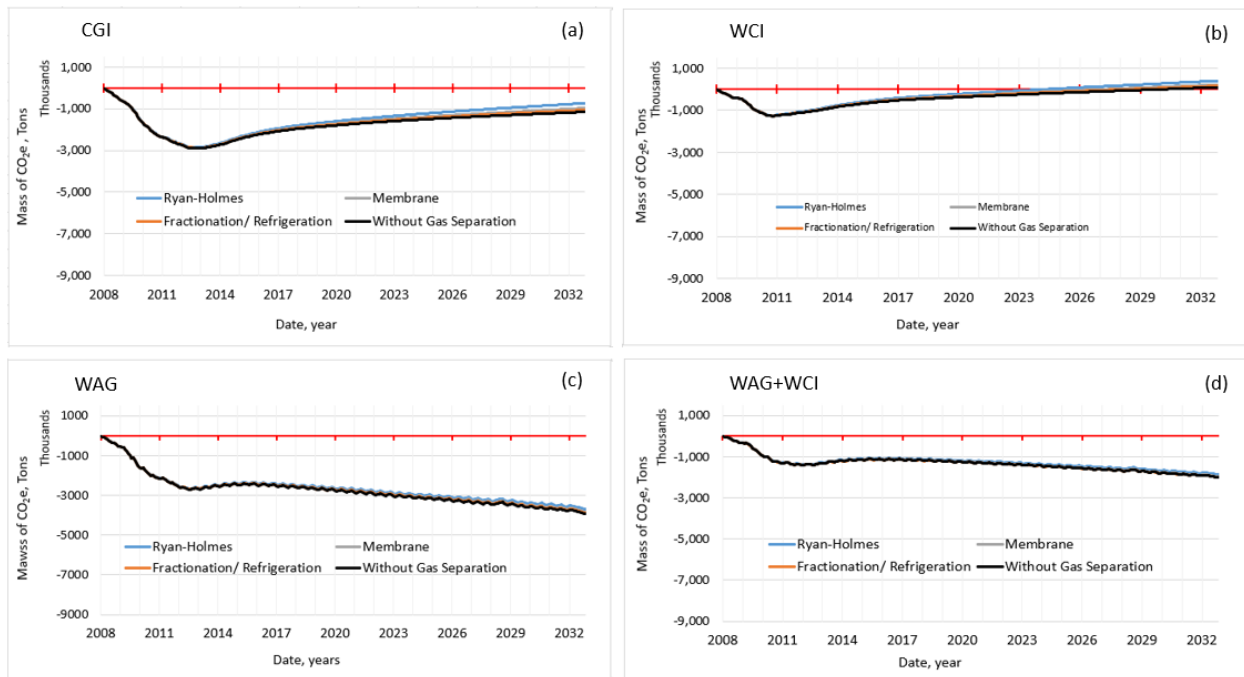


Figure 5.13. Effect of electricity displacement on the carbon balance (CO_2e emissions minus CO_2 storage) of the cradle-to-grave CCUS system with pulverized coal power plant for (a) continuous gas injection, (b) water curtain injection, (c) water-alternating-gas, and (d) the hybrid scenario.

3.4.2 Natural Gas Combined Cycle

Counter to intuition, the effect on the carbon balance of a system expansion with an NGCC plant is even more adverse than that of a PC plant (Figures 5.14 and 5.15). The adverse effect is caused by the significant increase in the electricity that the plant needs to generate in order to produce the CO_2 mass needed for the EOR flood. Figure 5.14 shows that GHG emission curves and CO_2 storage curves overlap during the first few years, so the system doesn't really produce NCNO, but carbon neutral oil during that time.

The same pronounced impacts on WAG strategies discussed in the previous section also apply, as the cyclic nature of WAG demands electricity generation throughout the EOR operation. Again this disadvantage in terms of gross upstream emissions (Figure 5.16) is compensated by a greater displacement.

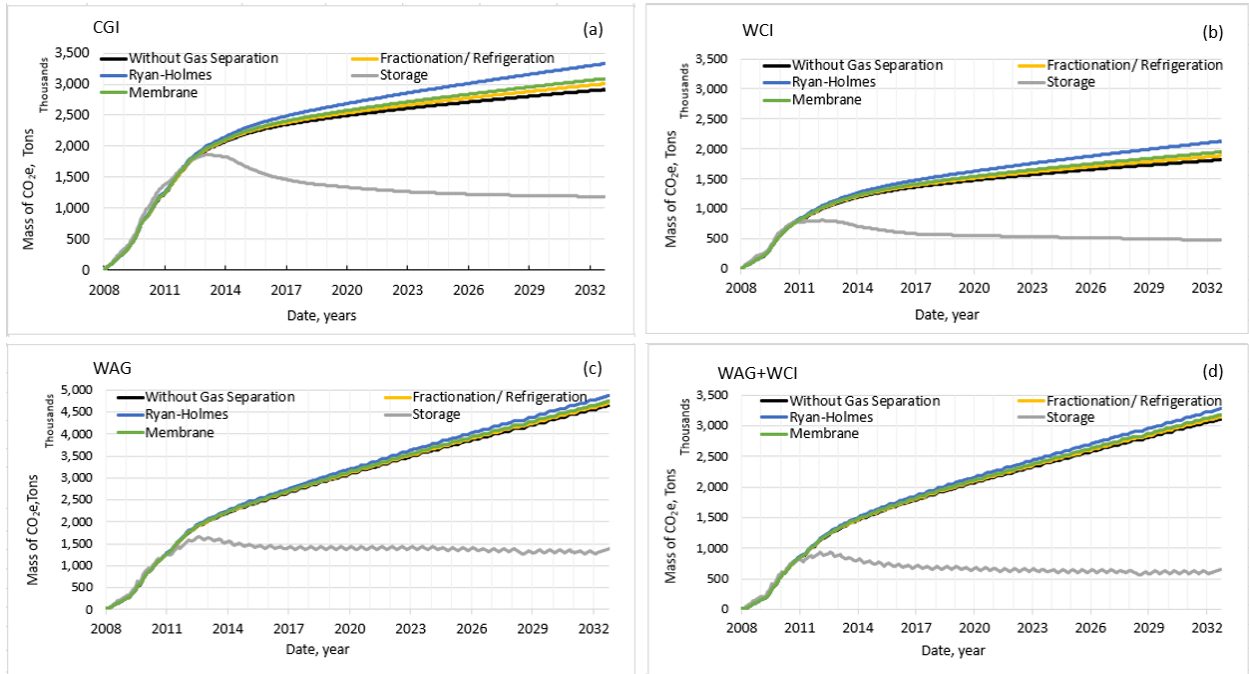


Figure 5.14. CO₂ storage mass (grey curves) versus CO₂e emissions (color curves) of the cradle-to-grave CCUS system with Natural Gas Combined Cycle power plant for: (a) continuous gas injection, (b) water curtain injection, (c) water-alternating-gas, and (d) the hybrid scenario.

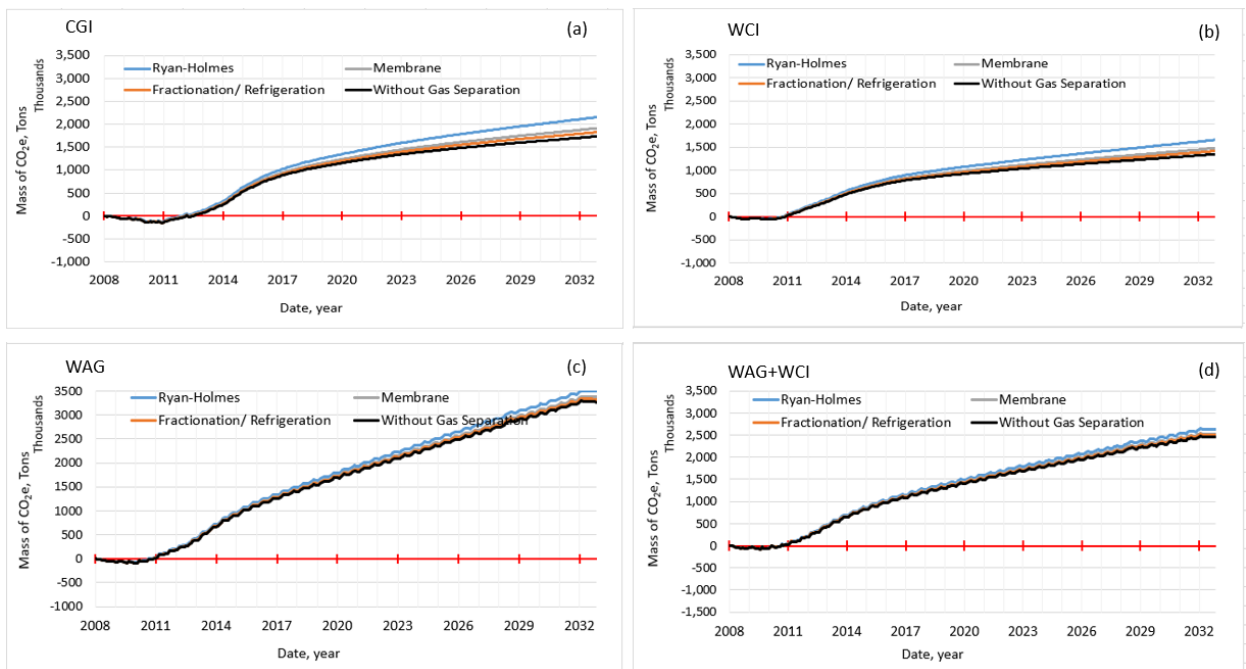


Figure 5.15. Carbon balance (CO₂e emissions minus CO₂ storage) of the cradle-to-grave CCUS system with Natural Gas Combined Cycle power plant for (a) continuous gas injection, (b) water curtain injection, (c) water-alternating-gas, and (d) the hybrid scenario.

Important cradle-to-grave decision making parameters at this transition point, such as cumulative oil production, cumulative carbon storage, length of the negative carbon footprint period, and CO₂e emission rates are included in Table 5.3.

Table 5.3. Important CCUS parameters at transition point (CO₂ storage = CO₂e emissions). Cradle-to-grave boundary with NGCC power plant.

Parameter at transition point	CGI				WCI			
	N/S	F/R	R-H	Mem.	N/S	F/R	R-H	Mem.
Cumulative oil production (million barrels)	1.23	1.20	1.03	1.18	0.45	0.48	0.45	0.45
Percent of ultimate incremental recovery (%)	38	37	32	36	15	20	19	19
Cumulative carbon storage (million tons)	1.80	1.79	1.65	1.78	0.78	0.78	0.79	0.79
Negative carbon footprint period (yrs.)	4.5	4.4	3.9	4.3	2.9	2.9	2.8	2.8
Negative carbon footprint period (% of project life)	18	18	16	17	12	12	11	11
Emission rate (tons CO ₂ e/barrel)	1.46	1.49	1.61	1.52	1.74	1.64	1.77	1.77

Table 5.3 (Cont.)

Parameter at transition point	WAG				WAG+WCI			
	N/S	F/R	R-H	Mem.	N/S	F/R	R-H	Mem.
Cumulative oil production (million barrels)	0.57	0.57	0.50	0.53	0.73	0.73	0.73	0.73
Percent of ultimate incremental recovery (%)	19	19	17	18	14	18	18	18
Cumulative carbon storage (million tons)	1.24	1.24	1.24	1.24	0.73	0.73	0.73	0.73
Negative carbon footprint period (yrs.)	2.9	2.9	2.7	2.8	2.7	2.7	2.7	2.7
Negative carbon footprint period (% of project life)	12	12	11	11	11	11	11	11
Emission rate (tons CO ₂ e/barrel)	2.17	2.17	2.48	2.33	1.00	1.00	1.00	1.00

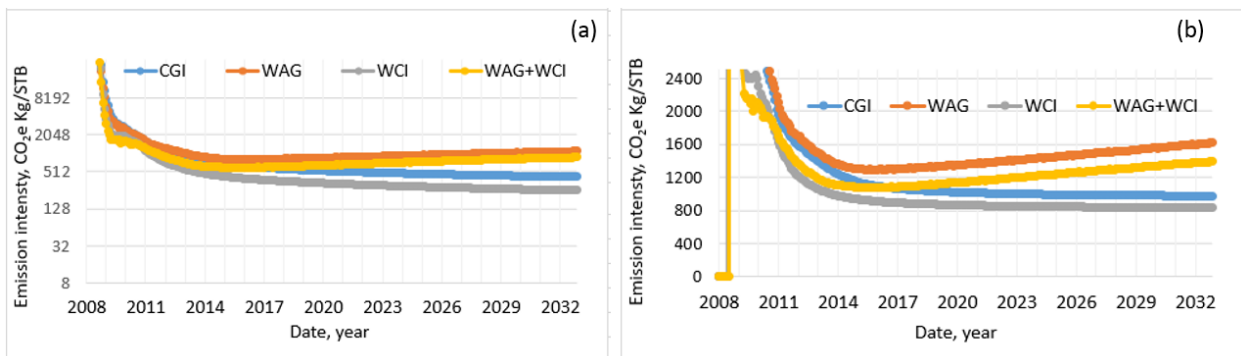


Figure 5.16. Evolution of efficiency rates: (a) components upstream of the CO₂-EOR site, (b) the cradle-to-grave NGCC – CCUS system.

Also in this case, if the capture facility displaces a conventional power source and credits are added for displacement, the adverse impact caused by the system expansion not only is reversed but transformed into a significant environmental benefit (Figure 5.17). The effect of the displacement more than compensates the emissions associated with the energy requirements for the production of CO₂, as much more electricity is displaced.

The same conditions that caused a disadvantage for this cleaner energy generation option (NGCC, low carbon intensity) now play in the system's favor, resulting in a beneficial environmental balance for all EOR operating scenarios, far exceeding the balance of the PC

option. With electricity displacement, all scenarios produce NCNO throughout the CO₂-EOR operation with the exception of WCI with Ryan-Holmes gas processing, which starts producing net carbon positive oil three years before the end of the operation. Please refer to Appendix D for complete set of results.

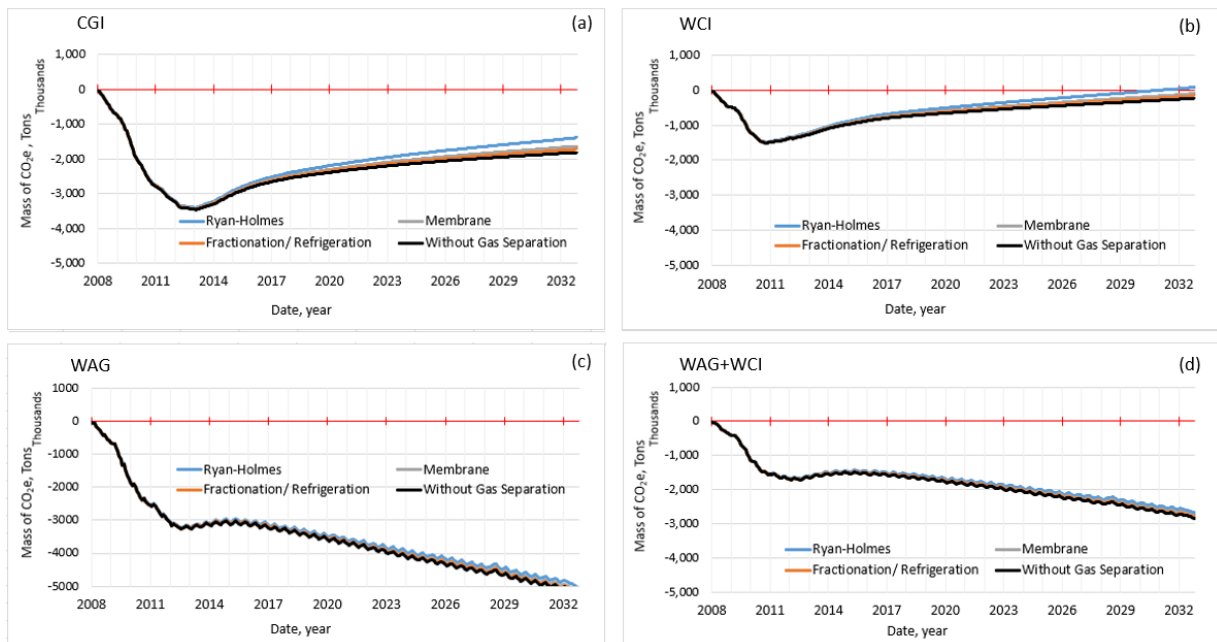


Figure 5.17. Effect of electricity displacement on the carbon balance (CO₂e emissions minus CO₂ storage) of the cradle-to-grave CCUS system with Natural Gas Combined Cycle power plant for (a) continuous gas injection, (b) water curtain injection, (c) water-alternating-gas, and (d) the hybrid scenario.

6. Conclusions

A dynamic assessment of reservoir performance coupled with energy consumption is necessary to understand the range and evolution of the carbon balance of CCUS systems. Our results show that in a gate-to-grave CCUS system all four CO₂ injection scenarios studied start operating with a negative carbon footprint and at some point transition into operating with a positive carbon footprint.

The length of the negative carbon period shortens significantly in a cradle-to-grave CCUS system boundary if conventional power is not displaced by the capture plant. However, the single fact that all CO₂-EOR operations produce NCNO during the first years of production is critical in the context of the urgency of climate change mitigation. Furthermore, our results suggest that the negative carbon footprint period can be engineered to last longer through operational changes.

If the capture facility displaces a conventional power source and credits are added for displacement, the adverse impact caused by the system expansion not only is reversed but transformed into a significant environmental benefit. The effect of the displacement more than compensates the emissions associated with the energy generation requirements for the production of CO₂, as much more electricity will be displaced. If electricity displacement occurs, the cradle-to-grave system has the potential of producing NCNO throughout the life of the operation.

In our reservoir simulations, the ultimate oil recovery in the CGI and WAG scenarios is largest, and so is the carbon storage at the end of 25 years of CO₂ injection. Results from CO₂ utilization ratio and oil production analysis show that the hybrid scenario, which combines a WAG flooding strategy with a water curtain injection, is the most EOR efficient. In this scenario, oil is recovered faster, producing earlier revenues and potentially the best project value. However, it does not perform well environmentally.

In a gate-to-gate system, the best initial environmental performance is achieved by the CGI scenario, even though WAG remains net carbon negative for as long as CGI does and produces 90% of the oil produced by CGI with only 58% of the injected CO₂. Based on our analysis, WAG appears to have a better potential for EOR/storage co-optimization, providing the best compromise between environmental and operational performance.

Our study demonstrates the variability of the net carbon balance of CCUS systems. Net carbon balance not only varies among different EOR settings, but it also varies depending on the strategy selected to develop reservoirs with the same geologic setting. In addition, net carbon balance also varies significantly through time, as projects mature. This variability is mostly due to the efficiency of the EOR process, which controls oil recovery and associated carbon storage.

Our results also provide an understanding of the interplay between environmental performance and economic oil production. This understanding can assist in the co-optimization of CO₂-EOR and geologic carbon storage. Most importantly, this study serves as confirmation that CO₂-EOR can be operationally designed to both enhance oil production and reduce greenhouse gas emissions to the atmosphere.

Nomenclature

HCPV	hydrocarbon pore volume
STB	stock tank barrel (at standard conditions)
kPa	kilopascal
CO _{2e}	CO ₂ equivalent
MWh	megawatt hour
VOC	volatile organic compounds
Tg	teragram = 10 ¹² grams = one million metric ton
EJ	exajoule = 10 ¹⁸ joules
MMscf	million standard cubic feet

Acknowledgments

This study was funded and managed by the Department of Energy's National Energy Technology Laboratory (DOE-NETL), under award number DE-FE0024433. The authors thank and acknowledge the Gulf Coast Carbon Center (GCCC) and the Hildebrand Petroleum and Geosystems Engineering Department of the University of Texas at Austin, as well as the Carbon Capture Project Phase 4 (CCP-4), for the cost sharing support. We also thank the Cranfield SECARB project (DE-FC26-05NT42590) for Cranfield data support.

References

1. Godec, M. L.; Kuuskraa, V. A.; Dipietro, P. Opportunities for Using Anthropogenic CO₂ for Enhanced Oil Recovery and CO₂ Storage. *Energy & Fuels* **2013**, *27* (8), 4183-4189, doi:10.1021/ef302040u
2. Verma, M.K. Fundamentals of carbon dioxide-enhanced oil recovery (CO₂-EOR)—A supporting document of the assessment methodology for z recovery using CO₂-EOR associated with carbon sequestration. U.S. Geological Survey Open-File Report **2015**, 1071, doi.org/10.3133/ofr20151071.
3. Mungan, N. Carbon Dioxide Flooding As an Enhanced Oil Recovery Process. Petroleum Society of Canada **1992**, 31, doi:10.2118/92-09-01
4. Hosseininoosheri, P.; Hosseini, S. A.; Núñez-López, V.; Lake, L. W. Impact of field development strategies on CO₂ trapping mechanisms in a CO₂-EOR field: A case study in the Permian Basin (SACROC unit). *International Journal of Greenhouse Gas Control* **2018**, *72*, doi:10.1016/j.ijggc.2018.03.002.
5. Han, W.S. *Evaluation of CO₂ Trapping Mechanisms at the Sacroc Northern Platform: Site of 35 years of CO₂ injection*; The New Mexico Institute of Mining and Technology: Socorro, NM, USA, 2008.
6. ISO 14040—Environmental Management—Life Cycle Assessment—Principles and Framework; International Standards Organization, **1997**; <http://www.iso.org/iso/en/prods-services/otherpubs/iso14000/index.html>.
7. Aycaguer, A. C.; Lev-On, M.; Winer, A. M. Reducing Carbon Dioxide Emissions with Enhanced Oil Recovery Projects: A Life Cycle Assessment Approach. *Energy Fuels* **2001**, *15* (2), 303-308, doi: 10.1021/ef000258a
8. Suebsiri, J.; Wilson, M.; Tontiwachwuthikul, P. Life-cycle analysis of CO₂ EOR on EOR and geological storage through economic optimization and sensitivity analysis using the Weyburn Unit as a case study. *Industrial & engineering chemistry research* **2006**, *45*(8), 2483-2488. Available online: <https://pubs.acs.org/doi/abs/10.1021/ie050909w>.
9. Hertwich, E. G.; Aaberg, M., Singh, B.; Strømman, A. H. Life-cycle assessment of carbon dioxide capture for enhanced oil recovery. *Chinese Journal of Chemical Engineering* 2008, *16*(3), 343-353. Available online: <https://www.sciencedirect.com/science/article/pii/S1004954108600853?via%3Dihub>.
10. Jaramillo, P.; Griffin, W. M.; McCoy, S. T. Life cycle inventory of CO₂ in an enhanced oil recovery system. *Environmental science & technology* **2009**, *43*(21), 8027-8032, doi: 10.1021/es902006h. Available online: <https://pubs.acs.org/doi/10.1021/es902006h>.
11. DOE-NETL. Electricity use of enhanced oil recovery with carbon dioxide (CO₂-EOR). *DOE/NETL-2009/1354* **2009**.
12. Fox, C.E. CO₂ EOR carbon balance at SACROC year 2007, *Kinder Morgan CO₂ Company, LP (Power Point Presentation)* **2009**.
13. Cooney, G.; Littlefield, J.; Marriott, J.; Skone, T. Evaluating the Climate Benefits of CO₂-Enhanced Oil Recovery Using Life Cycle Analysis. *Environmental science & technology* **2015**, Vol. 49, 12, 7491-7500. DOI: 10.1021/acs.est.5b00700. Available online: <https://pubs.acs.org/doi/abs/10.1021/acs.est.5b00700>.
14. Ampomah, W.; Balch, R.; Grigg, R.; McPherson, B.; Will, R.; Lee, S., Dai, Z.; Pan, F. Co-optimization of CO₂-EOR and storage processes in mature oil reservoirs. *International Journal of Greenhouse Gases Science and Technology* **2016**, *7*, 128-142, doi:10.1002/ghg.1618.
15. Leach, A.; Mason, C. F.; Velt, K. Co-optimization of enhanced oil recovery and carbon sequestration. *NBER working paper series # 15035* **2009**, Doc. 30p. Available online: <http://www.nber.org/papers/w15035.pdf>.
16. Dai, Z.; Viswanathan, H.; FessendenRahn, J.; Middleton, R.; Pan, F.; Jia, W.; Lee, S.Y.; McPherson, B.; Ampomah, W.; Grigg, R. Uncertainty quantification for CO₂ sequestration and enhanced oil recovery *Energy Procedia* **2014**, *63* (0) 7685- 7693.
17. Hadlow, R. E. Update of industry experience with CO₂ injection, Society of Petroleum Engineers. In proceedings

of SPE 67th Annual Technical Conference and Exhibition,, Washington, DC, U.S. October 4-7, 1992, 743-752, doi:10.2118/24928-MS.

18. Saneifar, M.; Heidari, Z.; Linroth, M.; Purba, S. Effect of Heterogeneity on Fluid-Injectivity Loss during Water-Alternating-Gas Injection in the Scurry Area Canyon Reef Operators Committee Unit, SPE Reservoir Evaluation & Engineering, **2017**, 20, 293-303, doi:10.2118/175064-PA
19. Gorell, S.B. Implications of Water-Alternate-Gas injection, for Profile Control and Injectivity, In Proceedings of the SPE/DOE Enhanced Oil Recovery Symposium, Tulsa, Oklahoma, USA, (22-25 April 1992), doi.org/10.2118/20210-MS
20. Hosseini, S. A.; Hamidreza, L.; Choi, J. W.; Nicot, J. P.; Lu, J., Hovorka, S. D. Static and dynamic reservoir modeling for geological CO₂ sequestration at Cranfield, Mississippi, U.S. *International Journal of Greenhouse Gas Control* **2013**, 18, 449-462. Available online: <https://www.sciencedirect.com/science/article/pii/S1750583612002721>.
21. Hosseini, S. A.; Alfi, M.; Nicot, J. P.; Nuñez-López, V.; Analysis of CO₂ storage mechanisms at a CO₂-EOR site, Cranfield, Mississippi. *International Journal of Greenhouse Gases Science and Technology* **2018**, 8, 469-482, doi: 10.1002/ghg, Available online: <https://onlinelibrary.wiley.com/doi/abs/10.1002/ghg.1754>
22. Nuñez-López, V., Gil-Egui, R., Gonzalez-Nicolas A., Hovorka, S. D., Carbon balance of CO₂-EOR for NCNO classification, 13th International Conference of Greenhouse Gas Control Technologies **2017**, Lausanne, Switzerland, 14-18 November 2016. Vol. 114, 6597-6603. Available online: <https://doi.org/10.1016/j.egypro.2017.03.1803>.
23. EPA. Emission Factors for Greenhouse Gas Inventories. URL:https://www.epa.gov/sites/production/files/2015-07/documents/emission-factors_2014.pdf (Archived by WebCite® at <http://www.webcitation.org/75HHcEzUt>).
24. U.S. Energy Information Administration (eia). Fuel Consumed at Refineries. WEB page 2018-06-25. URL:https://www.eia.gov/dnav/pet/pet_pnp_capfuel_dcu_nus_a.htm. (Archived by WebCite® at <http://www.webcitation.org/75HIDiuE7>)
25. Scull, B. D. et al. 2017. Upstream Emissions of Coal and Gas. New York, NY: Columbia University, School of International and Public Affairs.
26. NETL (2010). Cost and Performance Baseline for Fossil Energy Plants Volume 1: Bituminous Coal and Natural Gas to Electricity. DOE/NETL-2010/1397 Rev. 2.
27. Melzer, S., 2012. "Carbon Dioxide Enhanced Oil Recovery (CO₂ EOR): Factors Involved in adding Carbon Capture, Utilization and Storage (CCUS) to Enhanced Oil Recovery." Report for Center for Climate and Energy Solutions.
28. Juanes, R. Spiteri, E. J., Orr Jr., F. M., Blunt, M. 2006. Impact of relative permeability hysteresis on geological CO₂ storage. *Water Resources Research*, 42, W12418, doi:10.1029/2005WR004806.
29. Juanes, C. W. MacMinn, and M. L. Szulczewski. 2010. The footprint of the CO₂ plume during carbon dioxide storage in saline aquifers: storage efficiency for capillary trapping at the basin scale. *Transport in Porous Media*, **82**(1):19-30.
30. Yang, F., Bai, B., Dunn-Norman, S. 2011. Modeling the effects of completion techniques and formation heterogeneity on CO₂ sequestration in shallow and deep saline aquifers, *Environmental Earth Sciences*, 64, 841-849, DOI: 10.1007/s12665-011-0908-0.
31. Liu F., Lu P., Griffith C., Hedges S., Soong Y., Hellevang H., Zhu C., 2012. "CO₂-brine-caprock interaction: Reactivity experiments on Eau Claire shale and a review of relevant literature", *International Journal of Greenhouse Gas Control* 7, Elsevier, 153-157.
32. Lu, J. et al., CO₂-rock-brine interactions in Lower Tuscaloosa Formation at Cranfield CO₂ sequestration site, Mississippi, U.S.A. *Chemical Geology* 291 (2012) 269–277, doi:10.1016/j.chemgeo.2011.10.020.
33. Hovorka, S. D., Meckel, T.A., Treviño, R., 2012. Monitoring a Large-volume Injection at Cranfield, Mississippi - Project Design and Recommendations, *International Journal of Greenhouse Gas Control*.
34. Cavanagh, A. and P. Ringrose (2011). "Simulation of CO₂ distribution at the In Salah storage site using high-

resolution field-scale models." *Energy Procedia* 4(0): 3730-3737.

35. Lu, J., P. J. Cook, S. A. Hosseini, C. Yang, K. D. Romanak, T. Zhang, B. M. Freifeld, R. C. Smyth, H. Zeng, and S. D. Hovorka (2012), Complex fluid flow revealed by monitoring CO₂ injection in a fluvial formation, *J. Geophys. Res.*, 117, B03208, doi:10.1029/2011JB008939.
36. Whittaker, S. (2004). Theme 1: Geological Characterization, IEA GHG Weyburn CO₂ Monitoring & Storage Project Summary Report 2000-2004, Volume III, Vancouver, Canada.
37. Weaver and K. F. Anderson. Cranfield field, cranfield unit, basal tuscaloosa reservoir, adams and franklin counties, mississippi. 1966.
38. Spangler, L.H., Dobeck, L.M., Repasky, K.S. et al. A shallow subsurface controlled release facility in Bozeman, Montana, USA, for testing near surface CO₂ detection techniques and transport models. *Environ Earth Sci* (2010) 60: 227. <https://doi.org/10.1007/s12665-009-0400-2>
39. Feitz, A., Schroder, I., Phillips, F., et al. 2018. The Ginninderra CH₄ and CO₂ release experiment: An evaluation of gas detection and quantification techniques. *International Journal of Greenhouse Gas Control*. <https://doi.org/10.1016/j.ijggc.2017.11.018>

Appendix A

REVIEW AND ANALYSYS OF EXISTING MONITORING METHODS AND TOOLS

Geophysical methods

Acoustic methods

Time-lapse 3-D seismic methods for imaging the extent of the CO₂ plume have been one of the breakthroughs of CCS monitoring. The collection of repeat surveys prior to CO₂ injection and as the injection volume increased at the Sleipner and Weyburn projects and making these data accessible to multiple research teams have advanced the rigor with which plume evolution can be predicted, as discussed in the previous section. In addition, the reliability of the system is increased. Changes in seismic velocity are sensitive to both changes in fluids and pressure, both important in reservoir management. Research conditions have been useful in separation of the two contributing elements (Ajo Franklin, written communication). 4-D seismic is now being proposed as a technique for managing many types of reservoirs. Validation in geologic storage research environments will advance the technology.

Geologic sequestration has provided acceleration to research and development of other types of geophysical measurements also. The combination of federally funded large research programs that engage many researchers and make results publically available and experiments conducted in simplified brine-only fluid settings has accelerated tool development and data analysis. One of the contributions made for seismic interpretation from research-oriented storage projects is combination of seismic with other instruments, including borehole deployed technologies and other types of measurements.

Cross-well seismic and VSP

Higher resolution well-based acoustic data are typically collected in reservoir settings to augment a seismic survey to provide improved depth resolution and higher frequency data. These include sonic logs where both source and receiver are placed in the well, vertical seismic profiling, where receivers are deployed in the well and sources are placed at the surface, and cross-well arrays where the source array is placed in one well and the receivers in another. Storage projects have added to improved understanding of the reservoir where these tools were linked to other methods.

For example time-lapse cross well tomography conducted at the Frio test and at Cranfield provided the most resolved image of the plume evolution, and was used to constrain fluid flow data collected using introduced and natural tracers. At Frio, the baseline was collected prior to the start of injection in 2004 and then about 3 months after the end of injection. This images showed that plume swept fairly homogeneously through the reservoir, however gravity effects cause pronounced thinning over the 100 foot well spacing. At Cranfield a baseline was acquired in both observation wells prior to perforation and tubing completion and a repeat was conducted 9 months after start of injection when the wellbore logging and the geochemical sampling programs were completed. Results revealed strong heterogeneity in the distribution of CO₂ (Hovorka and others, 2012).

Crosswell seismic data is valuable, and complementary to well-logging data, as it provides an inversion of the CO₂ distribution in the interwell (fig. A-1).

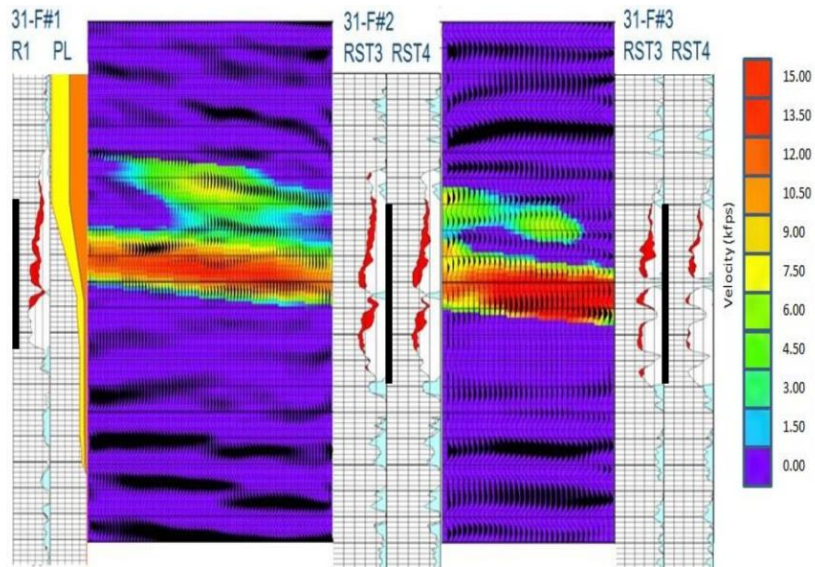


Fig. A-1. Crosswell seismic survey and RST integration at DAS. Injection well located on the left. From Butsch, 2012.

Two other tests of cross-well seismic provide important information on the limits of sensitivity of this technique. At the Nagaoka, Niigata prefecture, Japan, in an onshore experimental site where 10,400 metric tons of CO₂ were injected, the plume was imaged by time-lapse cross-well (Saito and others, 2006 and Zue and others, 2006). However the high frequency time-lapse logging (Mito and others, 2008) was able to resolve CO₂ arrival at wells when the cross-well did not image it. In addition, inversion of the image did not eliminate the possibility that changes could have occurred outside the target zone. Cross-well seismic was deployed at the Gaylord, Michigan CO₂ injection site (Battelle, 2011), and showed perturbations related to substitution of CO₂ for brine and increase in pressure below a regional seal. However, the effect of fluid substitution and pressure could not be separated, and uncertainty remained about the extent to which CO₂ was confined to the target reservoir (Bass Island Dolomite) or invaded overlying less permeable units, the Bois Banc Formation. These limitations are valuable because (1) recognitions of limits avoids investment failure, in that reliance on these tools can be designed with limitations in mind, and (2) additional research can be focused on limitations.

Cross-well Continuous Active Seismic Source Monitoring -CASSM- (Daley and others, 2007) was designed to deal with issues raised by monitoring geologic storage. In particular, placing a source at depth in a site under CO₂ injection requires removing the tubing and packers, which in turn requires that the well be filled with dense brine “kill fluid” to offset the pressure and buoyancy of injected CO₂. This kill fluid dramatically changes the near-well bore environmental at the perforations, which

damages the ability to measure saturation correctly with well based logging tools and may damage performance of other instrumentation. One solution to the need to kill the well is not to perforate the well in the injection zone, however this means that pressure and geochemical data cannot be collected. LBNL undertook designing a ceramic source conveyed on tubing (CASSM) to create a solution to this problem. The tubing is run through the source, providing access to the perforations as in a traditionally-completed well. The seismic source can be operated continuously, providing excellent repeatability and stacking. Multiple sources can be used in the same wellbore. CASSM was successfully deployed in the Frio test and documented the process of breakthrough. CASSM was undertaken between the two DAS observation wells at Cranfield to observe high frequency time-lapse changes in velocity caused by replacement of brine by CO₂. Valuable measurements of seismic response to pressure increase were obtained pre-injection during the hydrologic tests; however, failure of hydrophone seals prior to the CO₂ injection phase prevented data collection relevant to multiphase flow with this instrument (Hovorka, 2012). Additional deployment is recommended with improved receiver engineering that can withstand the downhole environment.

Electrical tomography

Electrical tomography methods have been traditionally, and successfully, used to monitor shallow subsurface fluid flow. Long-electrode electrical resistance tomography (LEERT) was evaluated for application at the Weyburn field (White, 2012). First, a numerical model was designed to assess the resolution and sensitivity of the method in a field environment. The modeling study indicated that none of the conditions that were considered produce data with adequate signal-to-noise ratio to image the resulting CO₂ plume. So, LEERT was concluded to be unsuited for direct CO₂ monitoring at the Weyburn field.

Placing an electrode array at depth greatly increases resolution; the main problem is to isolate the electrical field from the steel casing of the well. EM methods exist that are designed to be able to filter out the effect of the casing. A novel test was conducted at Lost Hills, during a water flood and CO₂ pilot, in which cross-well acoustic and EM were jointly inverted (Wilt and Morea, 2004; Lee and Uchida 2005). However an attempt to use borehole EM in a CO₂ environment to image CO₂ at the Frio test (K. Dodds, 2004) was not able to extract signal from the noise created by steel casings.

Cross well and surface to-well electrical resistivity arrays were first used in a CO₂ storage monitoring environment at the GFZ Ketzin site (Schmidt-Hattenberger and others, 2011) the Vertical Electrical Resistivity Array (VERA) was successful in observing and inverting a significant resistivity increase at the approximate depth of the injection zone.

At Cranfield, cross-well continuous electrical resistivity tomography (ERT) was undertaken successfully between the two DAS observation wells (Carrigan and others, 2009; X. Yang and others, in press). The technology consists of measurements between pairs of electrodes that provide high-frequency updates on conductivity changes introduced by changing CO₂ saturation. The installation

of such electrodes, however, requires nonconductive casing and a completion design that allows individual wires to be run from each electrode to the surface without damage. At Cranfield, installation caused high cost, suspected interference with other instruments (borehole seismic and borehole resistivity logs), and lost of connection to about ¼ of the electrodes. Improved technologies are required for easier and reliable installation of ERT before this tool can be deployed commercially at reservoir depths (Hovorka et al. 2012).

Although not completely tested in the public domain, GCS research results seem to indicate that the applicability of these new techniques to EOR and production settings holds high promise. New geometries and instruments are currently in development.

Gravity

Gravity collected from airplane, surface, or ship has been a resource exploration tool since early in the 20th century, with the value resulting from areas where higher or lower rock density signaled locations where structures such as salt domes formed oil traps. In recent decades, improvements in the resolution of gravity measurement have resulted in the use of this method in time lapse for assessing changes in fluids. Measurements fluid changes in near surface systems such as ice and groundwater have been made with the GRACE Satellite based platform (Adams, 2002). Time lapse gravity has been used for tracking fluid changes in the subsurface. In some cases the measurements have been made from the surface, which has the advantage of allowing dense spatial coverage for a number of producing fields under waterflood (Brady and others, 2002; Krahenbuhl and others, 2010.)

Gravity was pioneered for CO₂ injection at Sleipner (Alnes and others, 2011), where it provided a complementary measurement to seismic (Arts and others, 2004). This use of two complementary techniques is part of the benefit of large scale research, which validates and improves quantification of each technique.

In other cases, the change in gravity is too small to be detected with existing instruments at the surface. Gravity instruments that can be deployed closer to the fluid substitution by lowering them into the well are available. Time-lapse borehole gravity measurements were collected within the detailed area of study (DAS) wells at Cranfield Field Mississippi, as a CCP monitoring study conducted at the SECARB Early test. The borehole gravimeter data were evaluated for the sensitivity to both the larger scale geologic response and the smaller time-lapse signal from injected CO₂. All four data sets, two for each observation well, demonstrated distinct Poisson jumps at the boundaries of the Cranfield reservoir and are considered successful in reflecting the lower density of the reservoir of the site (Dodds, 2012). Assessment of the change in fluid is hampered by error in instrument relocation, noise and instrument drift. However final data are interpreted as showing a significant decrease in density within the reservoir as CO₂ was emplaced. Resolution is surprisingly good, showing the separation

between the upper and lower flow units. These uses in research mode show promise for additional commercial applications, including direct measurement of fluid substitution during production.

Wireline logging

Wireline logging is a workhorse of reservoir characterization. Several novel elements are contributed from experiments in geologic storage monitoring. Simpler fluid environments provide the same benefit as noted in the section on seismic, to increase quantitative rigor of saturation detection. Pre-injection baseline logging in a setting with only brine as a pore fluid, followed by detailed assessment of the ability of the formation to transmit fluids adds greatly to confidence and precision of measurements. Confidence and precision can then be translated to perturbed and complex reservoir settings. Significant two-phase experiments have been conducted and put in the public domain, where cross-lab and cross method comparisons can be made, including some of the first sets of public domain assessments of CO₂ saturation in the lab (Bachu and Bennion, 2008; Benson Lab, 2013; Akbarabadi and Piri, 2011).

Pulse neutron logging is a well understood technology that has been used for many years to monitor fluid movement in reservoirs. Results from pulsed neutron measurements are often the standard to which other monitoring measurements are compared. The Frio test was one of the first test to use RST in an experimental CO₂-brine setting (Sakurai et al, 2005). In the Cranfield DAS wells, even with complex wellbores and difficult logging conditions, the Schlumberger reservoir saturation tool (RST), a pulse neutron based tool, was able to provide insight on the saturations and volumes of the different fluids in the reservoir, and how these were changing with time (Butsch et al, 2012). However, uncertainty is introduced when correcting for change in tubing fluids when brine is replaced by CO₂. Other wireline tools, such as sonic and resistivity, had difficulty with noise at the DAS wells, perhaps because of interference by complex completions. RST is presently being successfully used in Gulf Coast commercial EOR applications. Pulsed neutron data was also collected at the Gaylord Michigan test injection (Battelle, 2011). The Gaylord test illustrated some of the uncertainties with pulsed neutron techniques, in low permeability carbonates.

Temperature monitoring

Thermal response is a classic tool for tracking fluids, especially in cases where flow is focused in a narrow zone, because temperature measurements are easily made and relatively simple to interpret. However, in-reservoir use is limited because the thermal mass of the reservoir buffers signal.

Fiber optic cables were deployed at the Cranfield DAS for distributed temperature sensing (DTS). DTS is a technology that consists of sending a pulse of light down a fiber optic cable installed along the

casing or tubing of a well from the surface to total depth and back. This technology produces quasi-continuous temperature profiles along the entire length of wells providing high temporal and spatial resolution. Borehole temperature data is used to determine the physical properties and the state of the CO₂ and to draw conclusions on flow processes inside the formation and along wells. At DAS, temperature measurements were acquired every meter along the wellbore, with sample rates that ranged from 2 to 15 minutes. Figure A-2 shows more than three hundred million temperature measurement recorded from November 2009 to July 2010, (Nuñez-Lopez, 2011).

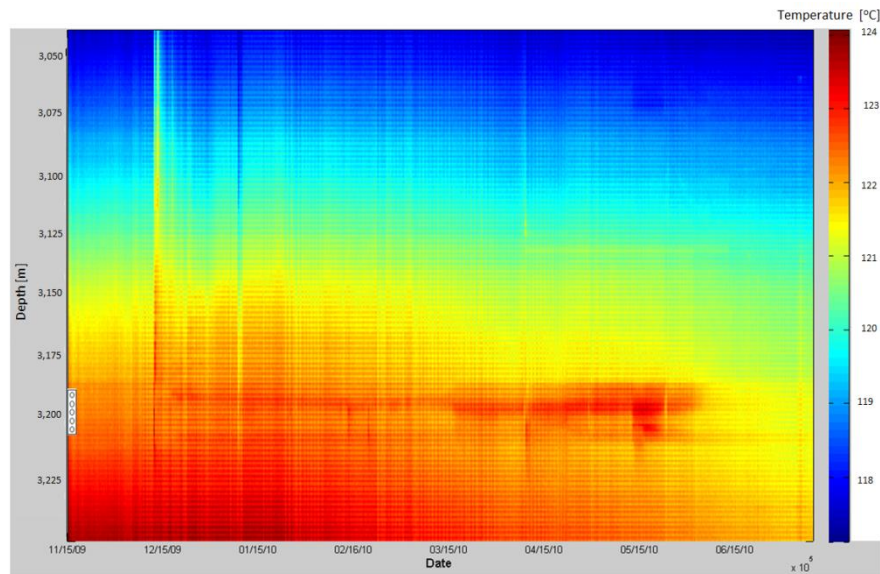


Fig. A-2. Temperature evolution, vertical distribution, and timing of temperature disturbances from Nov. 14th 2009 to July 7th 2010 at observation well F3.

A novel technique developed for a number of applications introduces a heater cable so that a controlled temperature increase can be induced. The speed of the recovery can be inverted to consider fluid flow and changes in the specific heat as the fluid composition changes. Perturbed pressure has been deployed at CO₂SINK project at the Ketzin field (Freifeld and others, 2007) and that the SECARB test at Citronelle. Perturbed temperature sensing has a potential applicability to EOR, to evaluate changes in fluid saturation that would be of high value in the assessment of the flood and in the modification of strategies as injection becomes mature. The demonstrations for CCS research provide information on the sensitivity of the method. Assessment of validity of the method has not been undertaken in the EOR context.

Pressure monitoring

Pressure monitoring in the reservoir is essential for commercial production, and a classic surveillance tool used for the calibration of numerical fluid flow models. Geologic storage projects have added value to this method by collecting novel and publically accessible data sets. Novel elements provided by geologic storage experiments include data collected (1) in minimally perturbed environments, (2) in close spatial distances, and (3) at high frequency. Integration of pressure data with geomechanical evaluation is also a novel approach. The value of these data for commercial application has not been fully developed, but opportunities are opened.

EOR is almost always conducted in a highly perturbed environment, where regional pressure drawdown from prolonged production has been partly offset by water injection. In these settings pressure evolution is so complex that a relatively coarse observation, for example by making episodic downhole measurements in some patterns is sufficient to document trends and constrain models. Storage tests have accessed relatively unperturbed fluid environments, which have allowed observation of much more subtle responses of the reservoir, which provide additional constrains to infer active processes in the reservoir. For example, the Frio tests at South Liberty Field Texas, Cranfield, Mississippi, Citronelle Alabama, and Gaylord Michigan tests were conducted in reservoir intervals that had not been produced for several decades prior to the test, allowing relatively simple measurements to be interpreted to high resolution not typically possible in the EOR context. Improved model matching methods can then be applied to more complex situations. Novel ideas, such as having a well out of the active pattern collect in-reservoir data that averages reservoir response and can be used to better calibrate the system come from these studies. For example, (Verma and others, -in press-) have documented the value of an idle well in passively accumulating changes in fluid composition during breakthrough without the cost of active sampling. Hosseini (in preparation) has modeled and is field testing a concept that uses time lapse changes in fluid compressibility to assess replacement of water by CO₂.

High-frequency pressure monitoring was confirmed as a highly valuable monitoring strategy at Cranfield. Pressure changes were observed in far-field wells, confirming reservoir architecture developed during characterization. Low cost pressure gauges installed in the well-heads of wells perforated in the injection zone can monitor pressure trends, as long as the pressure responses are calibrated to the density of the tubing fluids.

Above-zone pressure monitoring (AZMI)

Pressure surveillance in an above-zone monitoring interval (AZMI) has been used at gas storage sites for decades to assure that gas is not seeping out of the storage unit which is unacceptable both in terms of product loss and in terms of risk creation. This approach has been adapted for the same

purposes for geologic storage. AZMI pressure monitoring is conducted under the principle that any fluid intrusion into a shallower layer would cause a pressure increase on the hydrostatic pressure gradient (Zeidouni, 2012; Zeidouni and Pooladi-Darvish, 2012a; Zeidouni and Pooladi-Darvish, 2012 b). Careful selection of the AZMI is required as for this interval to be a successful monitoring element it needs to intercept as many hypothetical leakage paths as possible (Hovorka, 2012). An ideal AZMI is a laterally continuous thin zone that is sensitive to pressure perturbations.

Conceptual and analytical models were developed for interpreting continuous AZMI pressure and temperature monitoring data (fig. A-3) in the case that the wellbore is the monitoring leakage path (Tao et al, 2012). Results from modeling the pressure response and temperature response were consistent and proved that wellbore permeability can be estimated. If the results contradict, as it was observed in the case of the high volume injection observation well (EGL7), the wellbore is not the primary leakage pathway. The application to Cranfield data show that the dedicated observation well (EGL7) is unlikely to be leaking. However, this conclusion does not rule out the possibility that leakage can occur through other leakage pathways.

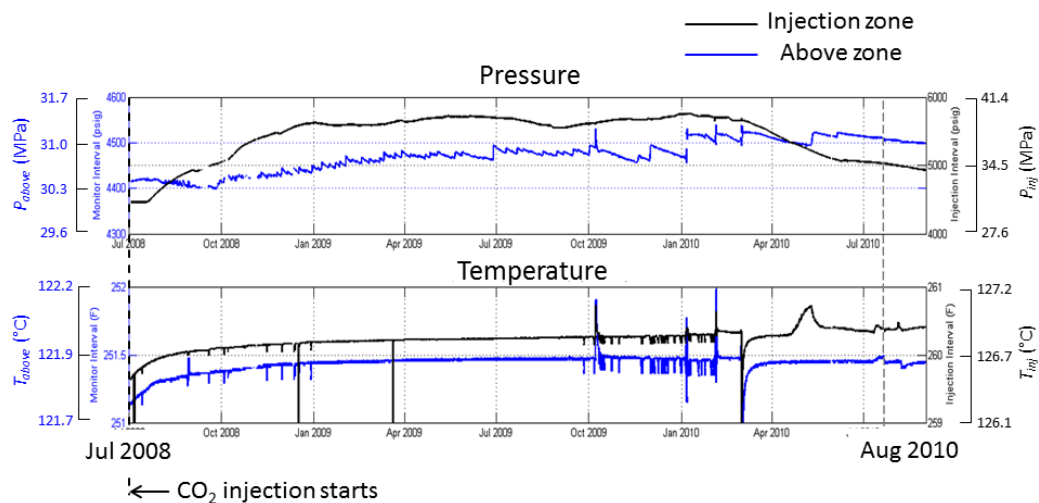


Fig. A-3. Plot of over 2 years (July 2008 to August 2010) of continuously recorded pressure and temperature data for the injection zone and AZMI (Meckel and Hovorka, 2010). Pressure in the injection zone rises within a month after CO₂ injection starts. Pressure in AZMI increases two months later, indicating a possible wellbore leak. Temperature data suggest a first-order isolation as both zones recover to distinct baselines, maintaining a linear correlation with a consistent differential of ~4.9°C (~8.8°F). From Tao, 2012.

It is well known that pressure-transient analysis provides information on the size and shape of the formation and its ability to produce/receive fluids. Pressure transients are also used as a metric for matching numerical flow model conformance with observed production/injection history. However, the identification of well leakage through pressure history matching can be challenging due to the subtle effects these leaks can have on the characteristic pressure magnitude evolution (Meckel, 2013).

At Cranfield, Meckel et al. (2010) developed a broadly applicable technique for the analysis of pressure transients in continuous time series. This technique uses a combination of theory, an analytically-derived synthetic reservoir pressure history example, and analysis of field pressure data. The analysis focuses on the second derivative (d^2P/dt^2) of the continuous pressure time series, and it shows that d^2P/dt^2 transients reveal consistent relationships with known (theoretical case) or induced (field case) pressure perturbations that are independent of prior pressure history. This fact makes the second derivative of the continuous pressure time series a very useful diagnostic tool for identifying and evaluating observed transients of unknown origin, such as well leakages.

A novel tool array, the Westbay multi-port sampler (Koch and Person, 2007), which has been deployed at a number of sites for monitoring high concern fresh-water aquifers, has recently been adapted for use at reservoir depths and pilot-tested at Midwest Geological Sequestration Consortium's CO₂ injection test site at Decatur, IL (Schlumberger Water Services, 2011). In this setting it is used to separately isolate and measure pressure and fluids across the injection reservoir and above the lowest seal. This tool may prove useful for understanding the response of a thick, hydrologically interconnected reservoir to flooding. For example, installation of such a multi-level sampler would be useful to understand how to efficiently exploit the ROZ of the Permian Basin, but the EOR application has not been tested in the public domain.

Groundwater monitoring

Groundwater monitoring is required for some industries that use the subsurface, such as mining and various types of near-surface waste disposal and not part of the expectations for deeper uses of the subsurface, such as deep fluid disposal under UIC class I, or oil and gas operations. However, groundwater monitoring may come to be expected more widely of various industries, in response to public concern, and is an expected activity in carbon storage projects under the US EPA UIC class VI rules. Carbon storage therefore provides a pioneer effort into what is feasible and productive and what is not useful in providing the wanted public assurance. GCS advances in this area could be useful for EOR if groundwater monitoring is required in the future.

The naïve assumption is that making measurements of groundwater chemistry prior to industrial activity will provide the baseline needed to prove that no contamination to potable water has occurred as a result of the CO₂ injection (U.S. EPA, 2009). As experience with monitoring groundwater builds, information about the complexity of achieving the desired finding increases. Four reasons for failure of "baseline" style monitoring are noted (Wolaver and others, in preparation):

- 1) Noise in the system measured is higher than the leakage or failure signal.
- 2) Ambient or introduced trend in the system measured overlaps the trend that would be induced by failure. For example climate change or urbanization may cause systematic changes that mimic leakage.

- 3) Failure or damage does not significantly and reliably perturb the system measured. For example the failure signal could be too localized or too transient to be detected by the monitoring array.
- 4) Pre-injection data collected in a different area than where changes resulting from injection are observed.

Robust and protective monitoring can only be achieved if the role of a pre-injection baseline in diagnosing indicators of loss of storage value or other damaging events is critically and quantitatively assessed. It is critical for monitoring success that characterization and explicit modeling of failure be conducted to define triggers that are to be detected by monitoring. One key function of pre-injection data collection is characterization and site-specific evaluation of noise, trends, frequency, and spatial variability of signal to determine the sensitivity of the monitoring array to leakage detection.

At the Weyburn field, more than 60 samples were collected during seven shallow groundwater surveys conducted between 2000 and 2009. Results (fig. A-4) revealed a highly variable composition in the area, generally of the Ca-Mg-SO₄-HCO₃ type. (Johnson, 2012)

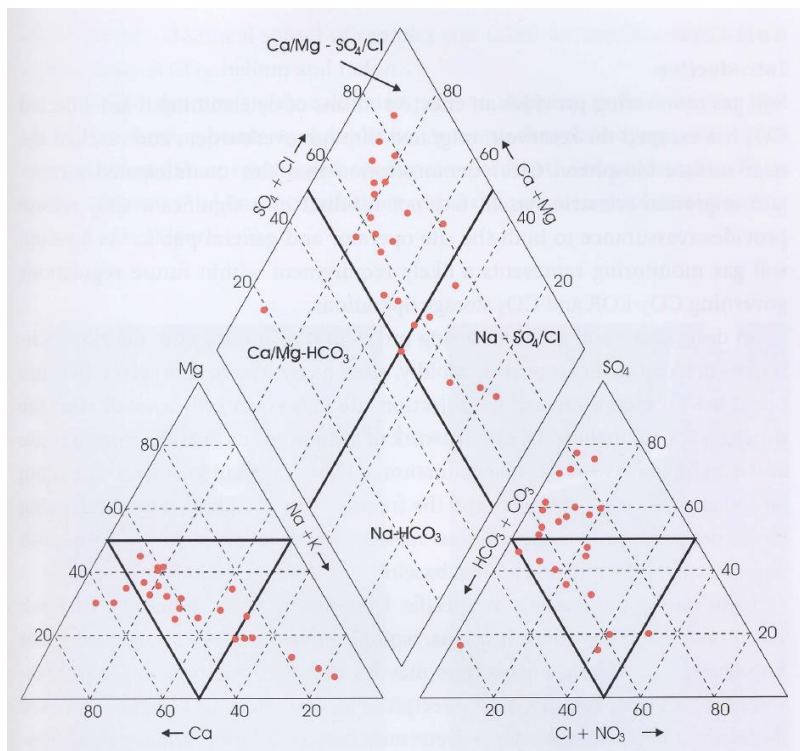


Fig. A-4. Piper plot of water composition from domestic and farm wells in the Weyburn project area. From Johnson, 2012.

An extensive sample-based study of groundwater geochemistry over SACROC did not find evidence that any leakage had occurred (Romanak and others, 2012), although the groundwater-rock-system is shown in models and in the lab to be sensitive to CO₂ leakage should it occur. However, Smyth (personal statement) warns that although the sampling data is quite dense and the signal well-assessed, a very strong statement that no leakage has occurred cannot be made, because reactive

transport modeling to show the sample density needed to document no-leakage between sampling points, and deep sampling have not been conducted. Exhaustive consideration of the leakage options would include more intensive characterization, modeling, and possibly additional sampling. This study which collected a large number of samples over a multi-year period over a large and mature EOR site provides an important and widely applicable recommendation not to underestimate the investment in terms of characterization and number and types of samples collected needed to conduct a valid groundwater monitoring deployment.

At Cranfield, groundwater evolution trends have not been interpreted as leakage. To increase the robustness of the interpretation of the data as no evidence of leakage, and shallow “controlled leakage” push-pull experiment was conducted, where groundwater from a shallow aquifer was extracted, saturated with CO₂, in reinjected to measure the parameters changed by in-situ rock-water, dissolved CO₂ reaction. The test showed that the rock water reaction at in-situ conditions was slightly weaker, although still considered similar in scale, than the reaction observed in laboratory studies (Yang and others, 2012).

Soil gas monitoring

Soil gas measurements are a tool widely used for assessing natural migration of fluid migration out of the subsurface. They are also used at contaminated sites to map the extent of contamination in cases where contamination produced a diagnostic signal, such as volatile organic carbons from an oil spill. Because the goal of monitoring geologic storage is to demonstrate retention of CO₂ in the subsurface, monitoring soil gas flux across the soil-air interface was identified as an attractive monitoring technology (Klusman, 2003). In addition, a number of variations on the exploration tools testing gas in the vadose zone and soil profile were identified as monitoring prospects.

Soil gases have a number of advantages as a monitoring approach, in that they are low cost ways to get a broad overview of a dynamic system. However, their suitability detection of leakage of CO₂ from a reservoir at depth is unproven. Uncertainties arise because 1) the transport distance is long, 2) transport mechanisms are understudied, 3) CO₂ is fairly soluble and natural analog studies (Gilfillan and others, 2010, Gilfillan and others, 2011) show that signal may be attenuated or delayed, 4) CO₂ generated by non-leakage processes may mimic or mask leakage signal, and 5) leakage signal may be focused in an area between sample points or outside of the sample pattern (Lewicki et al, 2005). Studies of natural analogs and controlled leakage experiments underway to support the development of this method may help to determine the usefulness and optimization of the methods.

The application to EOR might be limited to cases where storage falls under programs requiring such monitoring. However, other uses may become apparent as research matures. One potential benefit

is Romanak's "process-base" method for addressing leak allegations, discussed later in the Stakeholders Interactions section.

The first and most deeply studied controlled release site is the Zero Emission Research and Technology Center (ZERT) experiment, at the agricultural station at Montana State University, however growing number of tests are underway internationally in a wide variety of settings (Spangler, 2012).

One interesting synthesis of reported preliminary results from controlled releases is that lateral transport has been greater than expected at a number of sites, with the emergence of the CO₂ not over the release site but laterally some distance away. This fits a model shown by natural spring and vents, which can be focused at intersections of geologic features and structures (Lewicki et al, 2007).

Also at Cranfield, typical background vadose gas compositions were obtained through a reconnaissance soil gas survey undertaken in 2008 near historic wells, and through a repeat survey in 2010. An elevated concentration of methane and CO₂ was identified during the first survey beneath a plugged and abandoned production well scheduled to be reactivated for production was adopted as a study site (Yang et al, 2012). The anomaly was mapped utilizing an array of 3m-deep soil gas instruments deployed over an area of 100m², referred to as the *P-site* (fig. A-5). Mud-logs were used to assess the sources of deep methane. Workover activities found the cement plugs in good condition; the source and transport mechanism for the thermogenic methane is not well understood. CO₂ is plausibly a biodegradation product from methane. Perfluorocarbon tracers (PFT) were placed at bottom-hole during completion, and monitoring of soil-gas composition and tracers is continuing seeking evidence of Jackson Dome CO₂ in soil gases. Production records indicate that CO₂ arrived in the reservoir in this area before August 2010, monitoring continues to identify any compositional changes.

A novel "process-based" approach (Romanak and others, 2012) was developed as part of the Cranfield project for separating in-situ generated gases from exogenous gases. The process-based method considers the ratios of N₂, O₂, CO₂, and CH₄ to distinguish gases from processes that originated in the vadose zone from incoming gases that migrated from depth. An important value of this methodology over the traditional mapping of gas concentration is the reduced need for background measurements to identify leakage signals. This method was applied at Kerr Farm, a site in the vicinity of the Weyburn field, where farm owners claimed contamination with CO₂ from the EOR operation.

During Phase 1 of the Weyburn program, annual soil gas surveys were conducted from 2001 to 2005 and again in 2011, generally to measure CO₂ fluxes and stable isotopes. Three techniques were employed: (1) discontinuous gas measurements, (2) discontinuous depth profiles measurements, and (3) continuous monitoring. Results indicate that stable isotope data on their own are inconclusive. But in combination with the measured soil gas CO₂ content indicates there is a clear isotopic depletion

with increasing CO₂ concentration, which further supports the interpretation that the observed trend is caused by isotopic fractionation via biogenetic composition of organic matter (Johnson, 2012).

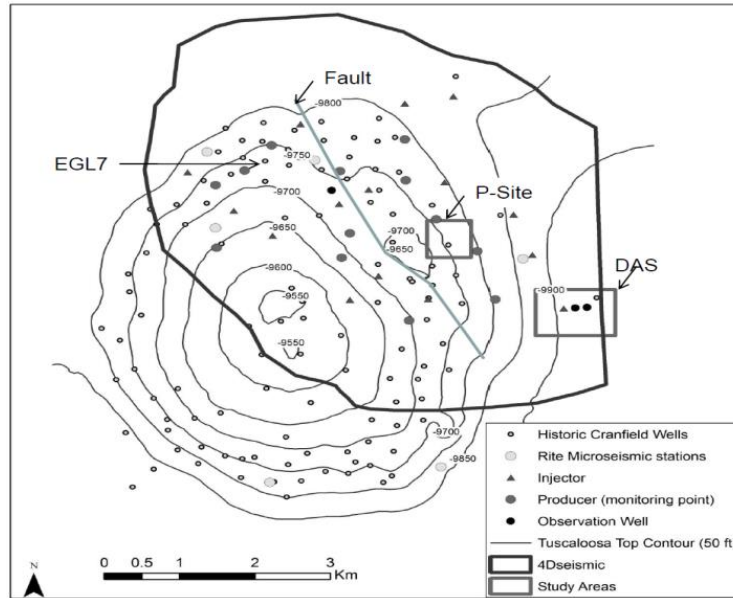


Fig. A-5. P-site and re-activated producer where the vadose zone was instrumented.

References

- Adam, D. 2002. Gravity measurement: Amazing grace. *Nature*, 416 (6876): 10-11.
- Akbarabadi, M. and Piri M. 2011. Geologic storage of Carbon Dioxide: An experimental study of permanent capillary trapping and relative permeability. Department of Chemical & Petroleum Engineering, University of Wyoming. This paper was prepared for presentation at the International Symposium of the Society of Core Analysts held in Austin, Texas, USA 18-21 september, 2011
- Alnes, Harvard; Eiken, Ola; Nooner, Scott; Sasagawa, Glenn; Stenvold, Torkjell and Zumberge, Mark. 2011. Results from Sleipner gravity monitoring: Updated density and temperature distribution of the CO₂ plume. *Energy Procedia*. Vol. 4, 5504-5511
- Arts, R., Eiken, O., Chadwick, R.A., Zweigel, P., Van Der Meer, L., and Kirby, G.A. 2004. Seismic monitoring at the Sleipner underground CO₂ storage site (North Sea). In: Baines, S. and Worden, R.J. (Eds.) *Geological Storage for CO₂ emissions reduction*. Geological Society, London, Special Publication 233, 181-191.
- Arts, R.; Chadwick R.A.; Eiken, Ola; Thibeau, Silvain and Nooner Scott. 2008. Ten years's experience of monitoring CO₂ injection in the Utsira Sand at Sleipner, offshore Norway in *First Break*. Vol 26, 65-72. http://www.ideo.columbia.edu/~snooner/Nooner/Publications_files/fbjan08_05.pdf
- Bachu, Stefan and Bennion Brant. 2008. E, Effects of in-situ conditions on relative permeability characteristics of CO₂-brine systems, *Environmental Geology*, June 2008, Volume 54, Issue 8, pp 1707-1722
- Battelle. 2011. Best Practice Manual for Midwest Regional Carbon Sequestration Partnership Phase II Geologic CO₂ Sequestration Field Validation Test. Prepared for the U.S. Department of Energy, NETL. April, 28. http://www.netl.doe.gov/technologies/carbon_seq/infrastructure/rcsp/mrcsp/mrcspmibasinvalidationrpt_final.pdf
- Bennion, B., Bachu, S., 2008, Drainage and imbibition relative permeability relationships for supercritical CO₂/brine and H₂S/brine systems in intergranular sandstone, carbonate, shale, and anhydrite rocks, *SPE Reservoir Evaluation Engineering*, 11, 487-496, DOI: 10.2118/99326-PA.
- Benson Lab. 2013. Relative permeability explorer: a data base of relative permeability. Accessed on January 25. <https://pangea.stanford.edu/research/bensonlab/relperm/index.html>
- Bolhassani, Behnaz, Hovorka, S. D., Hosseini, S. A., Young, M. H., Anderson, J.S., and Yang, C, 2017, Model-based assessment of the sitespecific cost of monitoring, *Energy Procedia*, 13th International Conference on Greenhouse Gas Control Technologies, GHGT-13, 14-18 November 2016, Lausanne, Switzerland.
- Busch, A., Alles, S., Gensterblum, Y., Prinz, D., Dewhurst, D.N., Raven, M.D., Stanjek, H., Krooss, B.M., 2008. Carbon dioxide storage potential of shales. *International Journal of Greenhouse Gas Control* 2, 297–308.
- Cavanagh, A. and P. Ringrose (2011). "Simulation of CO₂ distribution at the In Salah storage site using high-resolution field-scale models." *Energy Procedia* 4(0): 3730-3737.
- Cavanagh, Andrew. 2011. Calibration and prediction of the Sleipner CO₂ plume from 2006 to 2012. American Geophysical Union, Fall Meeting 2011, abstract #H42C-04. <http://adsabs.harvard.edu/abs/2011AGUFM.H42C.04C>

- Carrigan, C R ; Ramirez, A L ; Newmark, R L ; Aines, R and Friedmann, S. J. 2009. Application of ERT for tracking CO₂ plume growth and movement at the SECARB Cranfield site, presented at: 8th Annual Conference on Carbon Capture & Sequestration, Pittsburgh, PA, United States, May 4-7, 2009.
- Chadwick, R.A., Zweigel, P., Gregersen, U., Kirby, G.A., Holloway, S. and Johannessen P.N. 2004. Geological reservoir characterization of a CO₂ storage site: The Utsira Sand, Sleipner, northern North Sea. *Energy* 29, 1371-1381.
- Chadwick, R.A., Arts, R., Eiken, O., Williamson, P., and Williams, G. (2006). Geophysical monitoring of the CO₂ plume at Sleipner, North Sea: an outline review. In: Lombardi, S., Altunia, L.K., and Beaubien, S.E. (Eds.) *Advances in the Geological Storage of Carbon Dioxide*. Springer, Dordrecht, NATO Science, IV Earth and Environmental Sciences Vol. 65, 303-314.
- Daley, T.M., Myer, L.R., Peterson, J. E. Majer, E.L. and Hoversten, G.M. 2007. Time-lapse crosswell seismic and VSP monitoring of injected CO₂ in a brine aquifer, *Environmental Geology*, July. LBNL-62396.
- Doughty, C. Freifeld, B.M., Trautz, R.C., 2008, Site characterization for CO₂ geologic storage and vice versa: The Frio brine pilot, Texas, USA, as a case study, *Environmental Geology*, 54, 1635-1656.
- Gilfillan, S. , Wilkinson, M. , Haszeldine, R. S. , Nelson, S. & Poreda, R. Jun. 2010. He and Ne as tracers of natural CO₂ migration from a deep reservoir. In: *Geochimica et Cosmochimica Acta*. 74, 12, p. A331-A331. 1 p.
- Gilfillan, S. M. V. , Wilkinson, M. , Haszeldine, R. S. , Shipton, Z. K. , Nelson, S. T. & Poreda, R. 2011 He and Ne as tracers of natural CO₂ migration up a fault from a deep reservoir: *International Journal of Greenhouse Gas Control*. 5, 6, p. 1507-1516. 10 p.
- Hosseini, S. A., Lashgari, H., Choi, J. W., Nicot, J. P., Lu, J., Hovorka, S. D., 2012. Static and Dynamic Reservoir Modeling for Geological CO₂ Sequestration at Cranfield, Mississippi, U.S.A. *International Journal of Greenhouse Gas Control*. DOI: 10.1016/j.ijggc.2012.11.009
- Hovorka, S. D., Meckel, T.A., Treviño, R., 2012. Monitoring a Large-volume Injection at Cranfield, Mississippi - Project Design and Recommendations, *International Journal of Greenhouse Gas Control*.
- Jerry L. Brady, John F. Ferguson, John E. Seibert, Tianyou Chen, Jennifer L. Hare, Carlos V.L. Aiken, Fred J. Klopping, John M. Brown, Micro-g Solution, Inc; 2002, Surface Gravity Monitoring of the Gas Cap Water Injection Project - Prudhoe Bay, Alaska, SPE Annual Technical Conference and Exhibition, 29 September-2 October 2002, San Antonio, Texas 77513-MS, DOI 10.2118/77513-MS.
- Jordan, Preston and Doughty Christine. 2009. Sensitivity of CO₂ migration estimation on reservoir temperature and pressure uncertainty. *Energy Procedia* 1, 2825-2832.
- Johnson, J. W. et al. 2012. Geochemical Monitoring. In B. Hitchon (Editor), *Best Practices for Validating CO₂ Geological Storage*, 155-210. Geoscience Publishing.
- Krahenbuhl, Richard A; Li, Yaoguo and Davis, Tom. 2010. 4D gravity monitoring of fluid movement at Delhi Field, LA: A feasibility study with seismic and well data. Center for Gravity, Electrical & Magnetic Studies (CGEM). http://geophysics.mines.edu/cgem/pdf%20files/Krahenbuhl_Li_Davis%202010.pdf SEG Expanded
- Koch, Richard J. and Pearson, Steven G. 2007. Evaluation of Sampling Systems for Multiple Completion Regional Aquifer Wells at Los Alamos National Laboratory. LA-UR-07-4034. August, EP2007-0486, <http://permalink.lanl.gov/object/tr?what=info:lanl-repo/lareport/LA-UR-07-4034>

- Lee, Tae Jong and Uchida, Toshihiro. 2005. Electromagnetic travelttime tomography: Application for reservoir characterization in the Lost Hills oil field, California. *Geophysics*, May 2005; 70: 51 - 58.
- Lewicki, J.L., Hilley, G.E. and Oldenburg, C.M. (2005). An improved strategy to detect CO₂ leakage for verification of geologic carbon sequestration. *Geophysical Research Letters* 32(19): doi: 10.1029/2005GL024281. issn: 0094-8276.
- Lewicki, J.L., Birkholzer, Jens and Tsang Chin-Fu. 2007. Natural and industrial analogues for leakage of CO₂ from storage reservoirs: identification of features, events, and processes and lessons learned. *Environ Geol.* 52:457–467. DOI 10.1007/s00254-006-0479-7
- Liu F., Lu P., Griffith C., Hedges S., Soong Y., Hellevang H., Zhu C., 2012. “CO₂-brine-caprock interaction: Reactivity experiments on Eau Claire shale and a review of relevant literature”, *International Journal of Greenhouse Gas Control* 7, Elsevier, 153-157.
- Melzer, S., 2012. “Carbon Dioxide Enhanced Oil Recovery (CO₂ EOR): Factors Involved in adding Carbon Capture, Utilization and Storage (CCUS) to Enhanced Oil Recovery.” Report for Center for Climate and Energy Solutions.
- Meckel T.A. and Hovorka S.D., 2010. Above-Zone Pressure Monitoring as a Surveillance Tool for Carbon Sequestration Projects. SPE International Conference on CO₂Capture, Storage, and Utilization. New Orleans, Louisiana, USA, 10–12 November 2010.
- Mito, Seako, Xue, Ziqie and Ohsumi Takashi. 2008. Case study of geochemical reactions at the Nagaoka CO₂ injection site, Japan. *International Journal of Greenhouse Gas Control* 2. 309-318.
- Nicot, J. P., Hosseini, S.A., and Solano, S.V., 2011. Are single-phase flow numerical models sufficient to estimate pressure distribution in CO₂ sequestration projects? *Proceedings of the 10th International Conference on Greenhouse Gas Control Technologies GHGT10*, September 19-23, 2010, Amsterdam, The Netherlands, *Energy Procedia*. 4, 3919-3926. GCCC Digital Publication #11-14.
- Nicot, J.-P., C. M. Oldenburg, J. E. Houseworth, J.-W. Choi, this issue. Analysis of potential leakage pathways at the Cranfield, MS, U.S.A., CO₂ sequestration sit. *International Journal of Greenhouse Gas Control*.
- Nogues, J.P., Nordbotten, J.M., Celia, M.A., 2011. Detecting leakage of brine or CO₂ through abandoned wells in a geological sequestration operation using pressure monitoring wells. *Energy Procedia* 4, 3620-3627.
- Nordbotten, J.M., Kavetski, D., Celia, M.A., Bachu, S., 2009. Model for CO₂ Leakage Including Multiple Geological Layers and Multiple Leaky Wells. *Environmental Science & Technology* 43, 743-749.
- Nooner, Scott; Zumberge, Mark; Sasagawa, Glenn, Eiken; Ola and Stenvold, Torkjell. A Baseline Gravity Survey over the Sleipner CO₂ Sequestration Site.
- Núñez-López, Vanessa, Holtz, M., 2007. Quick-look assessments to identify optimal CO₂ EOR storage sites, Special Issue "Site Characterization for CO₂ Geological Storage". *Journal of Environmental Geology*. Springer-Verlag, DOI 10.1007/x00254-007-0940-2, 15 p.
- Núñez-López, V., 2011, Temperature monitoring at SECARB Cranfield Phase 3 site using distributed temperature sensing (DTS) technology. GCCC Digital Publication Series #11-10.

- Official Journal of the European Union. 2009. EU Directive on the Geological Storage of Carbon Dioxide; accessed April 18, 2012. <http://eurlex.europa.eu/LexUriServ/LexUriServ.do?uri=OJ:L:2009:140:0114:0135:EN:PDF>.
- Okamoto, I., Li, X., Ohsumi, T., 2005. Effect of supercritical CO₂ as the organic sol-vent on cap rock sealing performance for underground storage. *Energy* 30, 2344–2351.
- Oldenburg, C. M., Bryant, S. L., and Nicot, J. -P., 2009. Certification framework based on effective trapping for geologic carbon sequestration. *International Journal of Greenhouse Gas Control*. 3, 444–457.
- Panda, M., Nottingham, D., Lenig, D., 2011. “Systematic Surveillance Techniques for a Large Miscible WAG Flood”, June 2011 SPE Reservoir Evaluation & Engineering, 299-309.
- Philip, R.P., and Crisp, P. T., 1981, Surface geochemical methods used for oil and gas prospecting-a review. *Journal of Geochemical Exploration*.. 17, 1-34.
- Romanak, K. D., Smyth, R. C., Yang, C., Hovorka, S. D., Rearick, M., and Lu, J., 2012. Sensitivity of groundwater systems to CO₂: application of a site-specific analysis of carbonate monitoring parameters at the SACROC CO₂-enhanced oil field. *International Journal of Greenhouse Gas Control*, v. 5, no. 1, p. 142– 152.
- Romanak, K. D., Zhang, T., Gilbert, K., Yang, C., Bennett, P., and Hovorka, S., 2010. Evaluation of CO₂, He, C1-C5 gaseous hydrocarbons at an engineered CO₂ injection, Cranfield, Mississippi. GCCC Digital Publication Series #10-04.
- Romanak, K.D., Bennett, P. C., Yang,, Changbing, Hovorka, S.D.,2012. Process-based approach to soil gas monitoring at geologic carbon storage sites. *Geophysical Research Letters*. 39, L15405, doi:10.1029/2012GL052426
- Rutledge, E. M., Guccione, M.J., Markewich, H. W., Wysocki, D. A., and Ward, L. B., 1996. Loess stratigraphy of the lower Mississippi Valley. *Engineering Geology*. 45, 167-193 Solano, S., and Nicot, J. -P., 2010, Gas-cap impact on CO₂ plume migration for long-term storage in saline aquifers. *Gulf Coast Association of Geological Societies Transactions*. 60, 643– 655.
- Saito, H., Nobuoka, D., Azuma, H., Xue, Z. and Tanase, D., 2006, Time-lapse crosswell seismic tomography for monitoring injected CO₂ in an onshore aquifer, Nagaoka, Japan, *Exploration Geophysics*, 37, p30-36
- Sakurai, Shinichi, Hovorka, S. D., Ramakrishnan, T. S., Boyd, A., and Mueller, N., 2005, Monitoring saturation changes for CO₂ sequestration: Petrophysical support of the Frio Brine Pilot Experiment, in SPWLA 46th Annual Logging Symposium: Society of Petrophysicists and Well Log Analysts, Paper No. 2005-YY
- Studlick, J.R.J., Shew, R.D., Basye, G.L., and J.R. Ray, 1990, A giant carbon dioxide accumulation in the Norphlet Formation, Pisgah Anticline, Mississippi, In: Barwis, J.H. McPherson, J.G. and Studlick, J.R.J. (Eds.), *Sandstone Petroleum Reservoirs*. Springer-Verlag, Inc., New York, pp. 181-203.
- Schlumberger Water Services. 2011. Use of the Westbay system for multilevel monitoring at the Illinois Basin Decatur Project carbon capture and storage site. <http://sequestration.org/resources/PAGNov2011Presentations/08-WestbayDecaturPresentationNov2011.pdf>
- Schmidt-Hattenberger, Cornelia; Bergmanna, Peter; Kießling, Dana; Krüger, Kay; Rückerb, Carsten; Schütt, Hartmut and Group, Ketzin. 2011. Application of a Vertical Electrical Resistivity Array (VERA) for Monitoring

- CO₂ Migration at the Ketzin Site: First Performance Evaluation. *Energy Procedia* 4, 3363–3370. <http://www.co2sink.org/publications/CSH%20Energy%20Procedia%202011.pdf>2011.
- Spangler, Lee. 2012. Overview of monitoring controlled releases. http://www.ieaghg.org/docs/General_Docs/Natr%20rel%20worksop/SPANGLER_SEC.pdf
- Tao, Q., Bryant, S. L., and Meckel, T. A. this issue. Above-zone measurements of pressure and temperature for monitoring CCS Sites. *International Journal of Greenhouse Gas Control*
- Tao, Q., Bryant, S.L., Meckel, T.A. and Luo, Z., 2012. Wellbore leakage model for above-zone 36 monitoring at Cranfield, MS. Carbon Management Technology Conference. Orlando, 37 Florida, USA, 7-9 February. Tao et al. 2012.
- Tianyou, Chen, John F. Ferguson, Carlos L.V. Aiken, and Jerry Brady, 2005. Real-time data acquisition and quality control for gravity surveys. *The Leading Edge*, 24, 702-704
- U.S. Environmental Protection Agency (EPA). 2009. Mandatory Reporting of Greenhouse Gases Rule (74 FR 56260) 40 CFR Part 98 (Part 98). Published in the Federal Register (www.regulations.gov) on October 30, under Docket ID No. EPA-HQ-OAR-2008 0508-2278.
- Vasco, D. W., Rucci, D.A. Ferreti, A, Novali, A.F., R. C. Bissell, P. S. Ringrose, A.S. Mathieson and I.W. Wright, 2010. Satellite-based measurements of surface deformation reveal fluid flow associated with the geological storage of carbon dioxide. *Geophysical Research Letters*.37, L03303, doi:10.1029/2009GL041544
- Verma, Sandeep, Oakes, Charles, Ramakrishnan, T. S., Malkewicz, Nick, Hosseini, S.A., Hovorka, S. D., 2011. Carbon dioxide sequestration at Cranfield – analysis of injection and observation well fluid pressure, temperature and density measurements. Ninth Annual Conference on Carbon Capture and Sequestration. DOE/NETL, Pittsburgh, Pennsylvania.
- Verma, Sandeep; Oakes, Charles; Ramakrishnan T.S., Malkewicz Nick, Hosseini Seyyed A. and Hovorka, Sue. 2012. Carbon Dioxide Sequestration at Cranfield – Analysis of Injection and Monitoring Well Data, abstract, GHGT 11.
- Vlassopoulos, D., Riley, M., and Darby, E., 2011, Reactive transport model for the shallow aquifer at Cranfield, MS. Anchor-QEA, unpublished contract report.
- White, D. et al. 2012. Geophysical Monitoring. In B. Hitchon (Editor), *Best Practices for Validating CO₂ Geological Storage*, 155-210. Geoscience Publishing.
- Wilt, Michael and Morea, Michael. 2004. 3D Waterflood Monitoring at Lost Hills with Crosshole EM. *The Leading Edge*, May 2004; 23 No. 5: 489 - 493. doi: 10.1190/1.1756840
- Wood, L., and Wolfe, K., in review, Sequence stratigraphic and paleogeographic framework for the Lower Tuscaloosa Sandstone, eastern Gulf of Mexico Province, U.S.A.: Influences on sediment distribution and depositional environments.
- Wolaver, B. D., Hovorka, S.D., and Smyth, R.C., in prep. 2013. CO₂ Sequestration at Greensites and Brownsites: Contrasting Characterization, Risk Assessment, and Monitoring.
- Xue, Z., Tanase, D. and Watanabe, J. 2006. Estimation of CO₂ saturation from time-lapse CO₂ well logging in an onshore aquifer, Nagaoka, Japan, *Exploration Geophysics*, 37, p19-29.

- Yang, Changbing, Mickler, P. Reedy, R. Scanlon, B.R. and Larson, T., Assessing potential impacts of CO₂ leakage on Cranfield shallow groundwater chemistry with laboratory and field experiments. *International Journal of Greenhouse Gas Control*.
- Yang, F., Bai, B., Dunn-Norman, S. 2011. Modeling the effects of completion techniques and formation heterogeneity on CO₂ sequestration in shallow and deep saline aquifers, *Environmental Earth Sciences*, 64, 841-849, DOI: 10.1007/s12665-011-0908-0.
- Yang, C., Romanak, K.D., Hovorka S.D.; Trevino, R., Holt R.M., Linder J., Smith, F., Roeckner, F. Xia, Y., and Rickerts J. 2012. Large Volume CO₂ Injection at Cranfield Early Field Test of the SECARB Phase III: Near-Surface Monitoring, SECARB 7th Annual Stakeholders' Briefing http://www.secarbon.org/wp-content/uploads/2012/08_Romanak.pdf.
- Zhang, T., Davidson, D., Bryant, S.L., and Huh, C. 2010. "Nanoparticle-Stabilized Emulsions for Applications in Enhanced Oil Recovery," SPE Paper 129885, presented at SPE/DOE Symp. Improved Oil Recovery, Tulsa, OK., Apr. 26-28
- Zeidouni, M. 2012. Analytical model of leakage through fault to overlying formations: *Water Resources Research*, v. 48, W00N02, doi:10.1029/2012WR012582.
- Zeidouni, M., and Pooladi-Darvish, M. 2012a. Leakage characterization through above-zone pressure monitoring: 1—inversion approach: *Journal of Petroleum Science and Engineering*, v. 98-99, p. 95–106.
- Zeidouni, M., and Pooladi-Darvish, M. 2012b. Leakage characterization through above-zone pressure monitoring: 2—design considerations with application to CO₂ storage in saline aquifers: *Journal of Petroleum Science and Engineering*, v. 98-99, p. 69–82.
- Zeidouni, Mehdi, Nicot J.-P., Hovorka S.D., 2014, Monitoring the above-zone temperature variations associated with CO₂ and brine leakage from the storage aquifer: *Journal of Environmental Earth Sciences* September 2014, Volume 72, Issue 5, pp 1733–1747

Appendix B

GATE-TO-GATE & GATE-TO-GRAVE - RESULTS

NOTE

Relative permeability data used in reservoir simulations were obtained from laboratory experiments performed on Cranfield core funded by this project.

Injection and Production

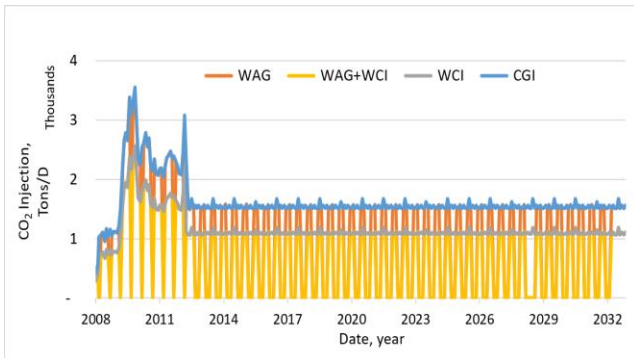


Figure 1- Mass of CO2 injected per Day



Figure 2- Cumulative Mass of CO2 injected

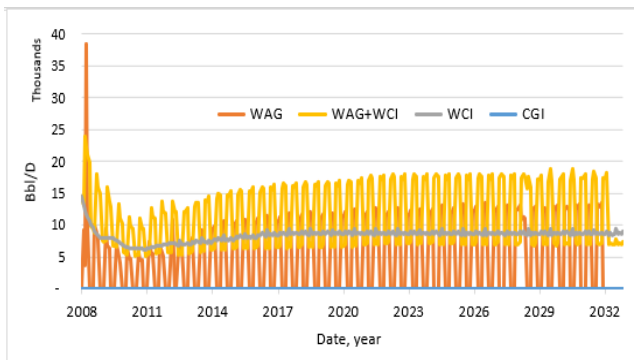


Figure 3- Water injection rate

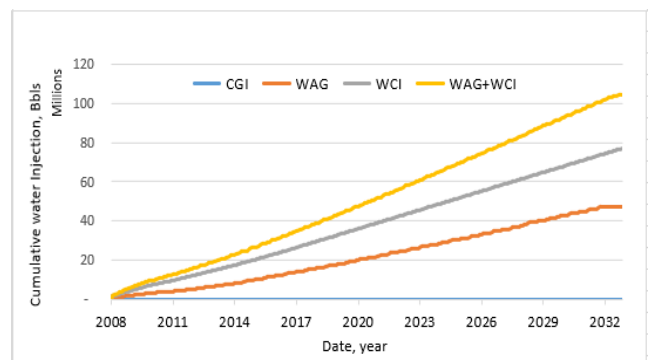


Figure 4- Cumulative water injection

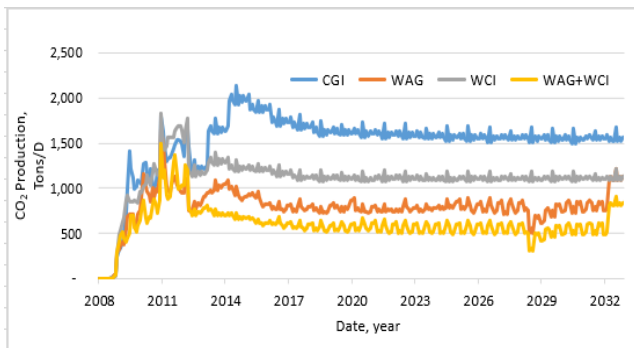


Figure 5- Gas production rate



Figure 6- Cumulative gas production

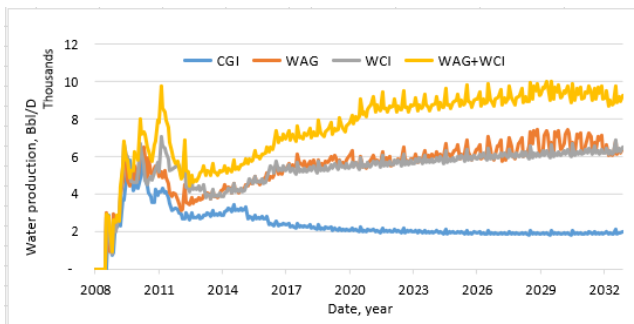


Figure 7- - Volumes of water produced

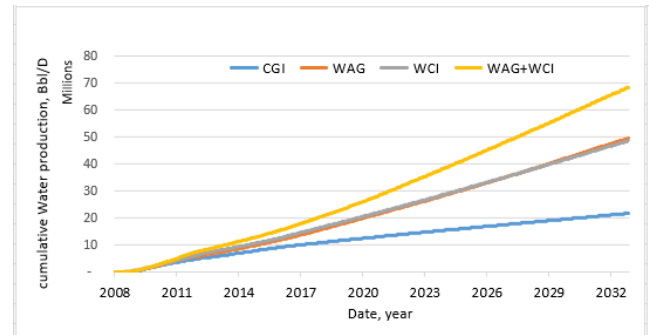


Figure 8- Cumulative water production

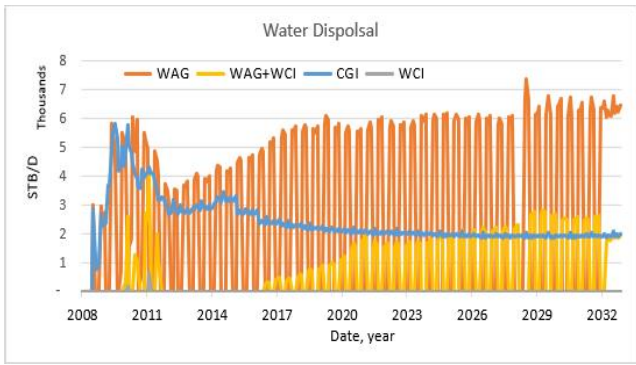


Figure 9- Water disposal rate

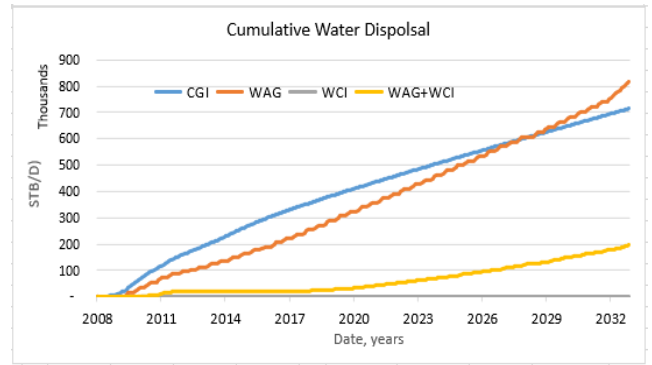


Figure 10- Cumulative volume of water disposal

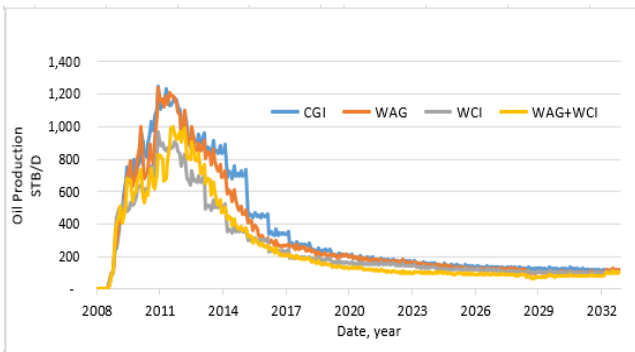


Figure 11- Oil production rate

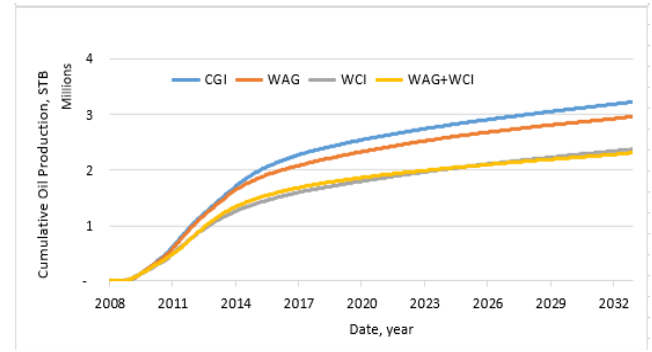


Figure 12- Cumulative oil production

Gate-to-gate emissions (major contributors)

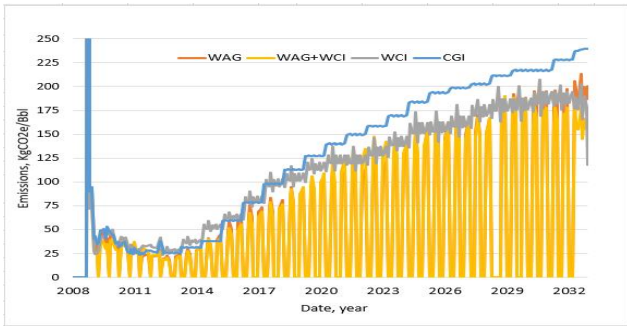


Figure 13- CO2 Injection emissions (gas compression)

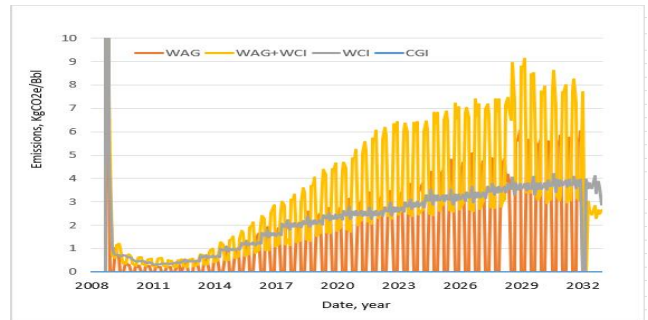


Figure 14- Water injection emissions

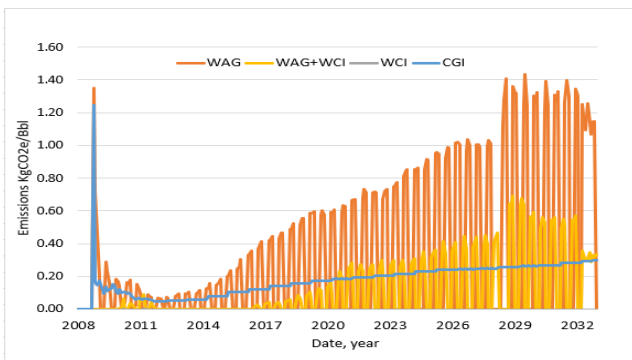


Figure 15- Water disposal emissions

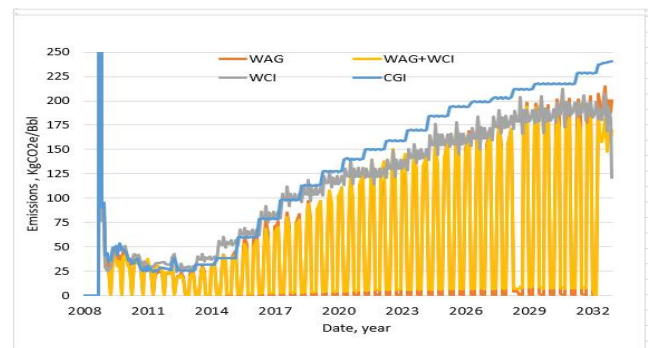


Figure 16- Total Gate-to-Gate emissions no Gas separation

Impact of gas separation emissions process

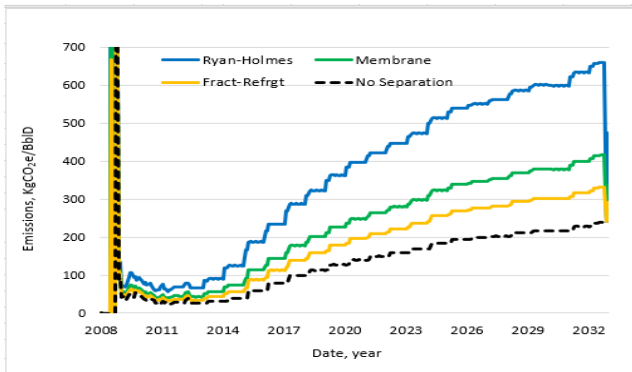


Figure 17- CGI: Total daily emissions per gas separation process

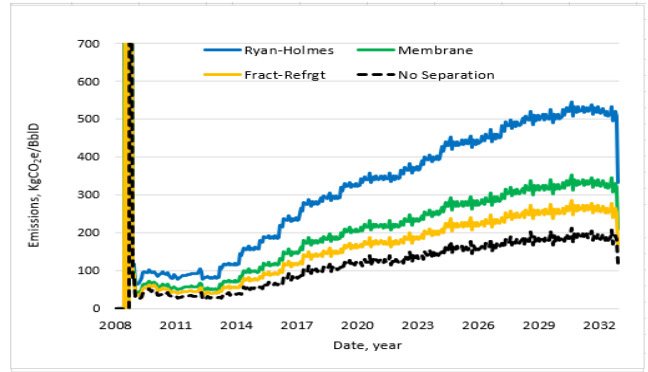


Figure 18- WCI: Total daily emissions per gas separation process

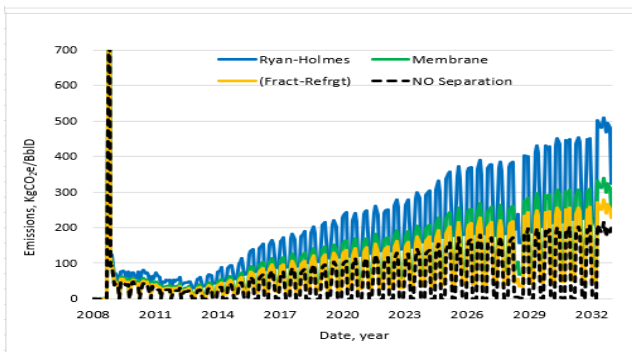


Figure 19- WAG: Total daily emissions per gas separation process

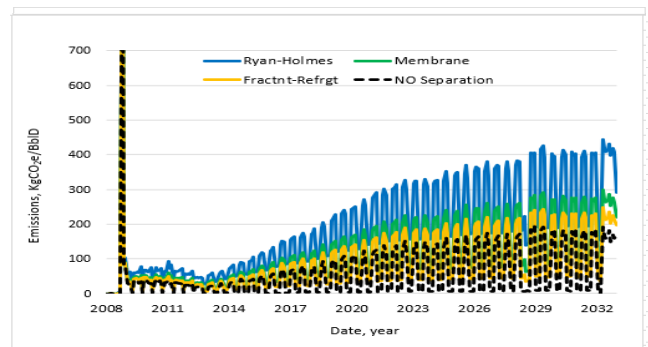


Figure 20- WAG+WCI: Total daily emissions per gas separation process

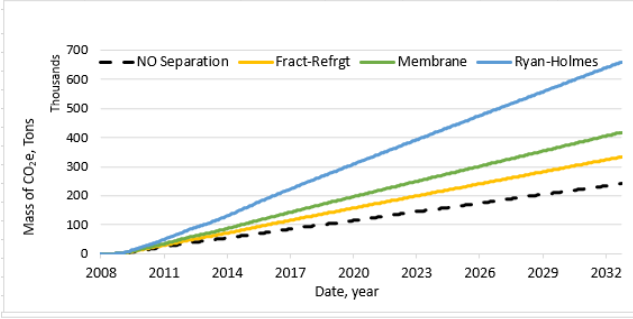


Figure 21- **CGI**: Cumulative GHG Emissions per Separation Process

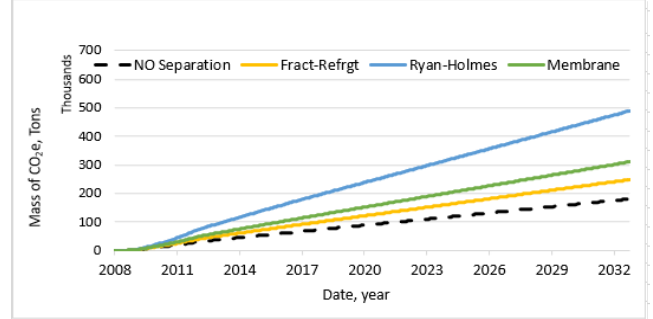


Figure 22- **WCI**: Cumulative GHG Emissions per Separation Process

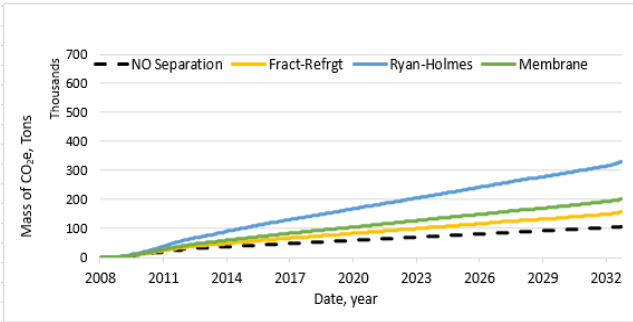


Figure 23- **WAG**: Cumulative GHG Emissions per Separation Process

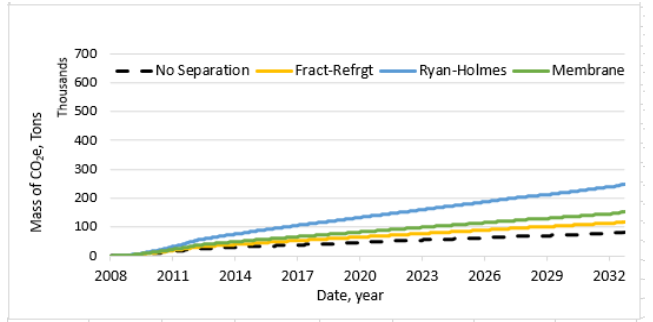


Figure 24- **WAG+WCI**: Cumulative GHG Emissions per Separation Process

Gate-to-gate Carbon Balance

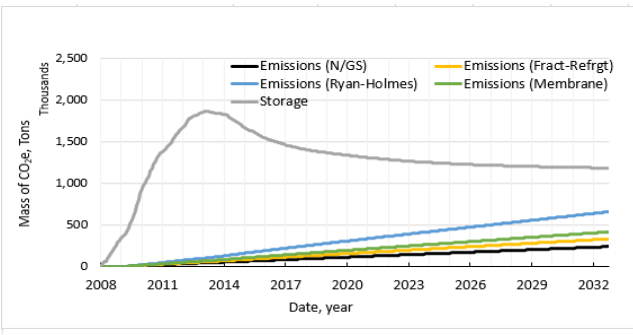


Figure 25- **CGI**: Emissions vs Storage

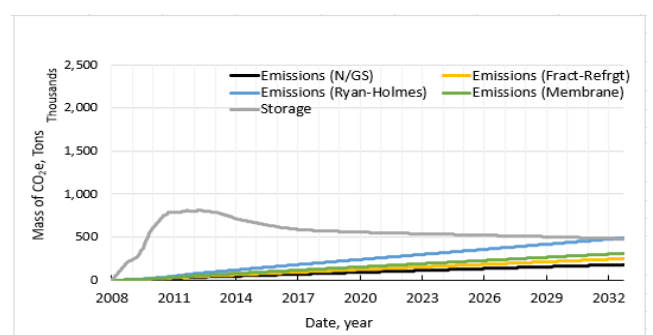


Figure 26- **WCI**: Emissions vs Storage

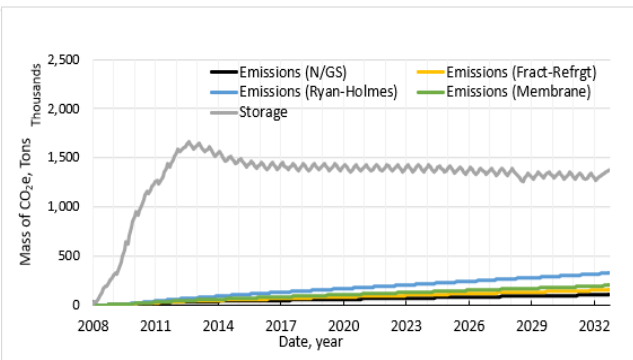


Figure 27- **WAG**: Emissions vs Storage

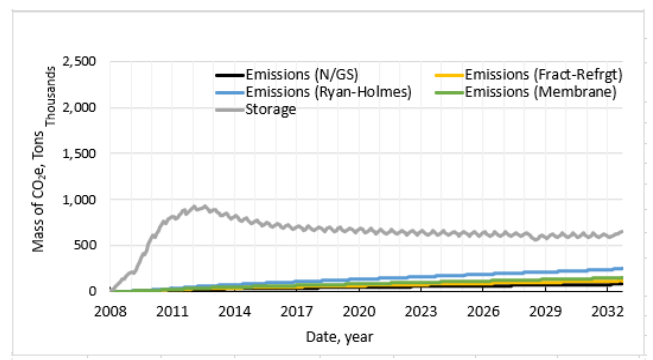


Figure 28- **WAG+WCI**: Emissions vs Storage

Gate-to-Grave Carbon balance

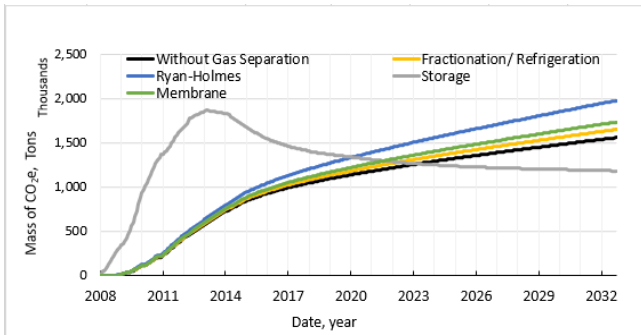


Figure 29- CO2 storage (gray curve), versus CO2e emissions (colored curves). CGI

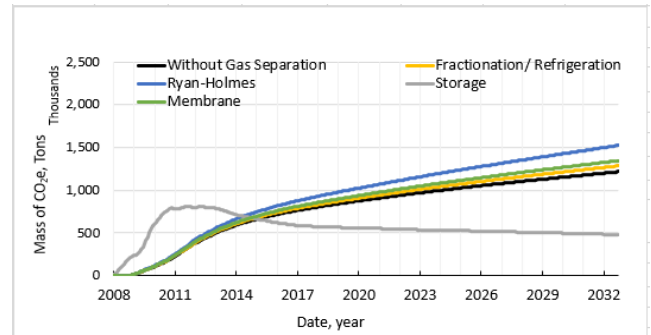


Figure 30- CO2 storage (gray curve), versus CO2e emissions (colored curves). WCI

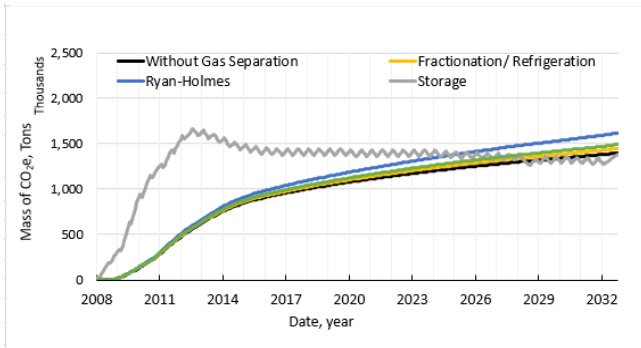


Figure 31- CO2 storage (gray curve), versus CO2e emissions (colored curves). WAG

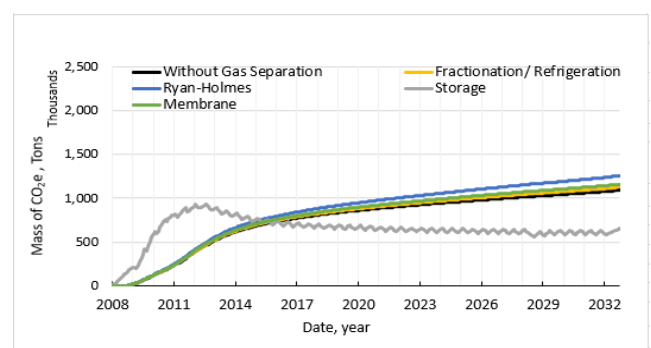


Figure 32- CO2 storage (gray curve) versus CO2e emissions (colored curves). Hybrid

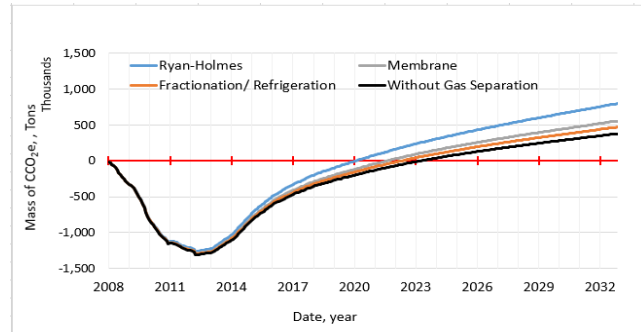


Figure 33- Carbon balance (CO2e emissions minus CO2 storage). CGI

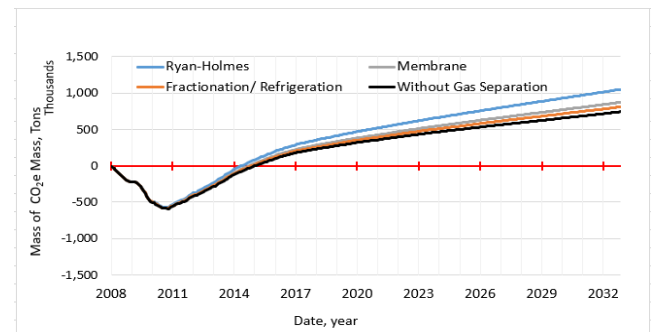


Figure 34- Carbon balance (CO2e emissions minus CO2 storage). WCI

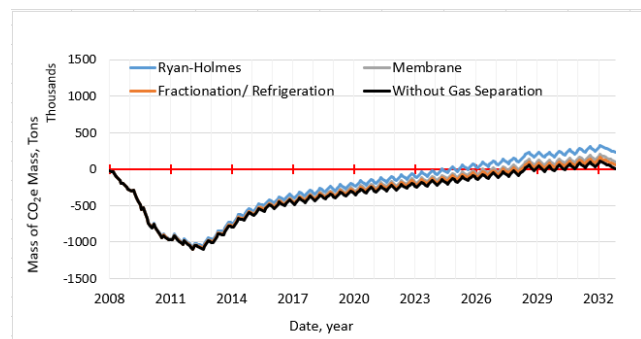


Figure 35- Carbon balance (CO2e emissions minus CO2 storage). WAG

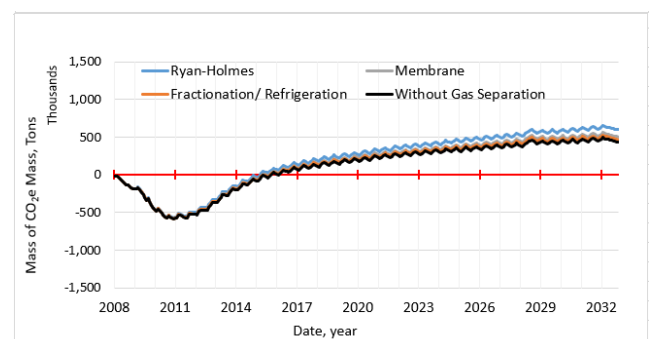


Figure 36- Carbon balance (CO2e emissions minus CO2 storage). Hybrid

Transition Point values

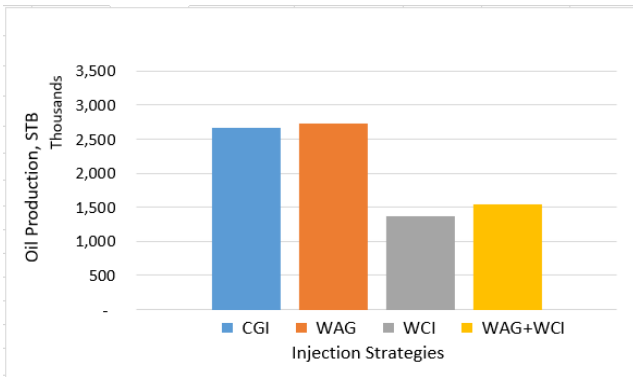


Figure 27- Cumulative NCNO production.

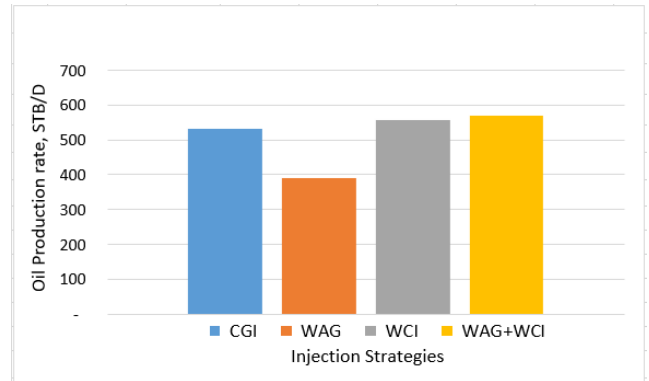


Figure 38- Daily NCNO production

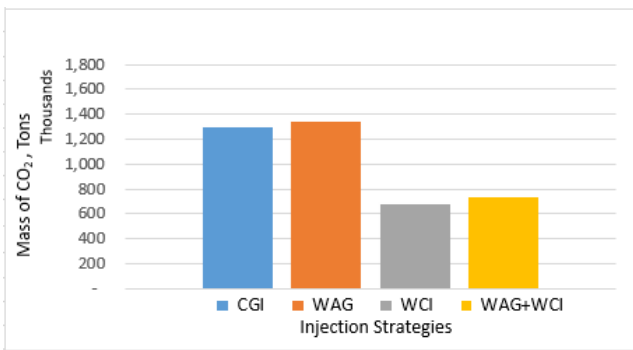


Figure 39- Cumulative mass of CO₂ stored at Transition Point

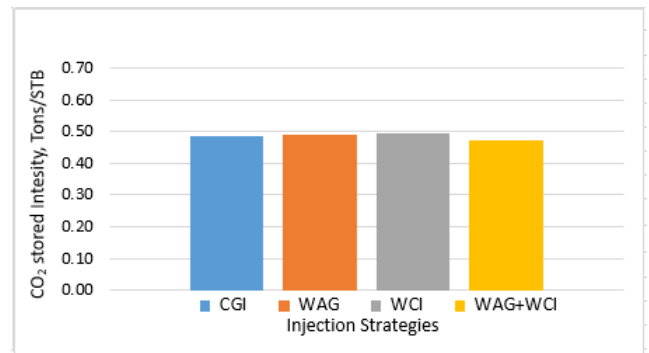


Figure 40- Mass of CO₂ storage per STB at Transition Point

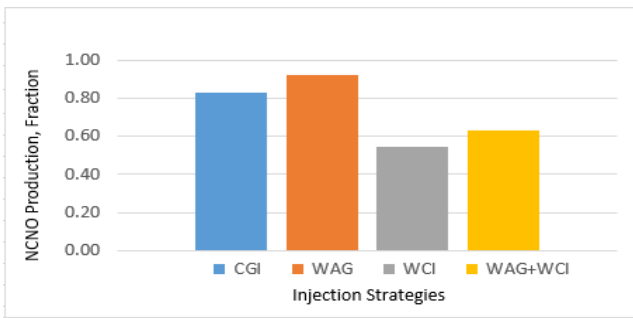


Figure 41- Cumulative NCNO production relative to Total

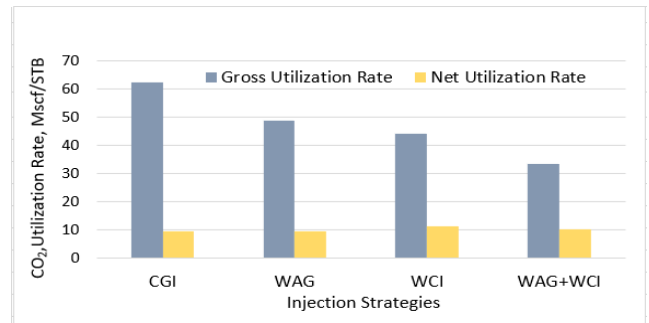


Figure 42- Average NCNO Utilization Rates (Gross & Net)

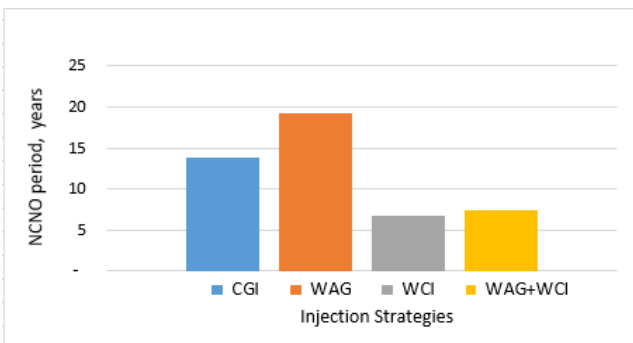


Figure 43- NCNO production period in years

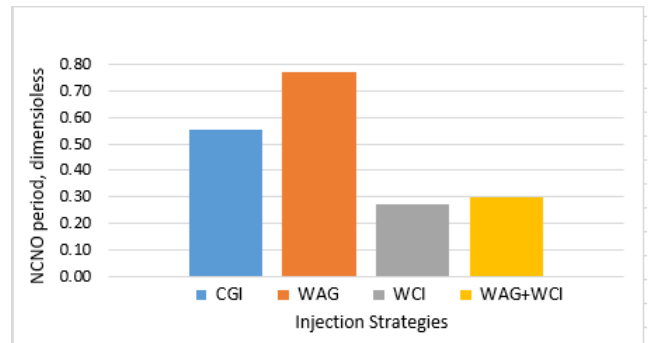


Figure 44- NCNO period relative to project life

End of project values

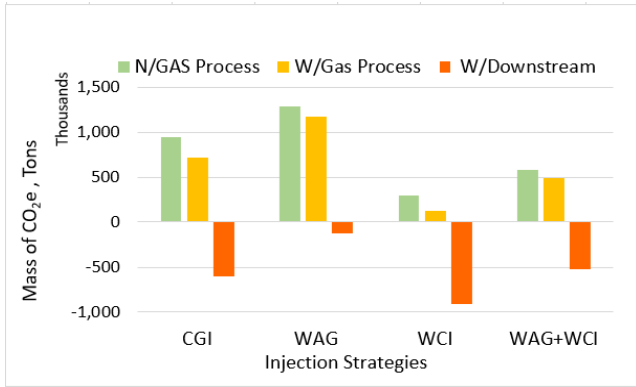


Figure 45- CO₂ Balance (Emission-Storage). Impact of different boundaries: Gate-to-Gate (No Gas Process and With Gas Process) and Gate-to-Grave (With Downstream).

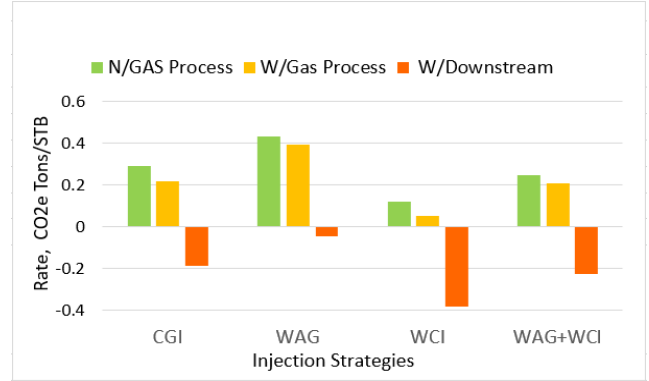


Figure 46- CO₂ Balance (Emission-Storage) per STB. Impact of different boundaries: Gate-to-Gate (No Gas Process and With Gas Process) and Gate-to-Grave (With Downstream).

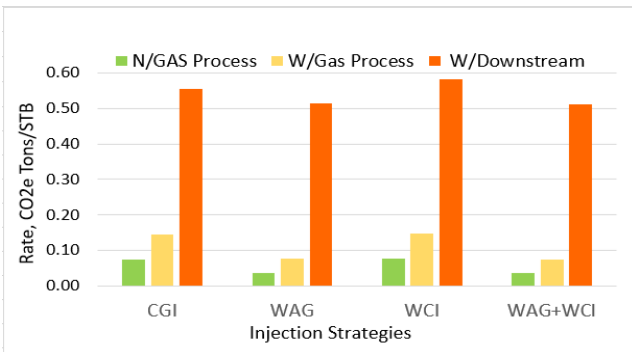


Figure 47- Production Emission Rate, CO₂e emission per STB. Impact of different boundaries: Gate-to-Gate (No Gas Process and With Gas Process) and Gate-to-Grave (With Downstream).

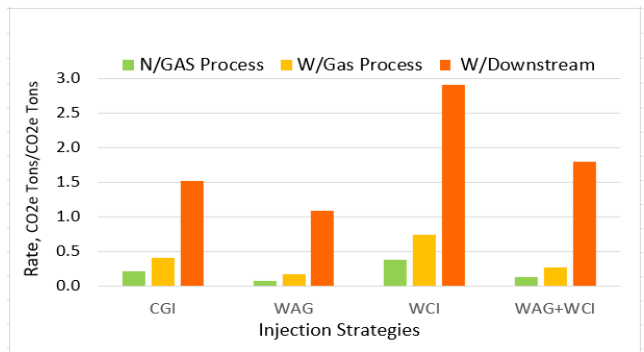


Figure 48- Storage Emission Rate, CO₂e emission per storage. Impact of different boundaries: Gate-to-Gate (No Gas Process and With Gas Process) and Gate-to-Grave (With Downstream).

Efficiency Rates Evolution

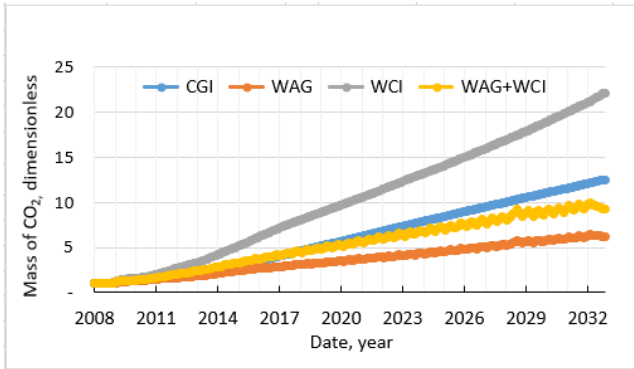


Figure 49- Mass of CO₂ injected per mass of CO₂ stored

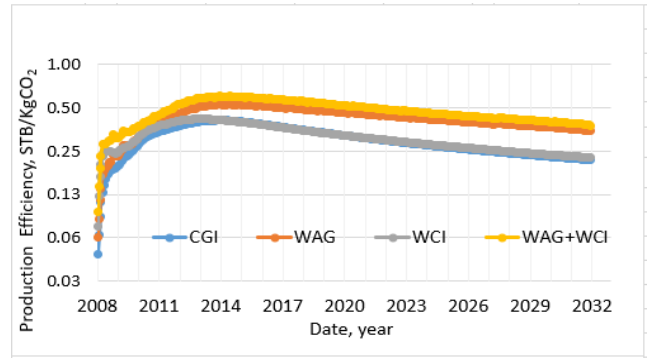


Figure 50- Oil Production efficiency in terms of CO₂ Kg injected

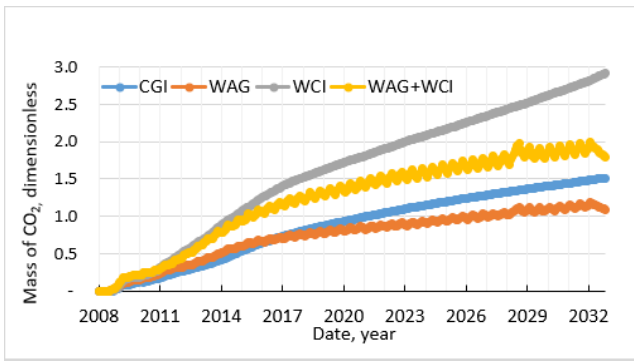


Figure 51- Gate-to-Grave mass of CO₂e emissions per mass of CO₂ stored

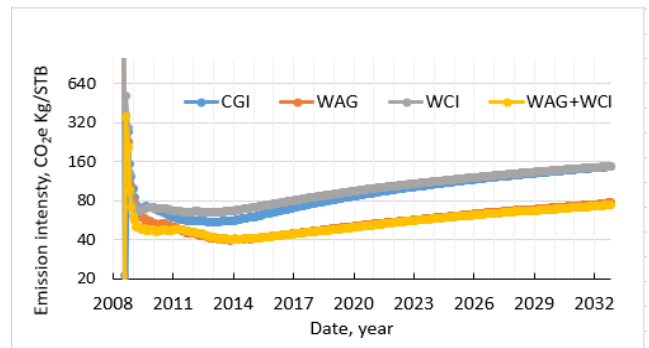


Figure 52- Gate-to-Gate CO₂e emissions intensity per STB

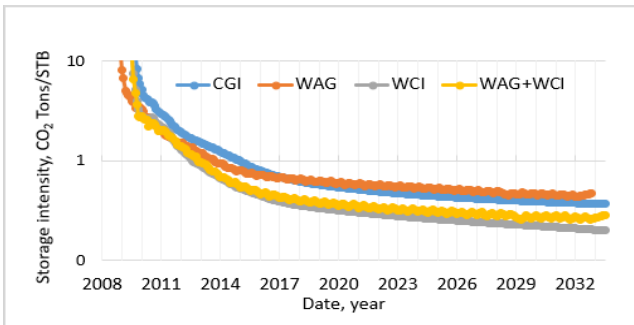


Figure 53- Mass of CO₂ stored per barrel of oil produced

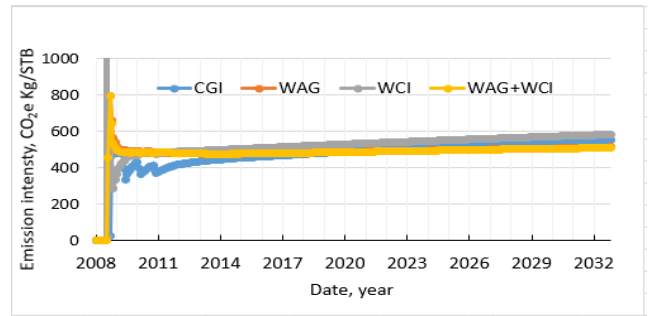


Figure 54- Gate-to-Grave CO₂e Emissions intensity per STB

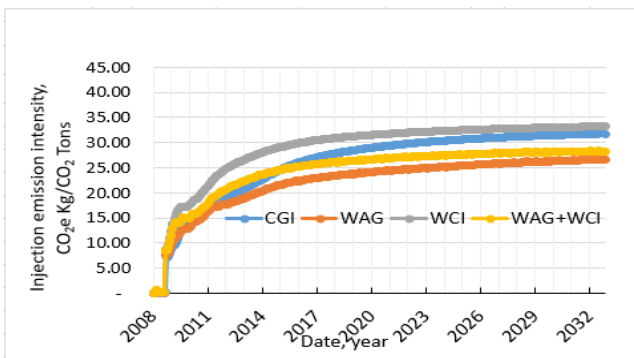


Figure 55- Gate to Gate CO₂e emissions intensity per CO₂ Injected

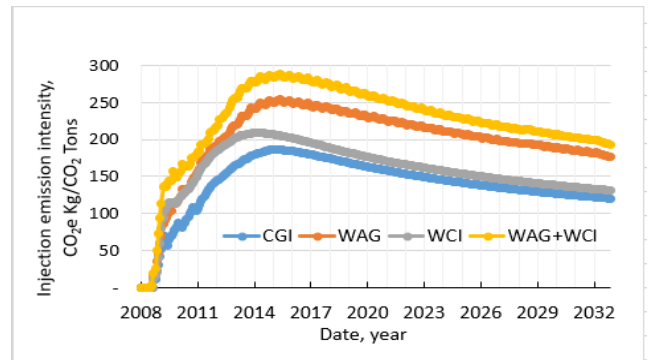


Figure 56- Gate-to-Grave CO₂e emissions per CO₂ injected

Appendix C

CRADLE-TO-GRAVE WITH PULVERIZED COAL (PC) POWER PLANT -
RESULTS

Cradle-to-Grave Carbon balance

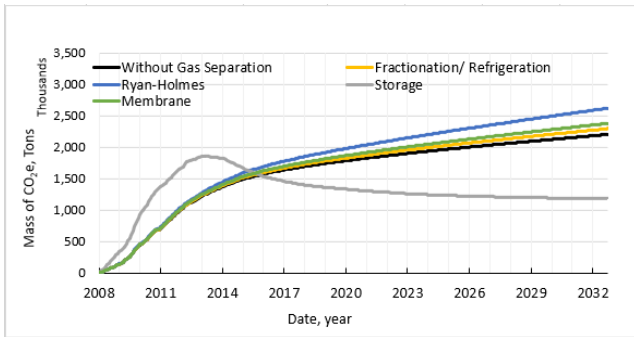


Figure C.1- CO2 storage (gray curve), versus CO2e emissions (colored curves). CGI

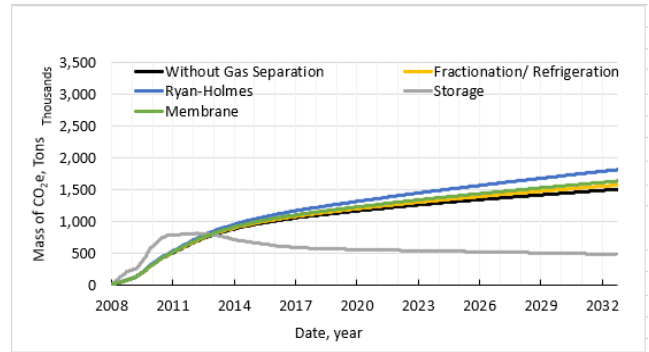


Figure C.2- CO2 storage (gray curve), versus CO2e emissions (colored curves). WCI

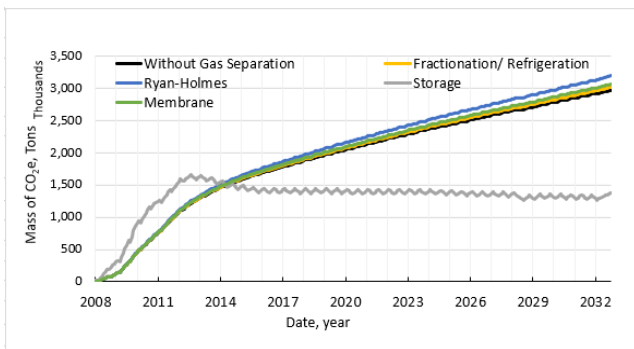


Figure C.3- CO2 storage (gray curve), versus CO2e emissions (colored curves). WAG

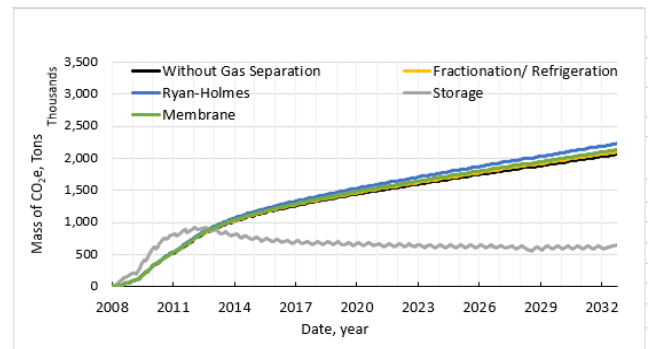


Figure C.4- CO2 storage (gray curve) versus CO2e emissions (colored curves). Hybrid

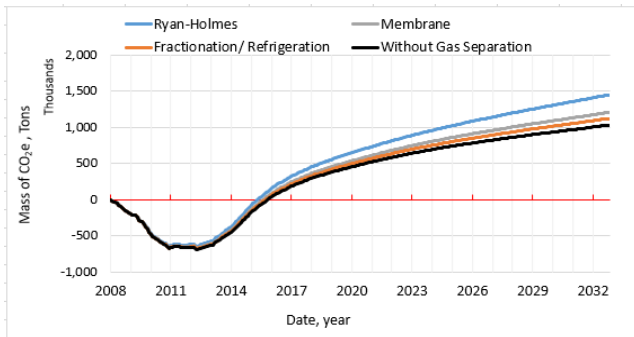


Figure C.5- Carbon balance (CO2e emissions minus CO2 storage). WAG

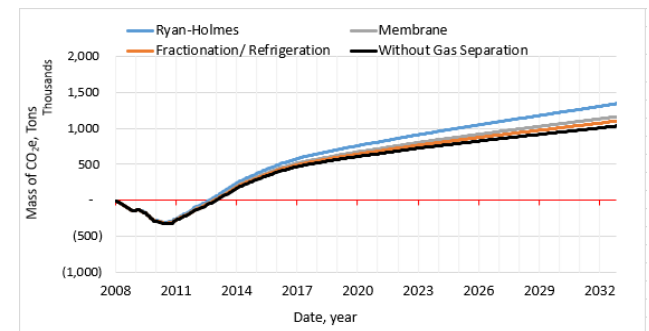


Figure C.6- Carbon balance (CO2e emissions minus CO2 storage) Hybrid

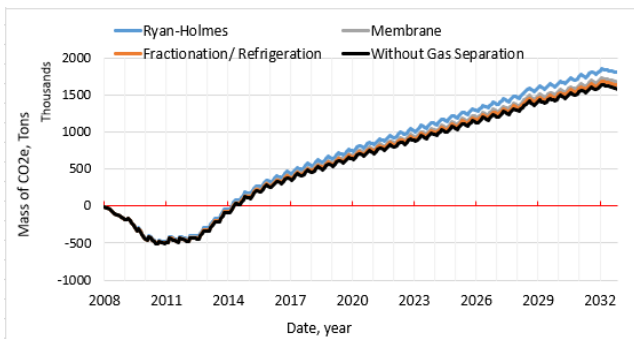


Figure C.7- Carbon balance (CO2e emissions minus CO2 storage). WAG

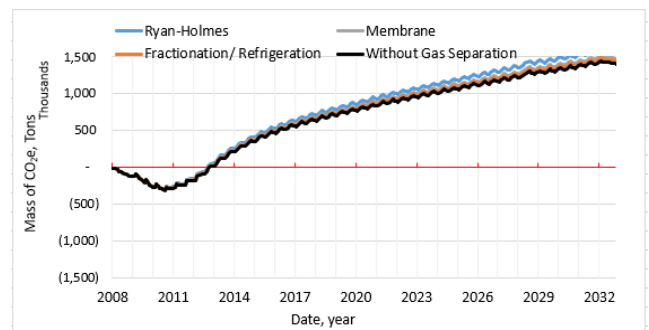


Figure C.8- Carbon balance (CO2e emissions minus CO2 storage). Hybrid

Transition Point values

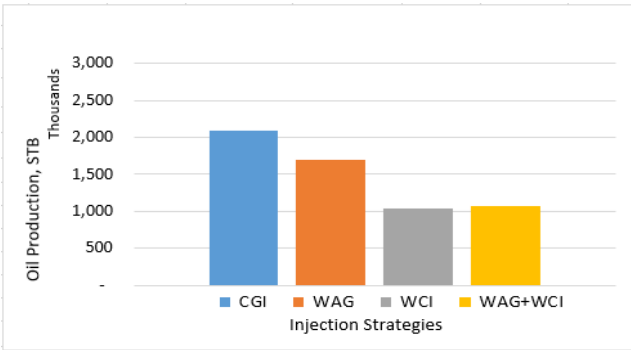


Figure C.9- Cumulative NCNO Production at Transition Point

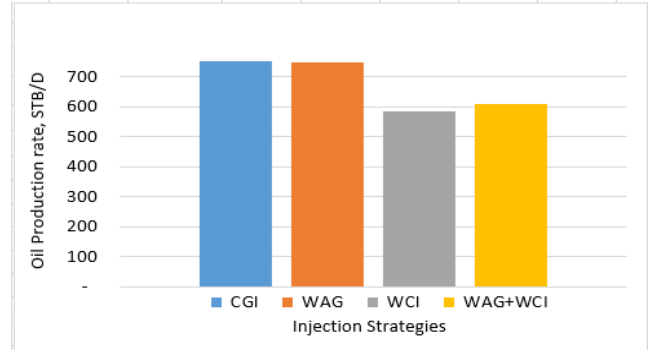


Figure C.10- Daily NCNO production at Transition Point

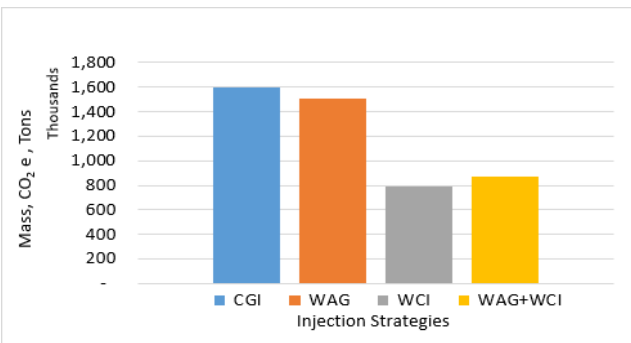


Figure C.11- Cumulative mass of CO₂ stored at Transition Point

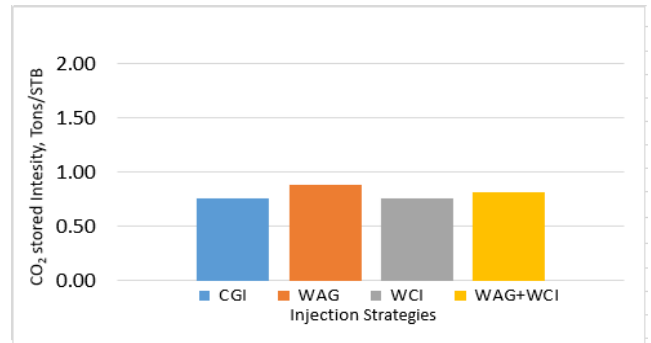


Figure C.22- Mass of CO₂ storage per STB at Transition Point

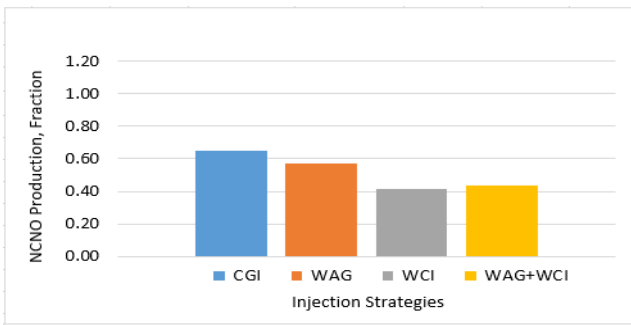


Figure C.13- Cumulative NCNO production relative to Total

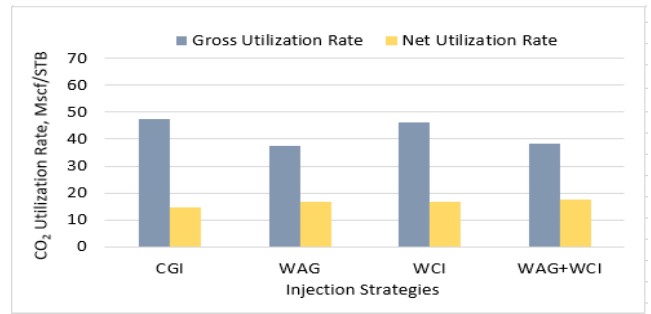


Figure C.14- Average NCNO Utilization Rates (Gross & Net)

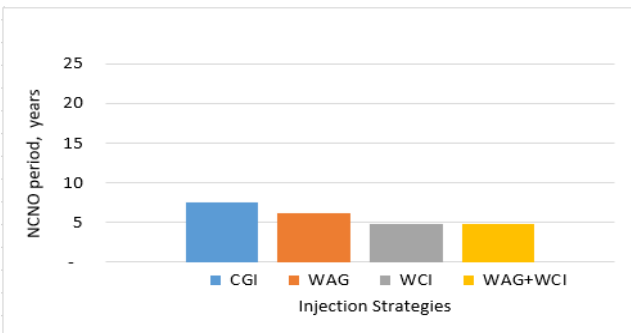


Figure C.15- NCNO production period in years

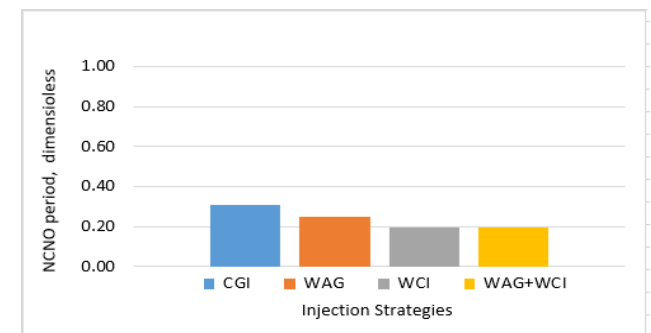


Figure C.16- NCNO period relative to project life

Cradle-to-Grave Carbon Balance plus electricity Displacement

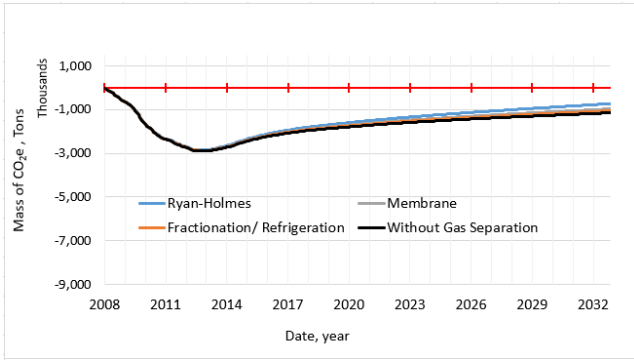


Figure C.17- Carbon balance (CO₂e emissions minus CO₂ storage) plus electricity displacement. CGI

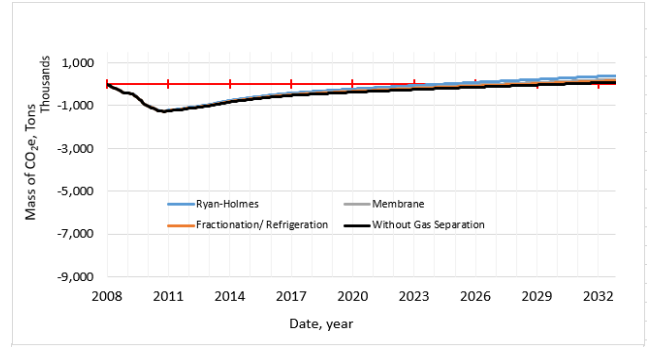


Figure C.18- Carbon balance (CO₂e emissions minus CO₂ storage) plus electricity displacement. WCI

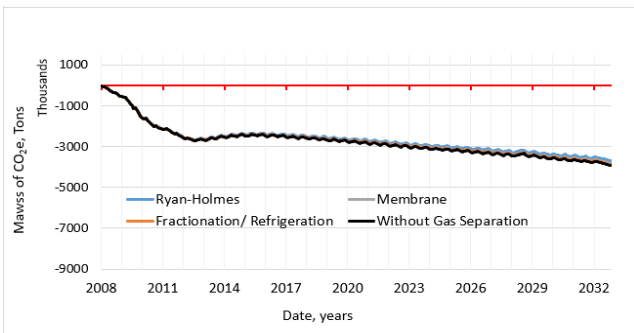


Figure C.19- Carbon balance (CO₂e emissions minus CO₂ storage) plus electricity displacement. WAG

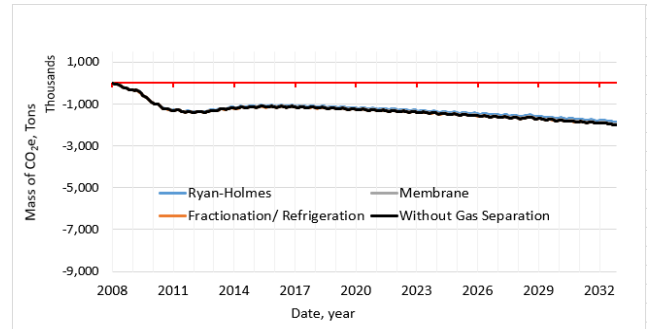


Figure C.20- Carbon balance (CO₂e emissions minus CO₂ storage) plus electricity displacement. Hybrid

End of project values

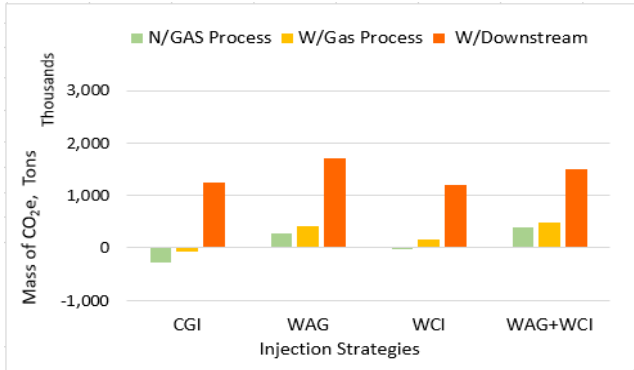


Figure C.21- CO₂ Balance (Storage- Emission). Impact of different boundaries: Cradle-to-Gate (No Gas Process and With Gas Process) and Cradle-to-Grave (With Downstream).

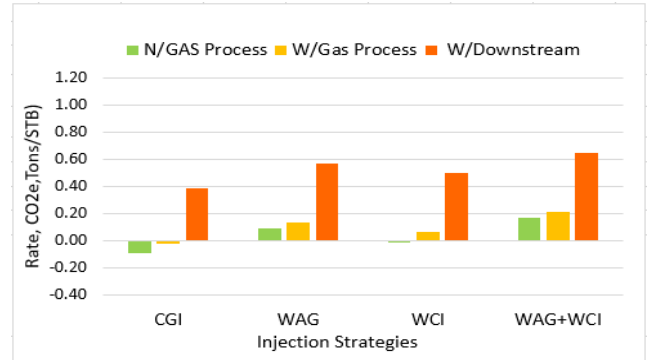


Figure C.22- CO₂ Balance per STB. Impact of different boundaries: Cradle-to-Gate (No Gas Process and With Gas Process) and Cradle-to-Grave (With Downstream)

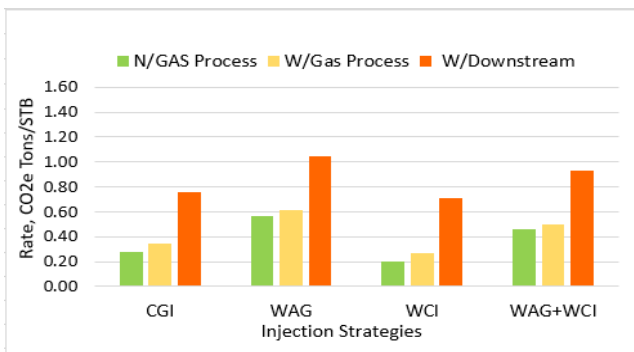


Figure C.23- Production Emission Rate, CO_{2e} emission per STB. Impact of different boundaries: Gate-to-Gate (No Gas Process and With Gas Process) and Gate-to-Grave (With Downstream).

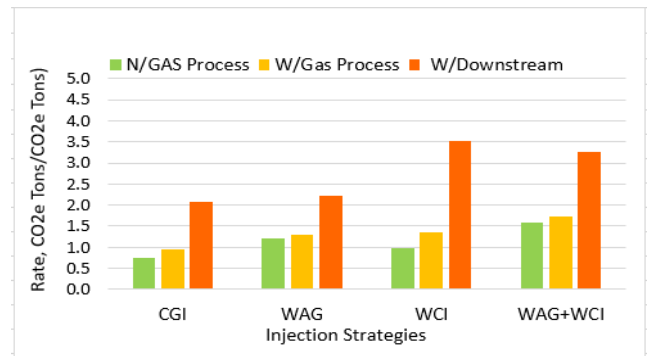


Figure C.24- Storage Emission Rate, CO_{2e} emission per storage. Impact of different boundaries: Gate-to-Gate (No Gas Process and With Gas Process) and Gate-to-Grave (With Downstream).

Intensity and efficiency rates evolution

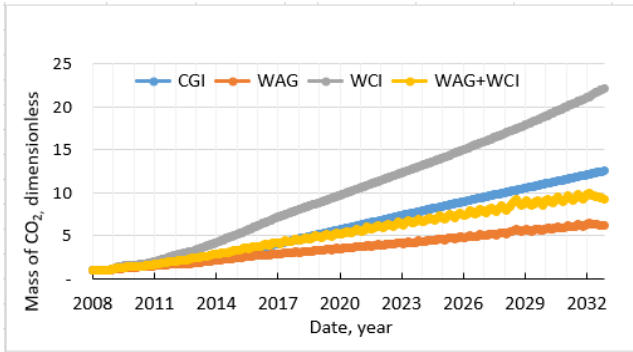


Figure C.25- Mass of CO₂ injected per mass of CO₂ stored

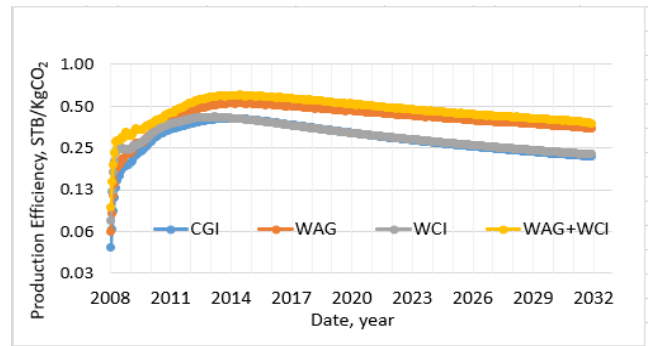


Figure C.26- Oil production efficiency in terms of CO₂ Kg injected

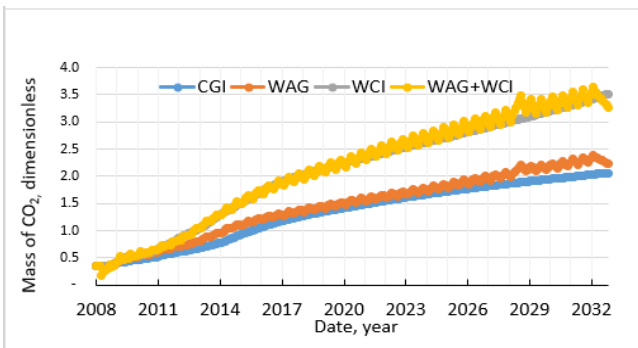


Figure C.3- Cradle-to-Grave mass of CO₂e emissions per mass of CO₂ stored

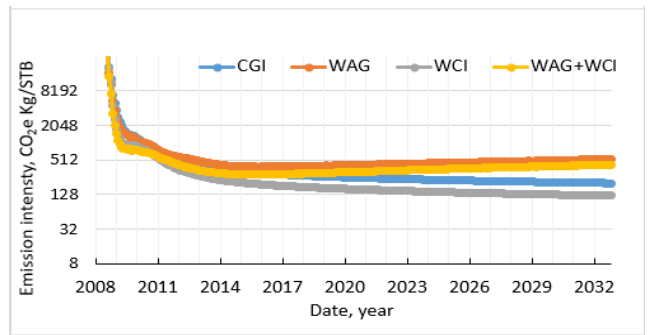


Figure C.28- CO₂e emissions intensity per STB for components upstream of the CO₂-EOR Site

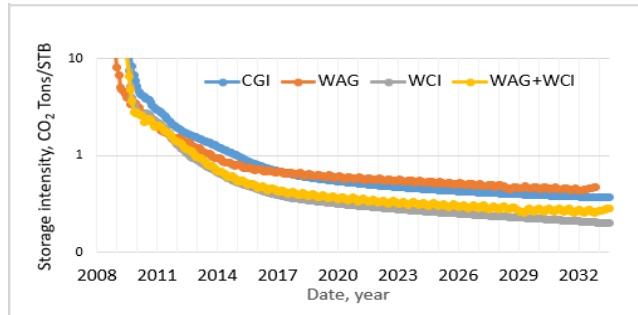


Figure C.29- Mass of CO₂ stored per barrel of oil produced

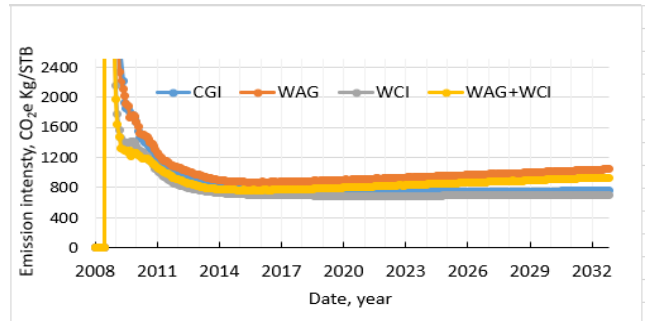


Figure C.30- Cradle-to-Grave CO₂e emissions per STB

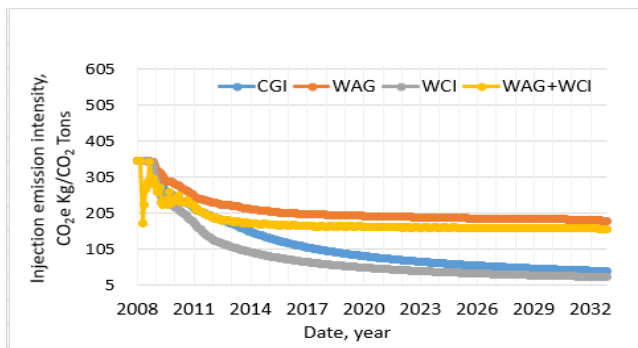


Figure C.31- Cradle-to-Grate CO₂e emissions intensity per CO₂ Injected

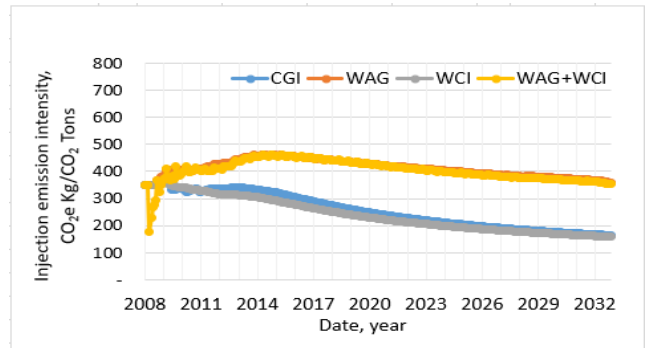


Figure C.32- Cradle-to-Grave CO₂ emissions per CO₂ injected

Appendix D

CRADLE-TO-GRAVE WITH NATURAL GAS COMBINED CYCLE (NGCC)
POWER PLANT - RESULTS

Carbon balance cradle-to-grave

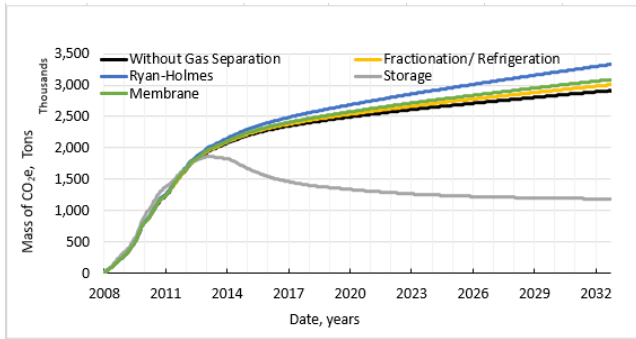


Figure D.1- CO2 storage (gray curve), versus CO2e emissions (colored curves). CGI

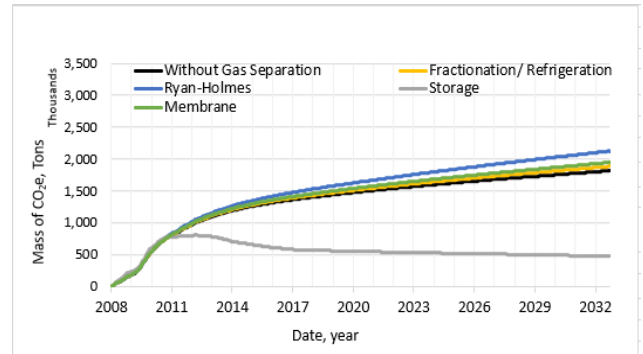


Figure D.2- CO2 storage (gray curve), versus CO2e emissions (colored curves). WCI

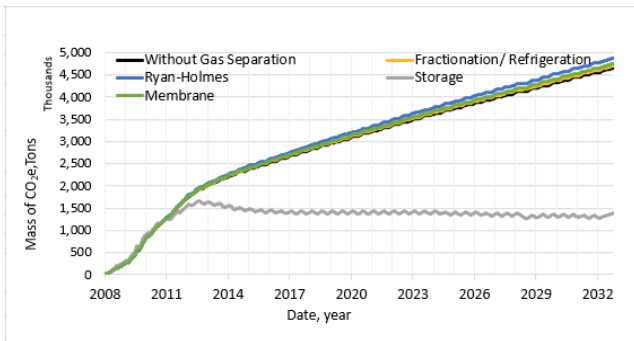


Figure D.3- CO2 storage (gray curve), versus CO2e emissions (colored curves). WAG

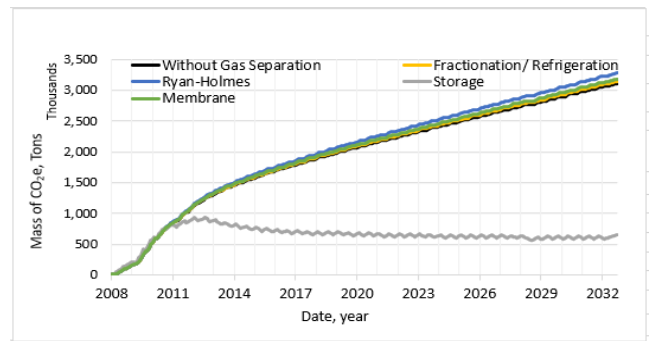


Figure D.4- CO2 storage (gray curve) versus CO2e emissions (colored curves). Hybrid

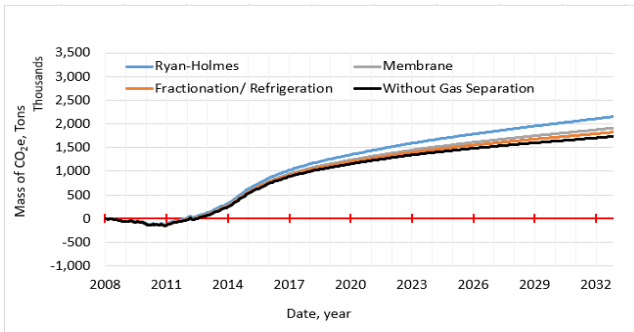


Figure D.5- Carbon balance (CO2e emissions minus CO2 storage). CGI

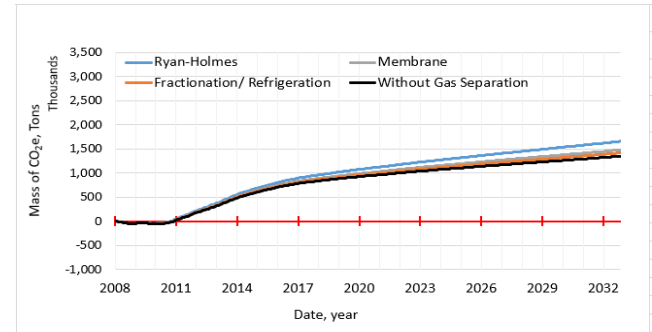


Figure D.6- Carbon balance (CO2e emissions minus CO2 storage). WCI

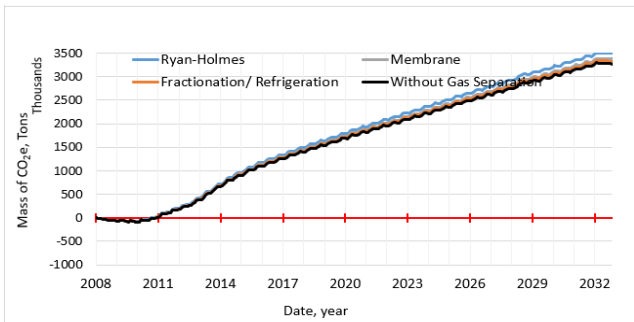


Figure D.7- Carbon balance (CO2e emissions minus CO2 storage). WAG

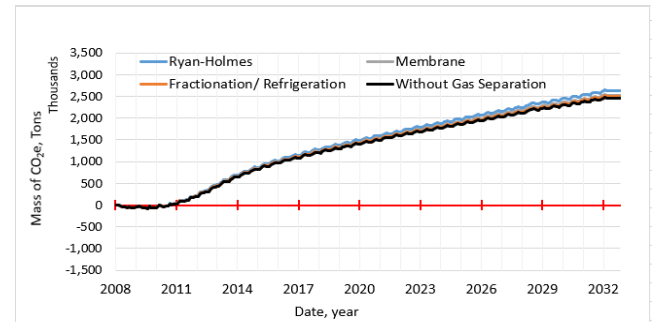


Figure D.8- Carbon balance (CO2e emissions minus CO2 storage). Hybrid

Transition point values

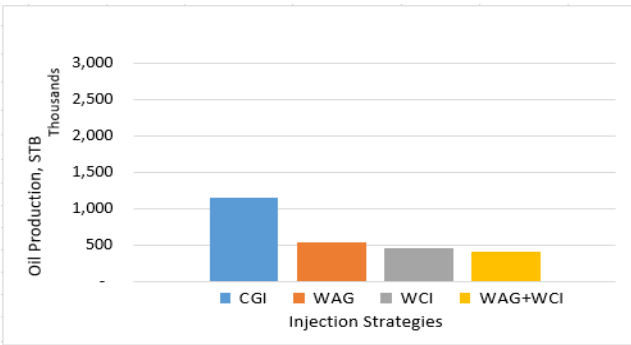


Figure D.9- Cumulative NCNO production.

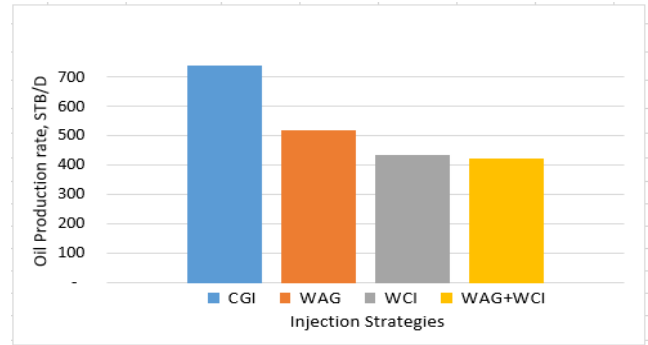


Figure D.10- Daily NCNO Production

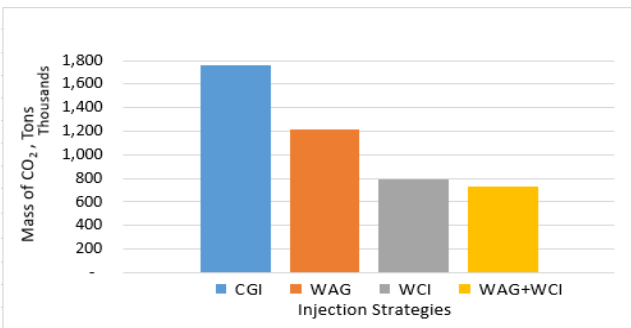


Figure D.11- Cumulative mass of CO₂ stored at Transition Point

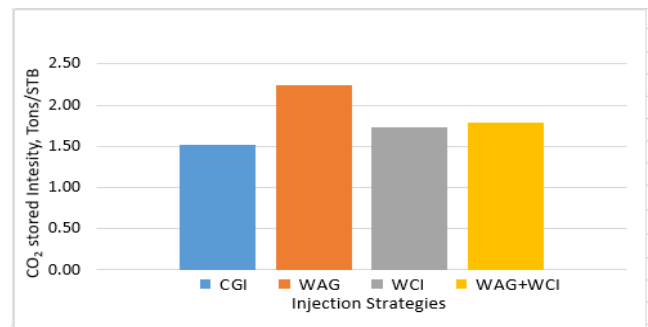


Figure D.12- Mass of CO₂ storage per STB at Transition Point

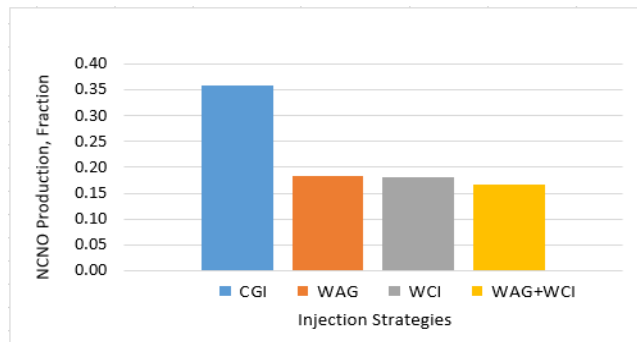


Figure D.13- Cumulative NCNO production relative to Total

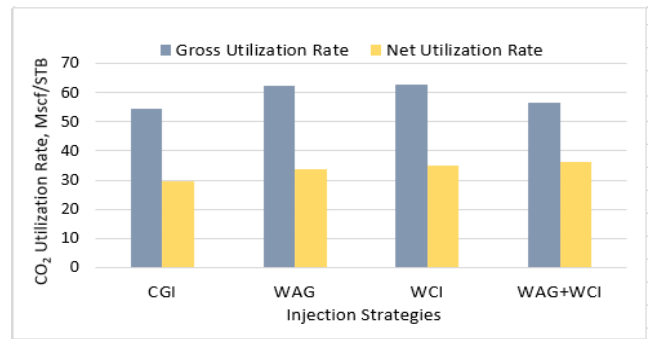


Figure D.14- Average NCNO Utilization Rates (Gross & Net)

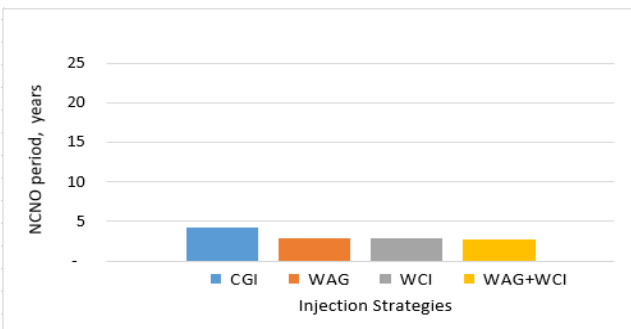


Figure D.15- NCNO production period in years

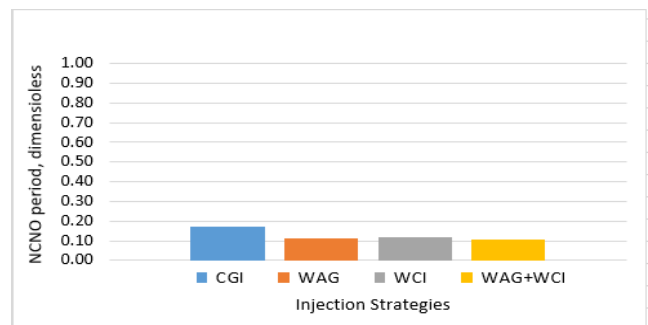


Figure D.16- NCNO period relative to project life

Carbon balance plus electricity displacement

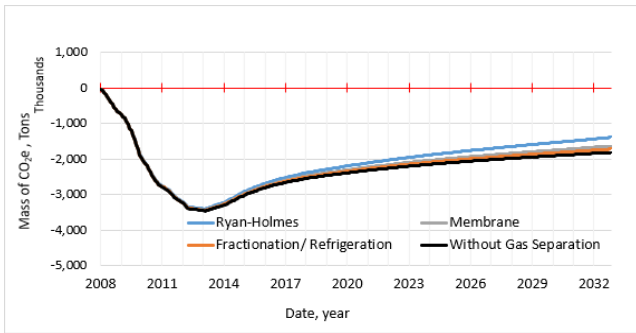


Figure D.17- Carbon balance (CO₂e emissions minus CO₂ storage). CGI

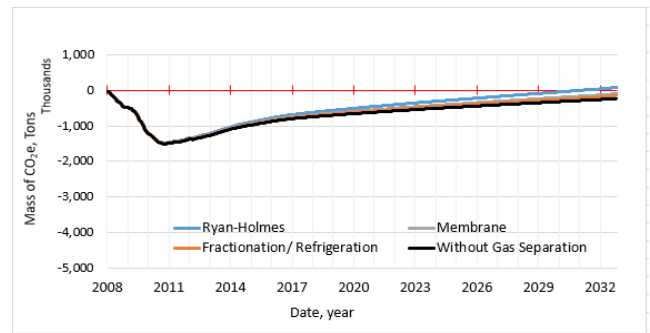


Figure D.18- Carbon balance (CO₂e emissions minus CO₂ storage). WCI

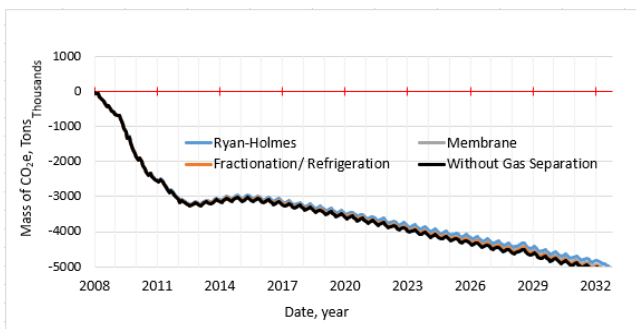


Figure D.19- Carbon balance (CO₂e emissions minus CO₂ storage). WAG

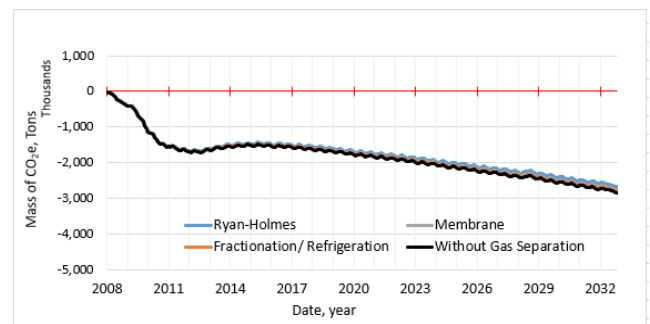


Figure D.20- Carbon balance (CO₂e emissions minus CO₂ storage). Hybrid

End of project values

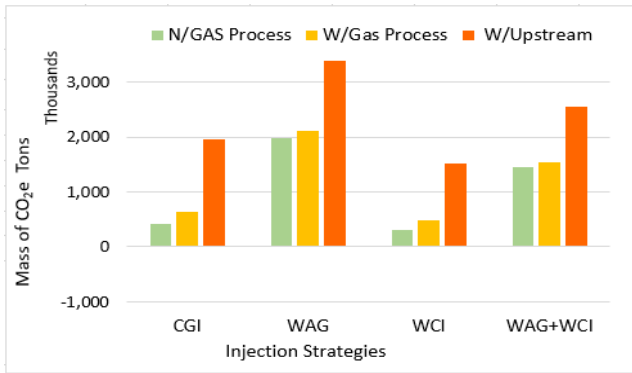


Figure D.21- CO₂ Balance (Emission-Storage). Impact of different boundaries: Cradle-to-Gate (No Gas Process and With Gas Process) and Cradle-to-Grave (With Downstream).

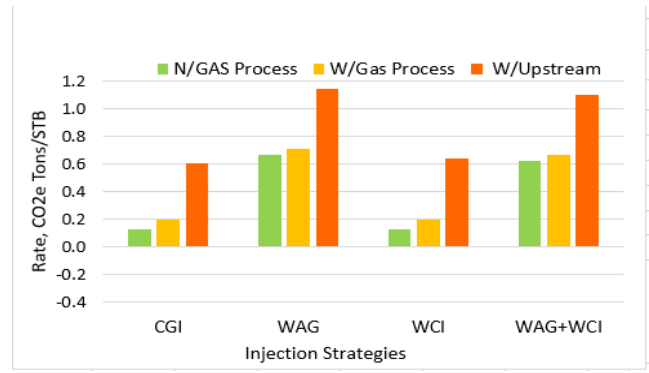


Figure D.22- CO₂ Balance (Emission-Storage) per STB. Impact of different boundaries: Cradle-to-Gate (No Gas Process and With Gas Process) and Cradle-to-Grave (With Downstream).

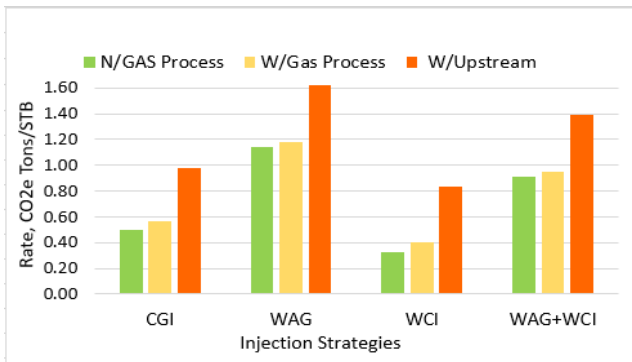


Figure D.23- Production Emission Rate, CO₂e emission per STB. Impact of different boundaries: Cradle-to-Gate (No Gas Process and With Gas Process) and Cradle-to-Grave (With Downstream).

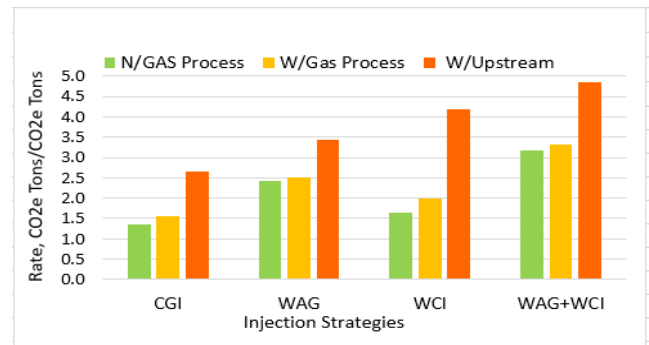


Figure D.24- Storage Emission Rate, CO₂e emission per storage. Impact of different boundaries: Cradle-to-Gate (No Gas Process and With Gas Process) and Cradle-to-Grave (With Downstream).

Efficiency rates evolution

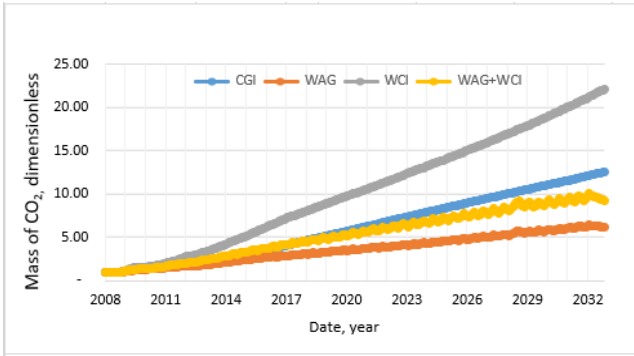


Figure D.25- Mass of CO₂ injected per mass of CO₂ stored

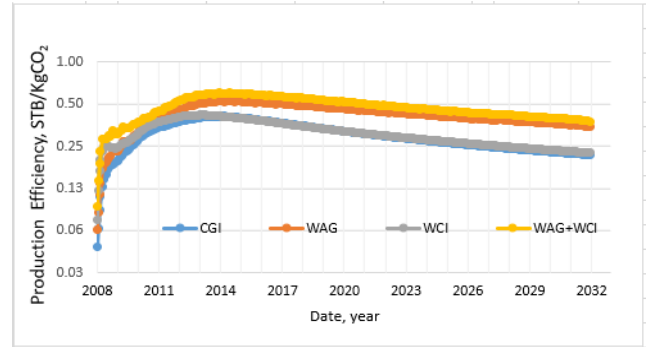


Figure D.26- Oil Production efficiency in terms of CO₂ Kg injected

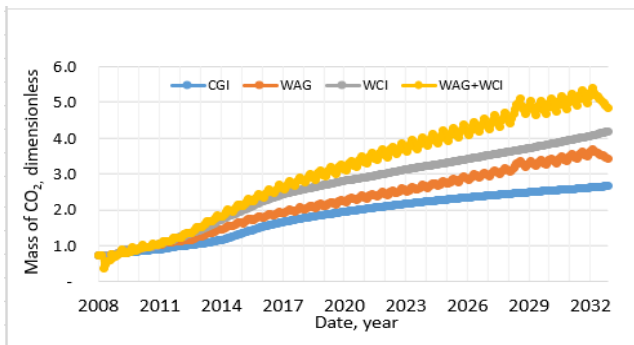


Figure D. 27- Cradle-to-Grave mass of CO₂e emissions per mass of CO₂ stored

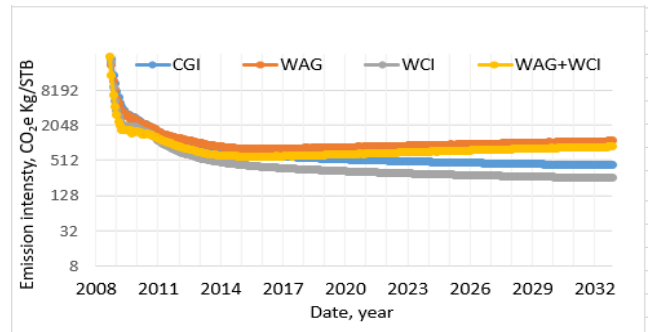


Figure D.28- Upstream CO₂e emissions intensity per STB

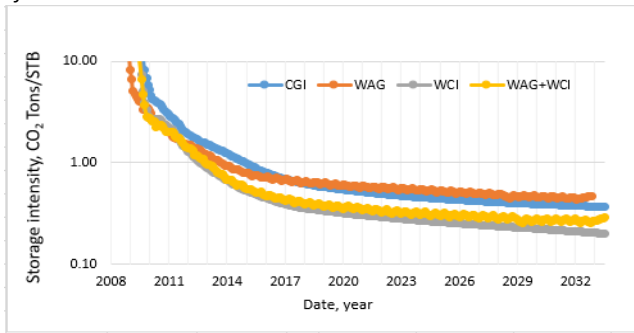


Figure D.29- Mass of CO₂ stored per barrel of oil produced

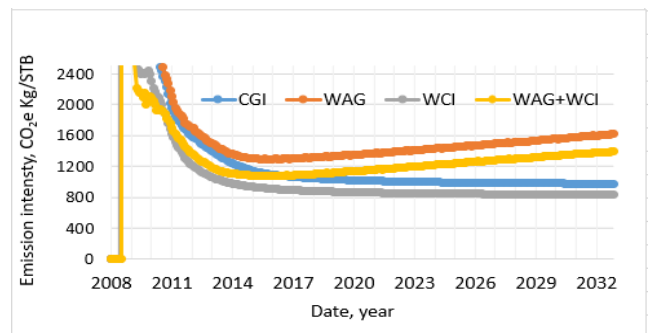


Figure D.30- Cradle-to-Grave CO₂e Emissions intensity per STB

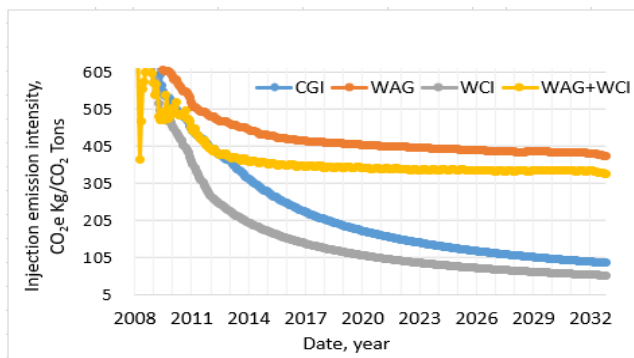


Figure D.31- Cradle-to-Gate CO₂e emissions intensity per CO₂ Injected

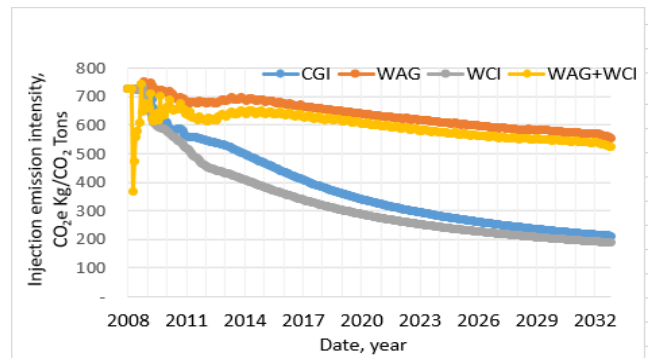


Figure D.32- Cradle-to-Grave CO₂e emissions per CO₂ injected

Appendix E

GATE-TO-GATE & GATE-TO-GRAVE – RESULTS OBTAINED THROUGH
RESERVOIR SIMULATION RUNS WITH PUBLIC CRANFIELD RELATIVE
PERMEABILITY DATA

Injection and Production

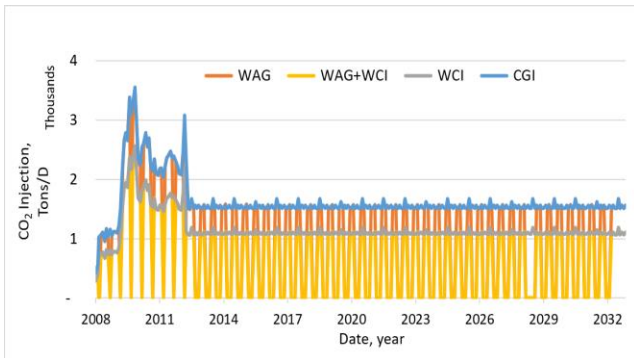


Figure E.1- Mass of CO2 injected pr Day



Figure E.2- Cumulative Mass of CO2 injected

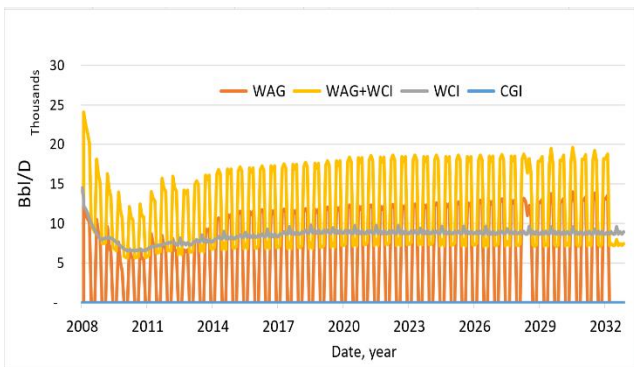


Figure E.3- Volume of Water Injected per Day

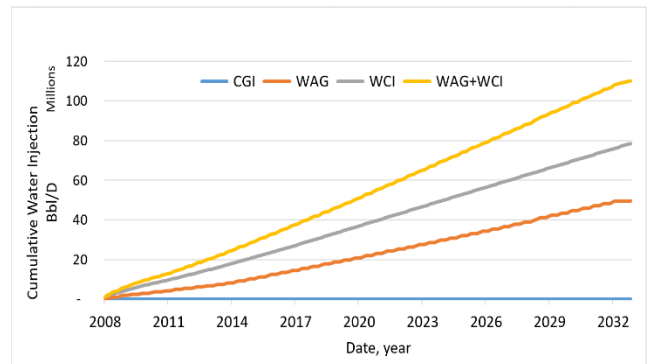


Figure E.4- Cumulative volume of Water Injected

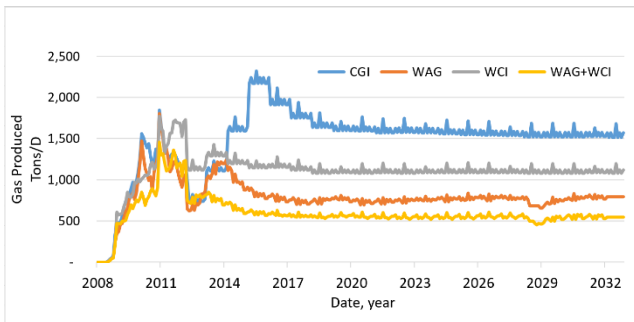


Figure E.5-Mass of Gas Produced per Day



Figure E.6- Cumulative Mass of Gas Produced

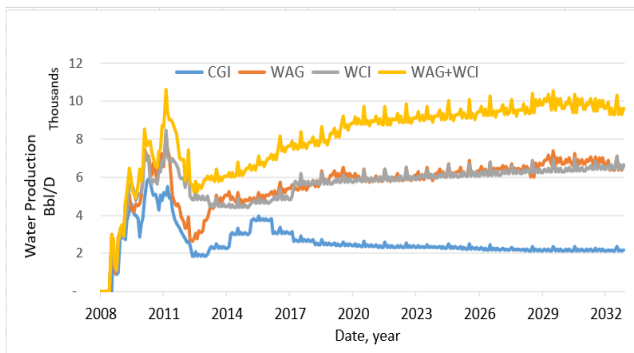


Figure E.7- Volumes of Water produced



Figure E.8- Cumulative volumes of Water produced

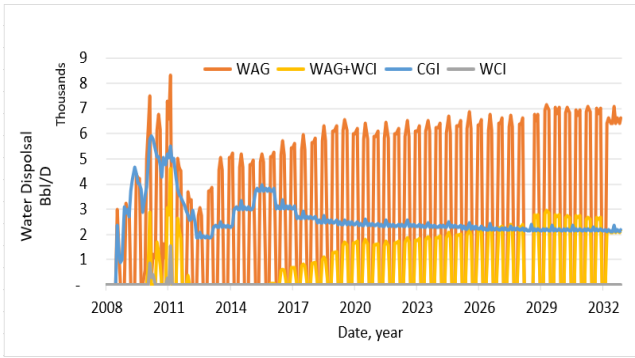


Figure E.9- Volume of Water disposal

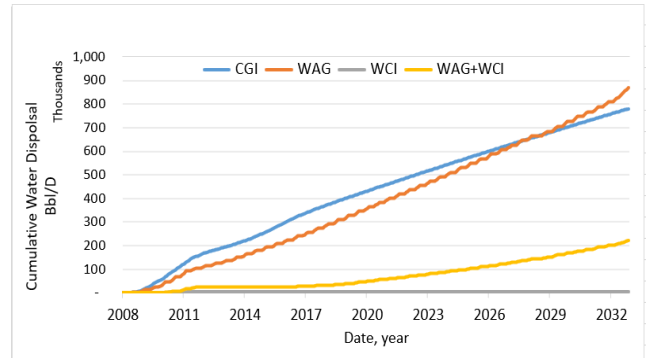


Figure E.10- Cumulative volume of Water disposal

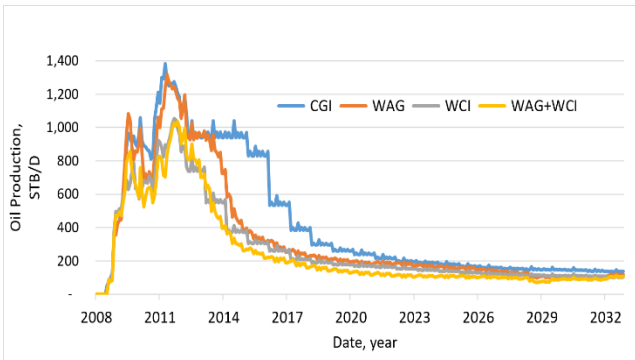


Figure E.11- Volume of Oil Produced per Day

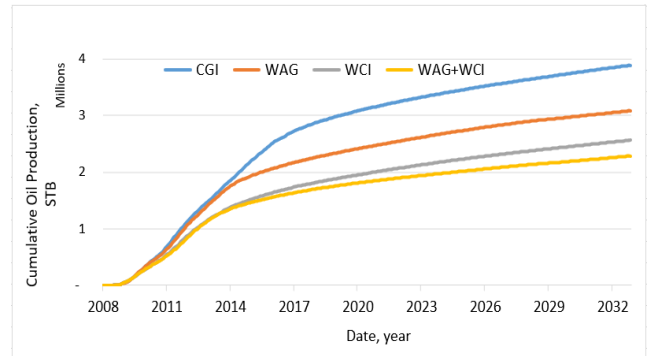


Figure E.12- Cumulative volume of Oil Produced

Gate-to-gate emissions (major contributors)

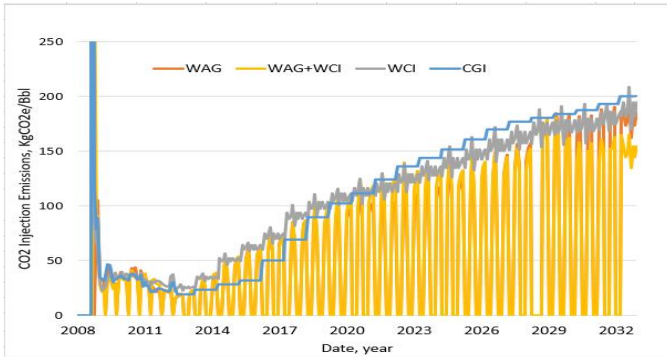


Figure E.13- CO2 Injection emissions

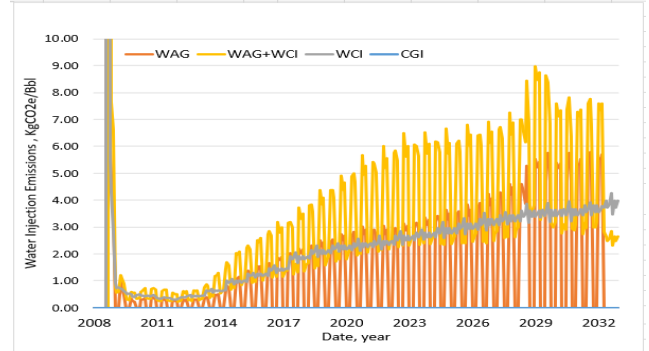


Figure E.14- Water injection emissions

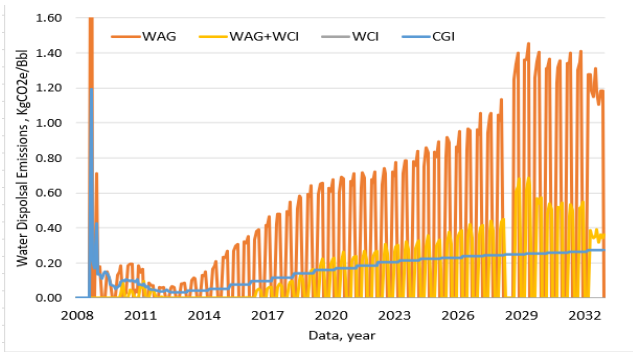


Figure E.15- Water disposal emissions

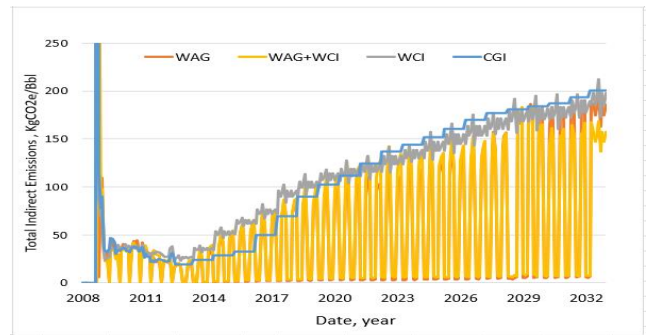


Figure E.16- Total Gate-to-Gate emissions without gas separation process

Impact of gas separation emissions process

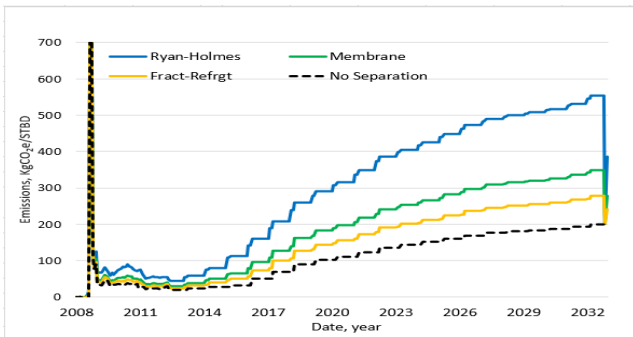


Figure E.17- CGI: Total daily emissions per gas separation process

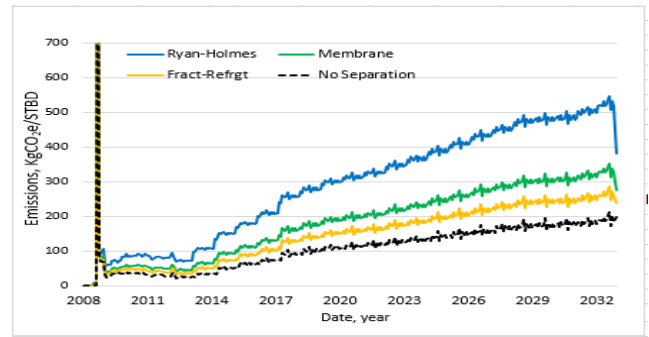


Figure E.18- WCI: Total daily emissions per gas separation process

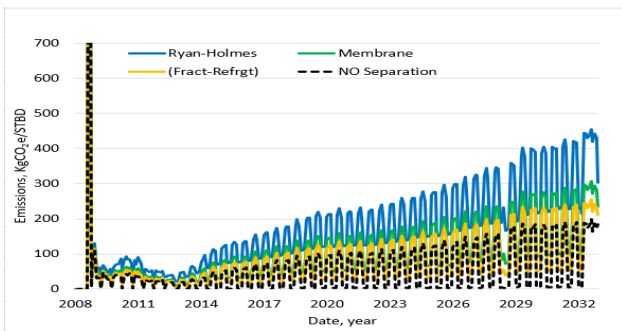


Figure E.19- WAG: Total daily emissions per gas separation process

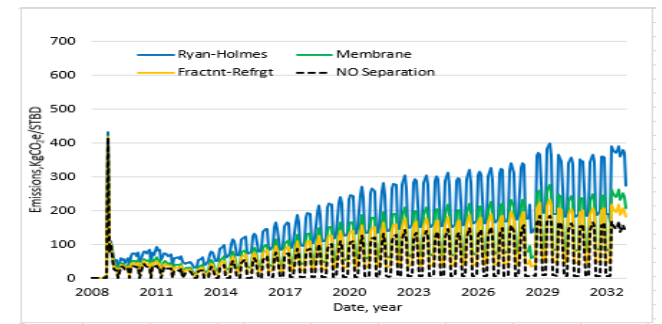


Figure E.20- WAG+WCI: Total daily emissions per gas separation process

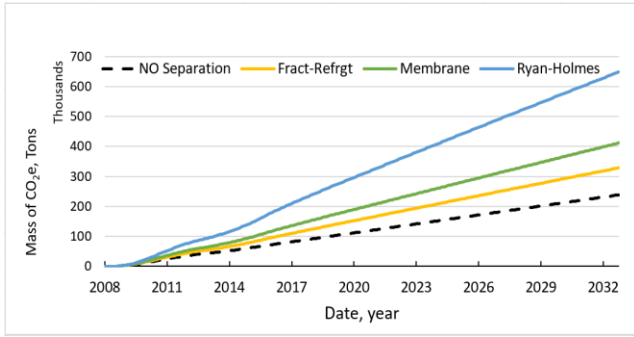


Figure E.21- **CGI**: Cumulative GHG Emissions per Separation Process

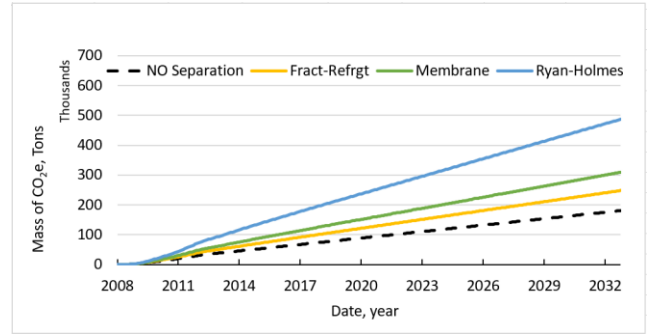


Figure E.22- **WCI**: Cumulative GHG Emissions per Separation Process

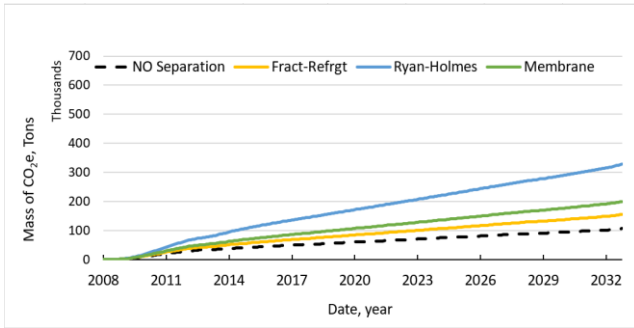


Figure E.23- **WAG**: Cumulative GHG Emissions per Separation Process

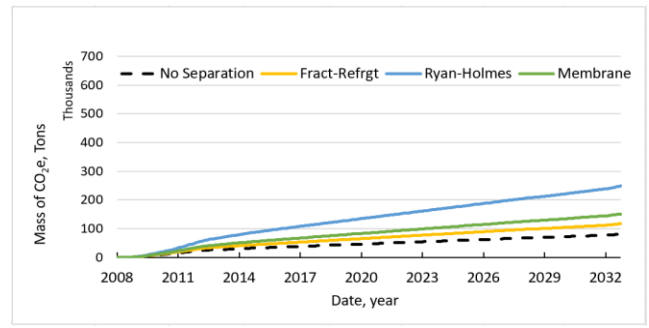


Figure E.24- **WAG+WCI**: Cumulative GHG Emissions per Separation Process

Gate-to-gate Carbon Balance

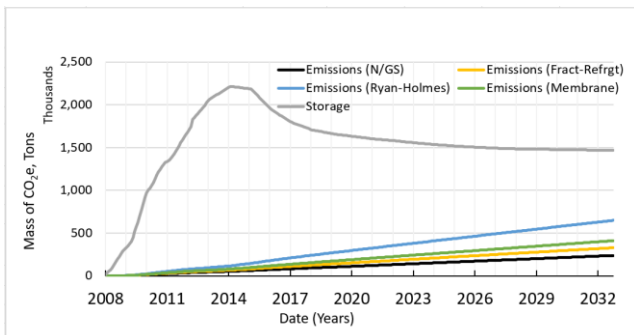


Figure E.25- **CGI**: Emissions vs Storage

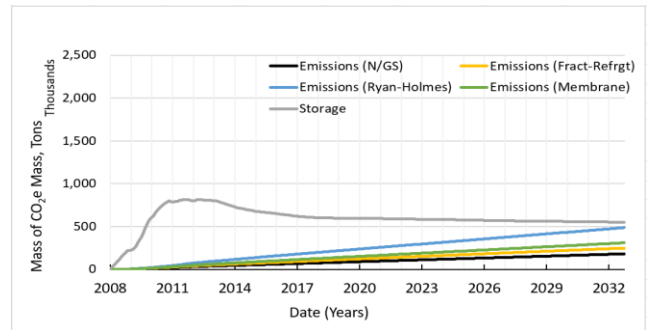


Figure E.26- **WCI**: Emissions vs Storage

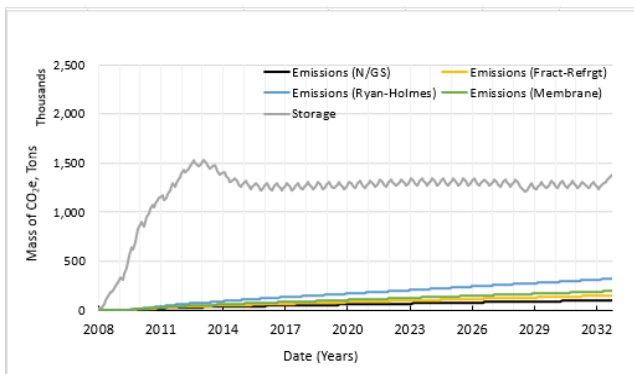


Figure E.27- **WAG**: Emissions vs Storage

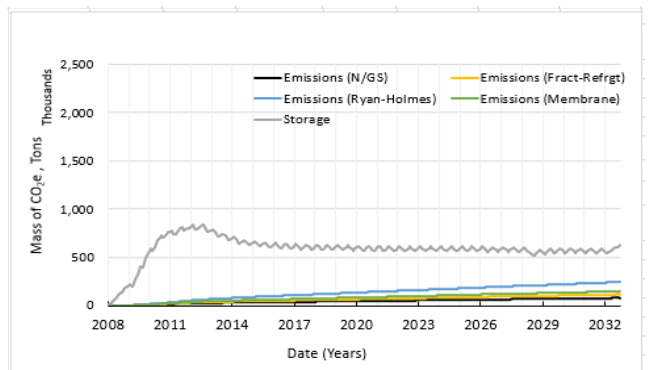


Figure E.28- **WAG+WCI**: Emissions vs Storage

Gate-to-grave Carbon balance

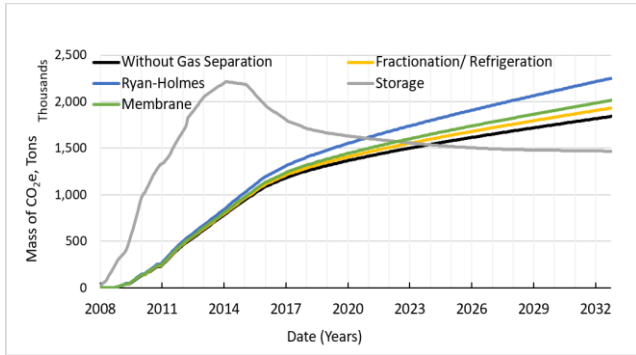


Figure E.29- CO2 storage (gray curve), versus CO2e emissions (colored curves). CGI

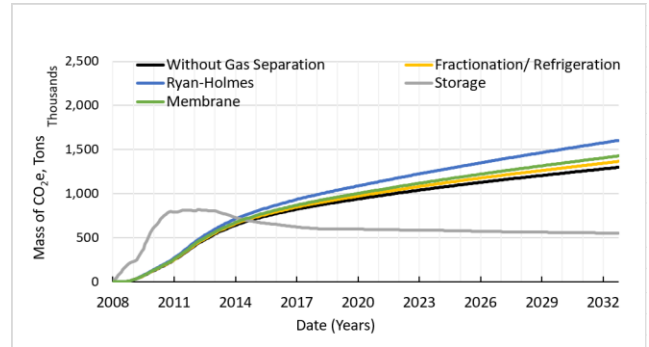


Figure E.30- CO2 storage (gray curve), versus CO2e emissions (colored curves). WCI

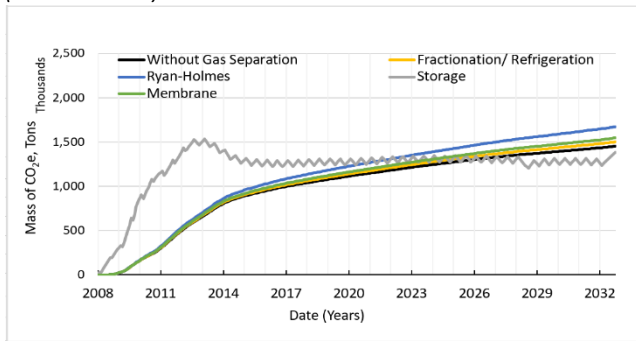


Figure E.31- CO2 storage (gray curve), versus CO2e emissions (colored curves). WAG

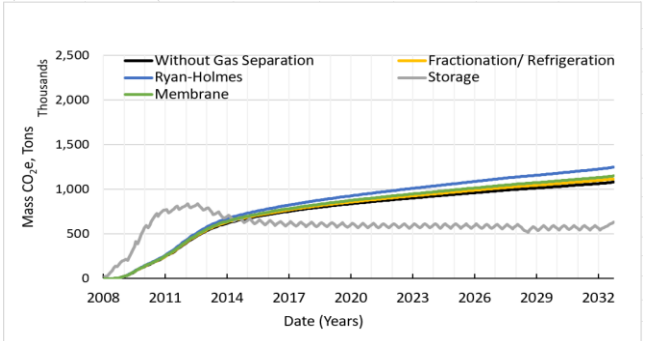


Figure E.32- CO2 storage (gray curve) versus CO2e emissions (colored curves). Hybrid

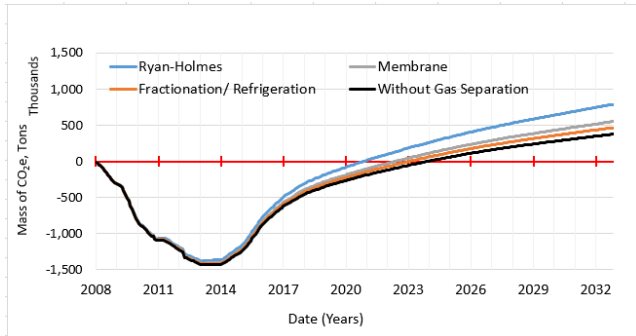


Figure E.33- Carbon balance (CO2e emissions minus CO2 storage). CGI

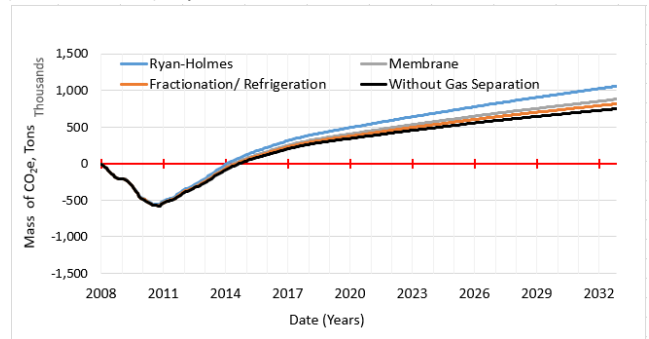


Figure E.34- Carbon balance (CO2e emissions minus CO2 storage). WCI

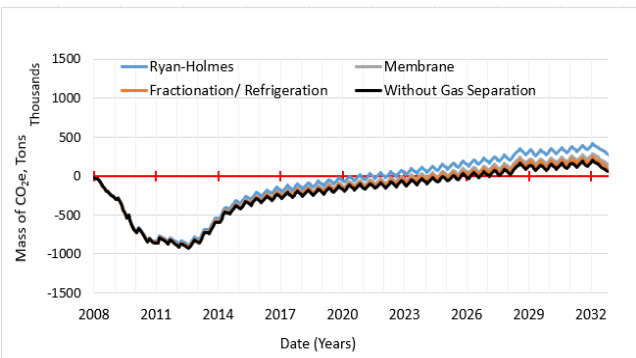


Figure E.35- Carbon balance (CO2e emissions minus CO2 storage). WAG

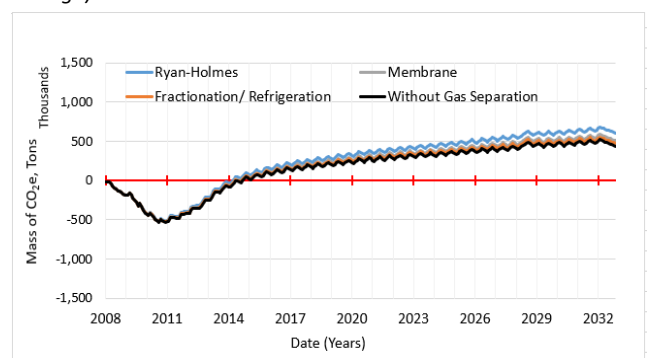


Figure E.36- Carbon balance (CO2e emissions minus CO2 storage). Hybrid

Transition Point values

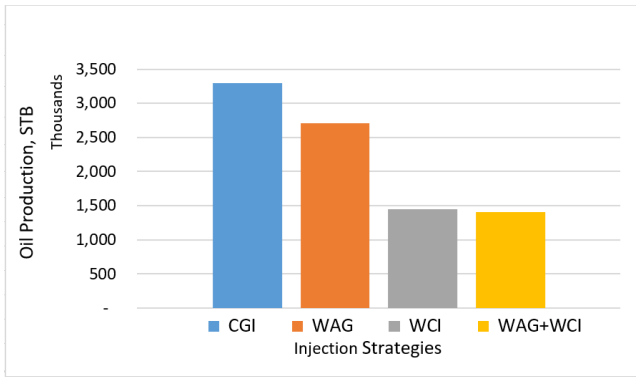


Figure E.17- Cumulative NCNO production.

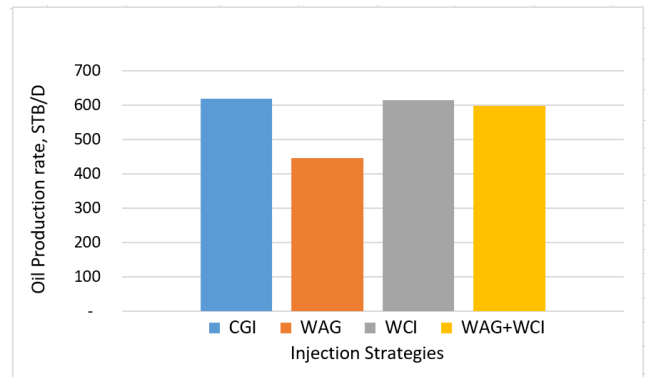


Figure E.38- Daily NCNO production

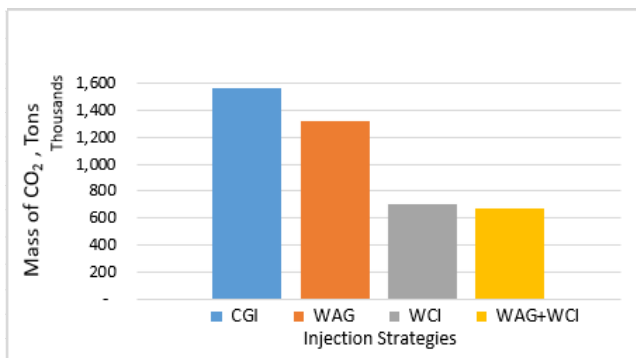


Figure E.39- Cumulative mass of CO₂ stored at Transition Point

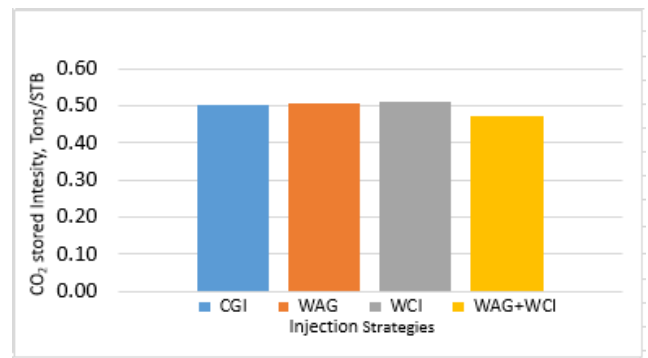


Figure E.40- Mass of CO₂ storage per STB at Transition Point

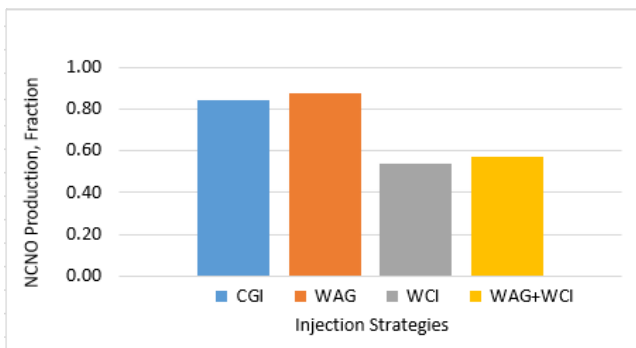


Figure E.41- Cumulative NCNO production relative to Total

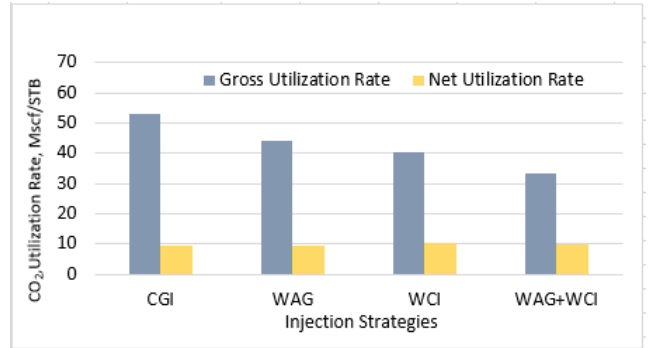


Figure E.42- Average NCNO Utilization Rates (Gross & Net)

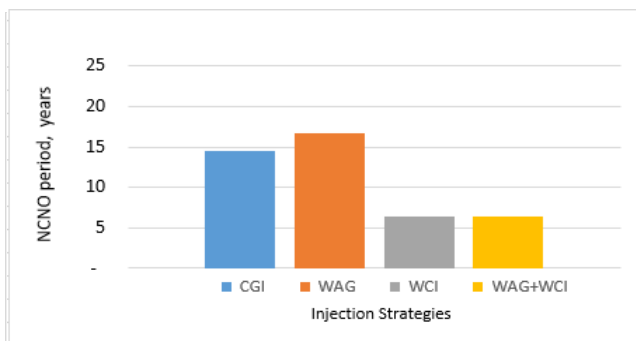


Figure E.43- NCNO production period in years

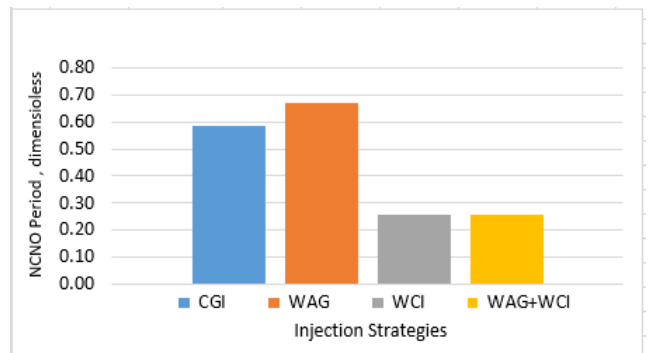


Figure E.44- NCNO period relative to project life

End of project values

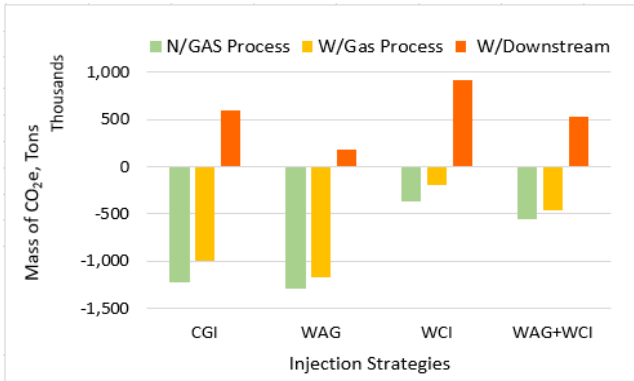


Figure E.45- CO₂ Balance (Emission-Storage). Impact of different boundaries: Gate-to-Gate (No Gas Process and With Gas Process) and Gate-to-Grave (With Downstream).

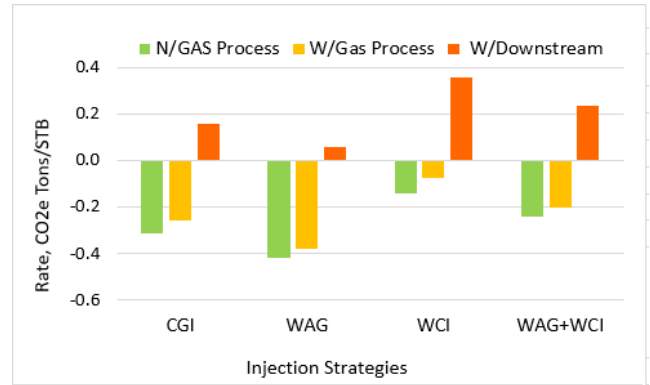


Figure E.46- CO₂ Balance (Emission-Storage) per STB. Impact of different boundaries: Gate-to-Gate (No Gas Process and With Gas Process) and Gate-to-Grave (With Downstream).

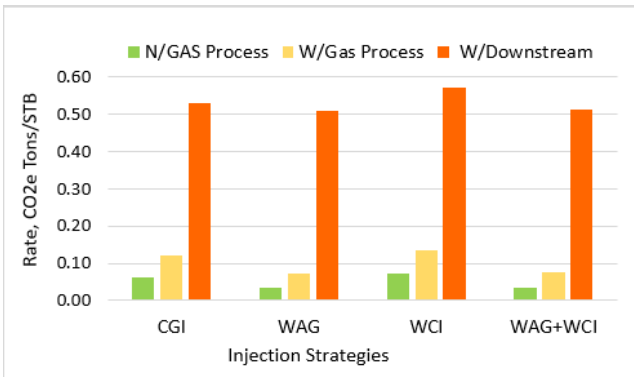


Figure E.47- Production Emission Rate, CO_{2e} emission per STB. Impact of different boundaries: Gate-to-Gate (No Gas Process and With Gas Process) and Gate-to-Grave (With Downstream).

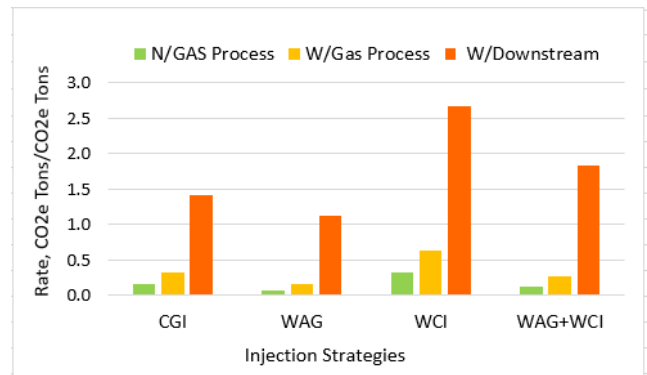


Figure E.48- Storage Emission Rate, CO_{2e} emission per storage. Impact of different boundaries: Gate-to-Gate (No Gas Process and With Gas Process) and Gate-to-Grave (With Downstream).

Intensity and efficiency rates evolution

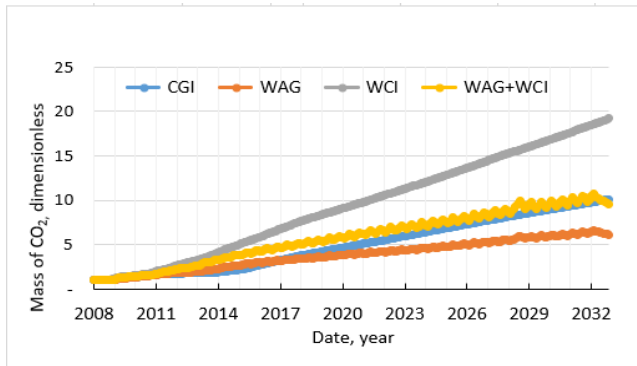


Figure E.49- Mass of CO₂ injected per mass of CO₂ stored

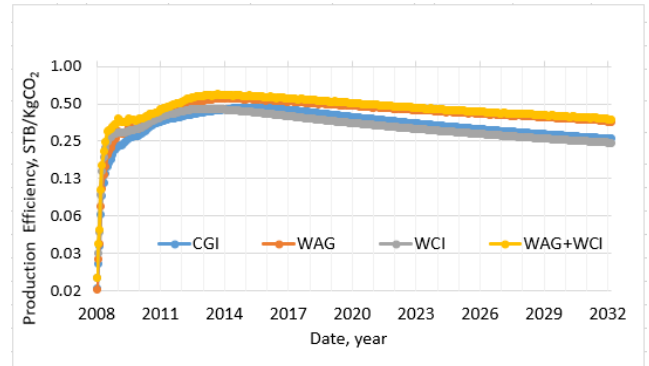


Figure E.50- Oil Production efficiency in terms of CO₂ Kg injected

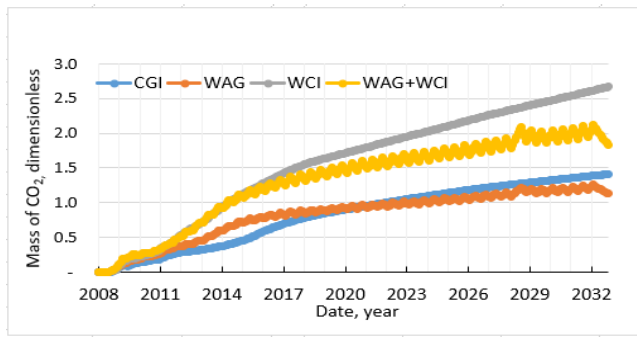


Figure E.51- Gate-to-Grave mass of CO₂e emissions per mass of CO₂ stored

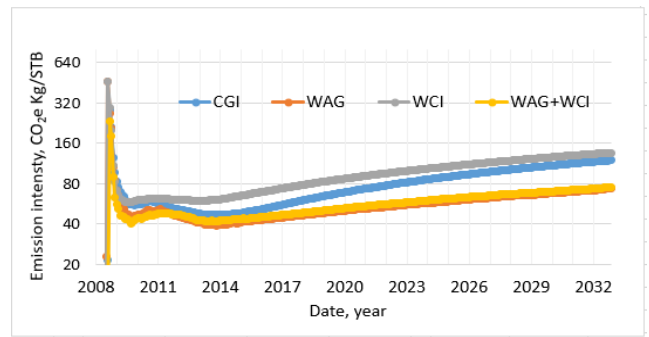


Figure E.52- Gate-to-Gate CO₂e emissions intensity per STB

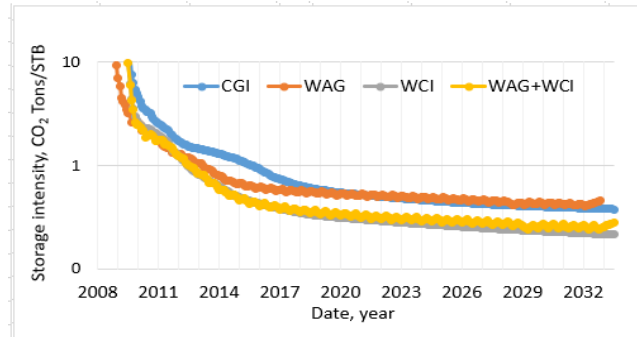


Figure E.53- Mass of CO₂ stored per barrel of oil produced

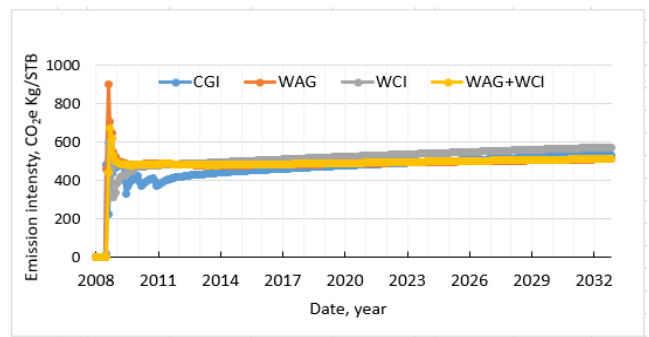


Figure E.54- Gate-to-Grave CO₂e Emissions intensity per STB

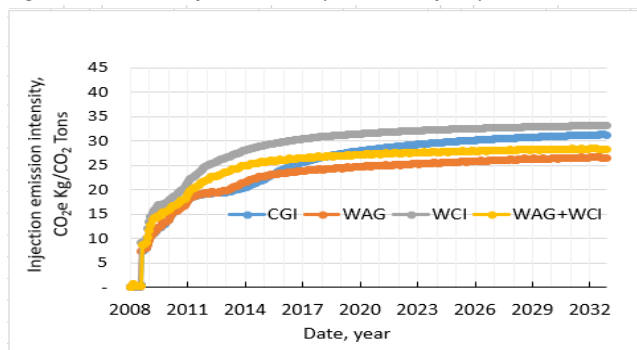


Figure E.55- Gate to Gate CO₂e emissions intensity per CO₂ Injected

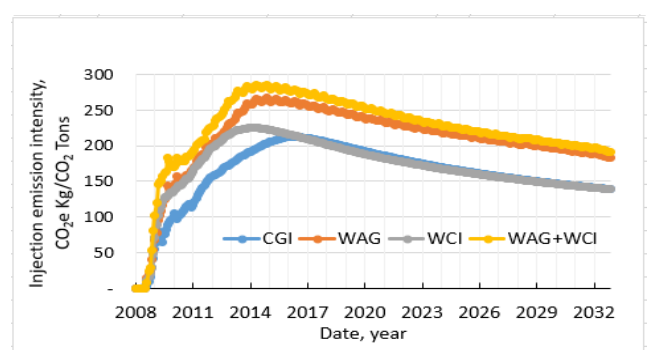


Figure E.56- Gate-to-Grave CO₂e emissions per CO₂ injected